ULTRAFAST SPECTROSCOPIC INTERROGATION OF STRUCTURAL DYNAMICS AND DISORDER OF EXCITED STATES IN CONJUGATED ORGANIC POLYMERS

By
Wenjian Yu

A dissertation submitted to Johns Hopkins University in conformity with the requirements for the degrees of Doctor of Philosophy

Baltimore, Maryland
September 2016

Abstract

The spectroscopy and dynamics of conjugated polymers have been widely studied in recent years, but there is limited empirical data that directly probes the role of structural dynamics and changes in conjugation length that occur during excited-state relaxation. An important challenge in the study of conjugated organic materials is to relate the properties of transient states that underlie macroscopic material responses directly with intra and intermolecular structure. We have studied the photo-induced relaxation dynamics of conjugated polymers (poly-(3-hexyl-thiophene) (P3HT) and poly-(3-cyclohexane-4-methyl-thiophene) (PCMT)) in solution using femtosecond broadband transient absorption spectroscopy (TAS), femtosecond stimulated-Raman spectroscopy (FSRS) and pump-dump-probe transient hole-burning spectroscopy. FSRS in particular provides a new perspective on dynamics of excited states according to the time-dependence of vibrational modes. Time-dependent studies with P3HT show that there are two different types of excited-state Raman signatures, which have been identified as modes along and peripheral to the exciton's backbone according to the time dependence of these features and from comparisons to Raman spectra of other states of the polymer. Comparison of spectra collected at different Raman pump wavelengths shows that the C=C stretching feature peaks at lower energies when interrogated with lower energy Raman pump pulses, which is known as Raman dispersion and reflects variations in effective conjugation length probed. Studies of PCMT using FSRS show

that there is time-dependent Raman dispersion: the C=C vibrational peak shifts to lower wavenumber on the time scales of 100-200 femtoseconds. This time-dependent Raman dispersion is consistent with an increase in ring-to-ring planarity and effective conjugation length, and offers a distinct spectroscopic signature of structural rearrangement in a polymer excited state. Transient hole-burning spectroscopy of RRa-P3HT in solution facilitated by population dumping through wavelength-selective stimulated emission exposes inhomogeneous broadening of the exciton absorption band in the near infrared. Dump-induced spectral diffusion of the exciton absorption band reflects structural fluctuations in locally excited polymer regions. This diffusion is observed to occur on timescales comparable to those observed in the non-equilibrium relaxation that follows direct excitation of the polymer (8-9 ps).

Advisor: Dr. Arthur Bragg
Thesis Committee:
Dr. Paul Dagdigian
Dr. Harris Silverstone

Acknowledgements

I gratefully thank all those who have worked with, helped and supported me during my Ph.D research.

First, I would like to express my great appreciation to my research advisor Dr. Arthur Bragg. Art is a nice person who has given me a lot of advice on my research projects. As one of the first graduate students in his group, I learned a lot from him not only from discussions of science but also regarding basic laser operation in the lab. He has also given me lots of suggestions about my future career. As an international student, my English is not good and he always listens to and talks with me with patience. I cannot thank him enough for all the help and support he has given me during my graduate studies.

Second, I thank all the members of the Bragg group. Thanks to Jiawang for the experiments that we did together. Thanks to Molly, Josh, Tim, Ken and Jamie for their suggestions on my research. Thanks to Paul for his contribution to my research.

Third, I would like to thank my thesis committee members, Prof. Dagdigian and Prof. Silverstone for their suggestions for my dissertation, and also because I learned a lot from their classes.

Fourth, I want to thank my friends at Johns Hopkins and in Baltimore, who helped me; we had lots of fun together during the past six years.

Finally, I want to thank my whole family: my parents, my grandma, my sister, and my aunts. Thanks for their support both in my childhood and in my education. I especially thank my

grandma, who is 90 years old and raised me while she was already old. Without her, I couldn't image how I can be.

Table of Contents

List of Figures

List of Tables

List of Charts

Chapter 1. Introduction

1.1. Application of conjugated organic materials in solar cells

Reliable energy sources are critically important for sustaining modern society. Fossil fuels, such as oil and coal, have been a traditional solution to human kind's great demand for energy, but there are two serious shortcomings associated with the use of fossil fuels: 1. Use of fossil fuels can generate poisonous environmental pollutants, as well as emission of greenhouse gases (CO_2).[1] 2. Fossil fuels reserves on earth are limited, so their use is not sustainable. Solar-cell technology presents an attractive alternative, with advantages of no direct pollution and technological sustainability.[2] Traditional solar cells are made using inorganic materials – such as silicon – and are quite costly to manufacture.[2] New organic solar cells are now under investigation with the potential to replace silicon-based solar cells. Organic solar cells are made using conjugated polymers and/or oligomers, materials that lower manufacturing cost compared to inorganic-based solar cells.[3] Another advantage of organic solar cells is easy fabrication, as organic molecules can be printed on different surfaces without concern for substrate shape. One critical issue with deployment of organic solar cells is their low efficiency. According to reports, the record for the highest efficiency for an organic photovoltaic is only 11%,[4] which is too low for useful solar-cell technology. Further fundamental research on the operation of organic solar cell materials (and photoresponses of conjugated organic polymers in general) are important to elucidate factors at the molecular level that can

impact device efficiencies. My thesis research has focused on the fundamental dynamics of isolated conjugated thiophene polymers using ultrafast transient laser techniques, which can provide insights on the structural dynamics and disorder of isolated polymer chains and how structure impacts dynamics of excitations on polymer chains.

1.2 Working principles of conjugated organic polymer solar cells

The currently accepted model for the working principles of bulk conjugated organic materials (solid state) includes four steps: 1. Exciton (electron-hole pair) generation through light/photon absorption by a conjugated polymer; 2. Exciton diffusion through polymer domains to a donor/acceptor interface; 3. Electron-hole pair separation; 4. Polaron pair dissociation into free charges.[5] In order to increase organic solar-cell efficiency, polymers with different chemical and/or conformational structures should be studied to correlate with exciton dynamics with structure. In contrast to the inorganic semiconductors they would replace, the behaviors of these materials are dictated by the dynamics of constituent molecules and their interactions with nearby (and even distant) molecules. Due to the complexity of the bulk materials, much research has focused initially on the study of relaxation behaviors in isolated conjugated polymer chains in dilute solution,[6-15] as these environments eliminate inter-chain and donor-acceptor interactions. In this way, the basic dynamics of excitation formation and relaxation on isolated conjugated chains can be investigated without the influence of intermolecular interactions. This information is useful for further investigation of solid state conjugated polymer and polymer mixtures with acceptors.

1.3 Steady-state spectroscopy of conjugated polymers: Evidence for structural heterogeneity and energetic relaxation along polymer chains

Ground state absorption and fluorescence spectra of P3HT have been reported previously for dilute polymer solutions.[6] The visible absorption spectrum of P3HT in solution shows a broad unstructured band centered around 430 nm, which corresponds to the lowest energy π-π^* inter-band transition.[6] As a comparison, the absorption spectra of conjugated thiophene oligomers show narrow features.[16] This indicates that in conjugated thiophene polymers there is a distribution of conjugation lengths or conformational domains that are excited. The corresponding emission spectrum is much narrower and displays a vibronic progression, with a peak at 580 nm that corresponds with the 0-0 transition. It has been reported that the emission spectrum of P3HT in dilute solution does not change with variation in excitation wavelength. This indicates that no matter which group of conformations have been excited, polymers relax to a common low-energy emitting intra-chain exciton state.[6] The emission spectrum of aggregated P3HT has been simulated using a Frank-Condon model, a Huang-Rhys factor of 1, and assuming that the 0.18 eV C=C stretching vibration predominantly couples to the electronic transition.[17]

1.4 Photoinduced dynamics in conjugated polymers from previous ultrafast studies

The photo-induced dynamics and spectroscopy of conjugated polymers in solution have been examined extensively over the last decade using various transient electronic spectroscopies, including transient absorption, stimulated emission, fluorescence up-conversion, and non-linear electronic spectroscopies.[6-15] From these studies it has been concluded that the dynamics underlying various phases of excited-state relaxation include: (1) Exciton self-trapping or localization, associated with transient spectral evolution over timescales of ~100 fs or less;[6,8,10,12,13] (2) Resonant excitonic energy transfer (EET)[6,9,14] through which energy migrates to lower-energy sites characterized by increased degree of delocalization and/or (3) local, long-range torsional relaxation, both occurring on timescales ranging from sub-ps to 10s of ps;[7,8,12,13,15] and (4) singlet exciton decay by emission and intersystem crossing (ISC), occurring on timescales of 100s of picoseconds.[6,15]

Spectroscopic evidence of the initial ultrafast self-trapping or localization has been reported by different groups.[10] Du et al. have reported the ultrafast geometrical relaxation of poly-[3-hexylthiophene-2,5-diyl]-[p-dimethylaminobenzylidenequinoidmethene] (PHTDMABQ) using real-time vibrational spectroscopy, which can obtain both electronic and vibrational dynamics under the same excitation and probing condition.[10] In their study, spectral changes in the electronic absorption spectrum and instantaneous

vibrational frequency have been observed and a 60-100 fs time scale has been identified, which was ascribed to geometrical relaxation from the free exciton to the exciton polaron.[10] Ruseckas et al have investigated fully conjugated poly[2-(2'-ethylhexyloxy)-5-methoxy-1,4-phenylenevinylene] (MEH-PPV) using photoluminescence and transient absorption and observed a reorientation of the transition dipole moment by ~30° on a sub-100 fs time scale.[18] On the contrary, partially conjugated MEH-PPV shows a much slower depolarization (>1 ps). This is explained by dynamic localization of initially delocalized excitons in the fully conjugated polymer driven by local geometrical relaxation from the more twisted geometry of the ground state to a planar quinoidal structure in the excited state.[18] A similar experiment performed on P3HT by Wells et al indicate that localization is dominated by only two phonon modes (0.18eV C=C stretching and a lower frequency torsional mode at ~0.016 eV) and is a correlated rather than stochastic process.[12] Banerji et al have investigated the ultrafast relaxation of both isolated P3HT and P3HT films using fluorescence up-conversion spectroscopy.[6] They concluded that primary photoexcitations in P3HT are highly delocalized, localizing in 100 fs to become an exciton.[6] All these results based on electronic spectroscopy point to a <100 fs ultrafast self-localization after the initial photoexcitation of conjugated polymer. Further experiments based on vibrational spectroscopy, such as Raman spectroscopy, would provide valuable insight on structural dynamics associated with this process.

After initial ultrafast self-localization, the exciton will further relax on picosecond timescales (>10 ps), with corresponding redshifts in emission features. Two mechanisms associated with this spectral dynamic have been discussed in past research: 1. Resonant excitonic energy transfer (EET), through which energy migrates to lower-energy sites characterized by different degrees of delocalization or conformational order.[6,9,14] 2. Local, long-range torsional relaxation, with dihedral angle decrease and exciton length increase.[7,8,12,13,15] Collini et al have investigated MEH-PPV using ultrafast transient anisotropy decay measurements and observed signatures of coherent intrachain energy transfer.[9] Further two-dimensional photon-echo measurements revealed the presence of long-lived intrachain electronic and vibrational coherences. They concluded that quantum transport effects occur when chemical bonds connecting donor and acceptor moieties help to correlate their energy-gap fluctuations.[9] Westenhoff et al have studied poly[3-(2,5-dioctylphenyl) thiophene] using femtosecond time-resolved transient absorption.[14] They claimed that torsional relaxation can be distinguished from EET by site-selectively exciting low-energy conjugated segments. Energy transfer simulations have been performed on chains with time-dependent site energies and conjugation lengths; these indicate that the exciton length increases about 2 monomers during torsional relaxation.[14] Busby et al investigated P3HT using pump-dump-probe spectroscopy. Their data shows that the ground state bleach does not exhibit a red shift that would be expected if EET occurs.[7] They therefore concluded that the primary mechanism for

excitonic relaxation is excited-state self-trapping by torsional relaxation and that EET makes a negligible contribution to exciton relaxation.[7] The debate about EET and torsional relaxation in excitonic relaxation requires additional time-resolved experimental results to resolve.

1.5 Ultrafast Transient Absorption Spectroscopy

Ultrafast transient absorption is a basic time-resolved spectroscopic method which has been used widely in the study of dynamic processes in chemical and material systems, including conjugated polymers.[19] In this method, a sample is excited electronically with an initial ultrafast laser pulse and photoinduced dynamics that result are interrogated according to changes in the transmission of a broadband ultrafast probe pulse. There are three general types of spectral features obtained from this method: 1. Ground state bleach (GSB), which corresponds to depletion of the transition between the ground and first excited states. 2. Stimulated emission (SE), which corresponds with the emission from first excited state back to the ground state. 3. Transient absorption (TA), which is the absorption from an excited state or a transient species (in conjugated polymers, usually the first excited states or exciton). Singlet transient states formed by the initial excitation can undergo inter-system crossing (ISC) to form triplet excited states. Using transient absorption, both singlet transient absorption (STA) and triplet transient absorption (TTA) can be detected at different time delays.

Although transient absorption is a powerful method to study ultrafast dynamics of conjugated polymers, it can only probe changes in electronic spectral features. Gaining greater insights on structural dynamics requires the use of vibrationally resolved methods.

1.6 Femtosecond stimulated Raman spectroscopy as a probe of structural dynamics in conjugated material systems

The role of structural dynamics in the relaxation of photoexcited conjugated materials would be more directly interrogated with vibrationally resolved techniques. Raman spectroscopy, in particular, has been used extensively to characterize conjugated polymers and polymer-based materials, and is a promising complement to electronic spectroscopies for interrogating the structural characteristics and dynamics of conjugated polymers in their excited states.[10,15] Conjugated polymers and oligomers exhibit very large ground-state Raman cross-sections, with spectra dominated by totally symmetric modes that coincide with the change in molecular geometry that accompanies polymer excitation.[20] Furthermore, vibrational frequencies of various Raman-active modes (most notably the in-phase C=C stretching frequency) are directly sensitive to the extent of delocalization along an oligomer or polymer backbone.[20,21] Given that excited states of conjugated oligomers and polymers are highly delocalized by nature, we anticipate that C=C stretching frequencies of excited states should be highly sensitive to variations or evolution in the excited-state delocalization length. Thus, time-resolved excited-state Raman spectroscopy could be used as a direct method for interrogating evolution in conformation and delocalization length that occurs through the course of excited-state relaxation of photo-excited conjugated polymers and oligomers.[15]

Our measurements have utilized femtosecond stimulated Raman spectroscopy (FSRS)

to provide a time-dependent measurement of Raman spectroscopy of transient species. Compared to time-resolved spontaneous Raman, the Raman signal of FSRS is large, which can accelerate data acquisition. As for TAS measurements, an initial excitation pulse, which is a femtosecond (< 100 fs) pulse centered at a specific transition energy, is used to excite the polymer into an excited state. With FSRS a pulse pair is used to measure stimulated Raman transitions over a broad wavelength range. This is accomplished using the combination of a Raman excitation pulse, which is a narrow band pulse with duration of a few picoseconds, and a broadband probe pulse, which has femtosecond duration. The time resolution of a transient FSRS measurement is determined by the cross-correlation of the pump and probe pulses, whereas the linewidths of vibrational features are determined by the bandwidth of Raman excitation pulses and dephasing rates of vibrational coherences in the excited state. Therefore FSRS generally enables both high time resolution and narrow feature bandwidth (~10-20 cm^{-1}). When FSRS is implemented using a multi chopper setup (described in 2.3), multiple spectroscopic signatures can be collected in a single experiment, including: transient absorption (TA), ground state Raman spectroscopy (GSR) and excited state Raman spectroscopy (ESR). This experimental approach provides advantages for signal processing and comparisons.[22]

1.7 Transient hole burning as a probe of excited-state heterogeneities

Previous work has shed little light on the structural characteristics of localized excitations and correlations between local structure and photo-physical properties, as the experimental methods applied generally have had limited ability to directly probe or differentiate among structural heterogeneities within an ensemble of photo-excited amorphous polymer, in either solution or films. This is noteworthy because polymer photo-physics typically have been interpreted within a simplified conceptual framework that assumes that structural disorder along the polymer backbone fragments the extended π network into a distribution of segments of variable length that are hosts for localized excitations;[23] thus, the photoexcitation of polymer is expected to prepare an ensemble of excitons characterized by a distribution of conjugation lengths determined by variation in intra-chain structure. The concept of an average, well-defined conjugated subunit is recognized to be an oversimplified paradigm for localized conjugated polymer (CP) excitons,[24, 25] yet, empirical data reporting characteristics of relevant structural motifs, their fluctuations, and how these impact exciton photo-physical properties have remained limited. Experimental interrogation of structurally induced photo-physical heterogeneities among CP excitons would provide further insights into mechanisms driving non-equilibrium relaxation of photo-excited CPs and how the nature of the local structure impacts processes such as intramolecular charge-pair formation.

In my research, I have used pump-dump-probe transient hole burning spectroscopy

to interrogate the inhomogeneity of isolated, amorphous conjugated polymer in solution. Three pulses are used in this technique. The first pulse is used to prepared a population of excited polymer by pumping the transition between the ground and the first excited state. After relaxation for 10-200 ps (shorter than the 500 ps exciton life time for P3HT), the initial ultrafast localization and torsional relaxation and/or excitonic energy transfer are complete and result in a quasi-equilibrated excited state population. Then a second pulse (with wavelength tunable within the polymer's emission spectrum) is used to selectively dump a subpopulation of polymer excitons from the first excited state back to the ground state and generate a spectral "hole" signifying formation of a non-equilibrated excited state population. Following application of the dump pulse the remaining population can only reequilibrate through structural fluctuation; these fluctuations are captured by changes in the transient absorption as probed by broadband absorption of a third pulse. .

1.8 References

1. W. Cees, *Resour. Energy Econ*. **16**, 235-242 (1994).
2. A. McEvoy, L. Castaner, T. Markvart, *Solar Cells: Materials, Manufacture and Operation*, 2nd Edition; Elsevier: Oxford, 2012.
3. O. A. Abdulrazzaq, V. Saini, S. Bourdo, E. Dervishi, and A. S. Biris, *Particul. Sci. Technol*. **31**, 427-442 (2013).
4. J. You, L. Dou, K. Yoshimura, T. Kato, K. Ohya, T. Moriarty, K. Emery, and C. Chen, *Nat. Comm.*, **4**, 1446 (2013).
5. M. Scharber and N. Sariciftci, *Prog. Polym. Sci*. **38**, 1929-1940 (2013).
6. N. Banerji, S. Cowan, E. Vauthey, and A. J. Heeger, *J. Phys. Chem. C* **115**, 9726-9739 (2011).
7. E. Busby, E. C. Carroll, E. M. Chinn, L. Chang, A. J. Moulé, and D. S. Larsen, *J. Phys. Chem. Lett.* **2**, 2764-2769 (2011).
8. J. Clark, T. Nelson, S. Tretiak, G. Cirmi, and G. Lanzani, *Nat. Phys*. **8**, 225-231 (2012).
9. E. Collini and G. D. Scholes, *Science* **323**, 369-373 (2009).
10. J. Du, Z. Wang, W. Feng, K. Yoshino, and T. Kobayashi, *Phys. Rev. B* **77**, 195205 (2008).
11. I. Hwang and G. D. Scholes, *Chem. Mater*. **23**, 610-620 (2011).
12. N. P. Wells and D. A. Blank, *Phys. Rev. Lett*. **100**, 086403 (2008).
13. N. P. Wells, B. W. Boudouris, M. A. Hillmyer, and D. A. Blank, *J. Phys. Chem. C* **111**, 15404-15414 (2007).
14. S. Westenhoff, W. J. D. Beenken, R. Friend, H., N. C. Greenham, A. Yartsev, and V. Sundström, *Phys. Rev. Lett*. **97**, 166804 (2006).
15. W. Yu, J. Zhou, and A. E. Bragg, *J. Phys. Chem. Lett*. **3**, 1321-1328 (2012).
16. D. Grebner, M. Helbing, and S. Rentsch, *J. Phys. Chem*. **99**, 16991-16998 (1995).
17. J. Clark, C. Silva, R. H. Friend, and F.C. Spano, *Phys. Rev. Lett*. **98**, 206406 (2007).
18. A. Ruseckas, P. Wood, I. D. W. Samuel, G. R. Webster, W. J. Mitchell, P. L. Burn, and V. Sundström, *Phys. Rev. B* **72**, 115214 (2005).
19. B. Rudi, G. Rienk, J. T. M. Kennis, *Photosyn. Res*., **101**, 105-118 (2009).
20. C. Castiglioni, M. Del Zoppo, and G. Zerbi, *J. Raman Spectrosc*. **24**, 484-494 (1993).
21. V. Hernandez, C. Castiglioni, M. Del Zoppo, and G. Zerbi, *Phys. Rev. B* **50**, 9815-9823 (1994).
22. W. Yu, P. J. Donohoo-Vallett, J. Zhou, and A. E. Bragg, *J. Chem. Phys*. **141**, 044201 (2014).
23. S. N. Yaliraki and R. J. Silbey. *J. Chem. Phys.* **104**, 1245-1253 (1996).
24. W. J. Beenken and T. Pullerits, *J. Phys. Chem. B* **108**, 6164-6169 (2004).
25. B. J. Schwartz, *Nat. Phys.* **7**, 427-428 (2008).

Chapter 2. Experimental Methods

2.1 Laser setup.

The experiments described in this dissertation utilize an ultrafast laser system, which consists of a femtosecond oscillator, regenerative amplifier, femtosecond optical parametric amplifier (OPA) and picosecond OPA. The oscillator is used to generate ultrafast pulses. The amplifier boosts the power of the seed pulse to a >4 W output. Half of the output from the amplifier is used to pump the femtosecond OPA, which is used to generate excitation pulses (covering UV, visible, and Near-IR wavelengths) that are used for experiments. One quarter of the output from the amplifier is used to pump the picosecond OPA and generate spectrally narrow picosecond pulses that are used for Raman excitation in FSRS experiments.

2.1.1 Generation of ultrafast pulses in a mode-locked oscillator

A commercial mode-locked Titanium:Sapphire oscillator (Coherent Mantis) is used to generate femtosecond laser pulses.[1] The Ti:Sapphire lasing medium of the oscillator is excited using a 5W continuous-wave (CW) excitation source at 532 nm; this green excitation light is generated by frequency doubling the output of an optically pumped semiconductor (OPS) laser (1064 nm) in a Lithium triborate (LBO) nonlinear crystal. When pumped with this excitation source the oscillator will lase in a CW mode centered near 800 nm prior to modelocking. Modelocking requires a fixed phase relationship between the longitudinal modes of the laser's resonant cavity, resulting in generation of

pulses with short duration (picosecond to femtosecond). The oscillator employs a passive mode-locking technique, which does not require an active shutter or modulator with externally controlled timing. Passive modelocking of the oscillator results from a nonlinear optical effect (Kerr lensing) that results in different focusing conditions for high- and low-intensity light in the optical cavity: The beam diameter at a critical aperture is large when the oscillator is not mode-locked (i.e. CW lasing), but becomes smaller when mode-locked; this means that there are fewer optical losses under mode-locked conditions. Pulse dispersion in the resonator cavity is balanced with sets of chirped mirrors.

Oscillator alignment involves three steps: 1) OPS pump beam alignment through the Ti:Sapphire rod; 2) Oscillator cavity alignment and optimization (CW lasing); 3) Mode-locking. The output of the oscillator is 400-500 mW, center around 800 nm and with an 80M Hz frequency at normal operation.

2.1.2 Amplification of ultrafast pulses

A Coherent Legend Elite ultrafast regenerative amplifier is used in our lab and is seeded with the output from the oscillator.[2] The seed pulses are first stretched in time and then amplified by several trips through a Ti:Sapphire gain medium pumped by 20 W of 527 nm light from a pulsed Nd:YLF laser (Coherent Evolution). Amplified pulses are then compressed in time to regain time resolution. Output pulses are centered at 800 nm, with 40 fs pulse duration, 1 kHz repetition rate, and with compressed output power of

4-4.5 W.

2.1.3 Tunable excitation pulses from a femtosecond Optical Parametric Amplifier (OPA)

A commercial OPA from Light Conversion is used in our lab to generate femtosecond pulses with tunable excitation energy.[3] Half of the output from the amplified Ti:Sapphire laser is used to pump the OPA, with tunable output wavelengths ranging between 300 and 2500 nm and power ranging 10 to 150 mW (wavelength specific).

The OPA is seeded with a white-light continuum that is pre-amplified by a low intensity pump beam to generate a near-IR signal beam. A high intensity pulse is used to amplify the signal beam, generating high intensity signal ("S", 1150-1600 nm) and idler ("I" 1600-2650 nm) outputs. Second harmonic signal ("SHS", 575-800 nm) and second harmonic idler ("SHI", 800-1325 nm) are generated by Mixer 1, which is a computer controlled carousel of nonlinear crystals, each cut for different non-linear processes. Sum frequency signal ("SFS", 470-530 nm) and sum frequency idler ("SFI", 530-610 nm) are generated by mixing S and I outputs with 800 nm light pulses in Mixer 1. Note that the delay of the fundamental 800 nm pump pulses relative to S and I can affect the output SFS and SFI intensities. Fourth harmonic signal ("FHS", 290-4700 nm) and fourth harmonic idler ("FHI", 400-470) outputs are generated by doubling the SHS and SHI signals using Mixer 2. I, FHI and FHS outputs all have horizontal polarizations, while all

the other outputs (S, SHI, SHS, SFI, SFS) have vertical polarization.

2.1.4 Picosecond OPA for generation of Raman excitation pulses

A Raman excitation pulse with narrow spectral bandwidth is needed in order to acquire vibrationally resolved Raman features using FSRS. Due to the Fourier transform relationship between time and frequency, a narrow bandwidth corresponds with a long duration pulse. In our lab, we use a commercially manufactured second harmonic bandwidth compressor (SHBC) to convert the femtosecond pulses (20-500 cm^{-1}) at the 800-nm amplifier fundamental to picosecond pulses (3-10 cm^{-1}) at 400 nm.[4] The working principle of SHBC is to drive second harmonic generation with oppositely chirped pulses. The 800 nm input is split 50/50, with each half phase conjugated, such that the two beams have opposite temporal chirp. The output pulse (400 nm) generated by mixing these in a non-linear crystal is chirp free and is used to pump a picosecond OPA to generate Raman excitation pulses at various visible (horizontally polarized) and near-IR (vertically polarized) wavelengths for our measurements.

2.1.5 Probe generation, polarization and optical delay control, and detection

White light generation: A few mW (~a few μJ/pulse) of the laser fundamental at 800 nm is focused onto a 2-mm thick sapphire crystal to generate both visible (410-750 nm) and near-IR (850-1100+ nm) white light probe continua. CaF_2 can also be used to

generate a near-UV continuum covering 310-380 nm.[6] The laser damage threshold of CaF_2 is much lower than that of Ti:Sapphire, such that it must be moved continuously with a translation stage in order to prevent damage.

Polarization control: In order to eliminate signatures of transient polarization anisotropy in our pump-probe TAS experiments, the relative linear polarizations of pump pulses and probe pulses are set at magic angle (54.7^o). In our lab, wire-grid polarizers are used to align the probe light polarization at magic angle relative to the pump beam polarization. Note that the pump beam polarization can be horizontal or vertical (relative to the table), as determined by the non-linear optical method for generating the pump .

For three-pulse experiment like FSRS and pump-dump-probe transient hole-burning, the two excitation pulses (photoexcitation and Raman excitation; or photoexcitation and "dump") are set to be polarized parallel. If the polarizations of the two pulses are not parallel as generated by OPAs or other non-linear optical methods, a periscope is required to rotate one of the beam polarizations by 90^o.

Collecting/isolating probe light for detection: The probe beam is focused to a spot size of ~100 microns in the photoexcited region of the sample using a parabolic reflector. After the probe transmits through the sample it is filtered prior to detection. Residual excitation scatter is blocked with apertures ("spatial filtering"); a long pass filter can be used if the pump pulse is at much higher energy than the probe range. The white light continuum is also filtered to eliminate detector saturation near the WLG driving

wavelength and to eliminate second order diffraction (i.e. if a visible probe is desired, the near-IR portion is filtered; if near-IR probing is desired, the visible portion is filtered.

Optical delay lines: For ultrafast spectroscopy (fs), the relative time of arrival of the pump and probe pulses at the sample is determined by their relative optical path length. In our lab, a translation stage equipped with a retroreflector is used to change the optical path length of excitation pulses relative to the probe. Although this configuration can be problematic if pump beams are not collimated sufficiently, this configuration is required such that the probe and Raman excitation pulse timing can be fixed for FSRS measurements. The optical delay of the Raman excitation pulse relative to the broadband probe is controlled by passing the ps pulse off of a reflector attached to a smaller motor-controlled translation stage.

2.2 Home-made automated data-acquisition program

An automated data-acquisition program written with Labview is used for our measurements.[6,7,8] This program was written to control the movement of the translation stages (optical delay control), to synchronize the camera operation with beam choppers and the laser repetition rate, to receive output from the camera, and to calculate and average output signals during data collection. This program will separate probe spectra collected by the camera that correspond with different choppers phase combinations (for one choppers, these are pump "on" vs. "off"; for chopping two beams these include, on/on, on/off, off/on, off/off), and label them correctly.

Translation stages are used to control the time delay between laser pulses. At each fixed translation state position signals are collected in two different steps: First, signals from the camera corresponding to different chopper phase combinations are collected, with transient absorption calculated using the following formula:

$$\text{Absorption} = -\log(I/I_o) \qquad (2.1)$$

This process is repeated for several thousand laser shots and absorption averaged to decrease influence of shot-to-shot signal fluctuations. Second, the signal will be averaged again by cycling through translation stage delays. This second cycle enables averaging over fluctuations in pump intensity or other factors that vary with measurement time. These cycles are controlled by nested "while" loops in the Labview acquisition program.

2.3 Multiple-phase data collection methods

Figure 2.1: Chopper wheels with different chopping patterns

For pump-probe spectroscopy, two laser pulses are used and one chopper is needed to chop the pump in order to get the final pump-probe signal.[6] A simple chopper (Figure 2.1, left) is sufficient for this measurement. In this configuration, two different signals (two phases) are detected by the camera shot-to-shot (i.e., each signal at 500 Hz): a pure probe signal and a pump-probe signal (which means the probe transmitted through the sample is affected by sample excitation with the pump pulse that creates transient states that can absorb part of probe). Many samples can fluoresce when excited by the pump, which can affect the calculated transient absorption. In order to eliminate fluorescence, a two choppers configuration is needed, whereby choppers are used with both the pump and probe beams.[8] In this way, four different signals (four phases) can be detected: pure pump (which includes fluorescence and pump beam scatter), pure probe, pump-probe, and a dark background; these correspond with pump/probe: on/off, off/on, on/on and off/off. In this way the pure fluorescence signal can be subtracted from the pump-probe signal prior to calculation of absorption. This can be implemented with two choppers as

shown in Figure 2.1 (left) or one specialized chopper (Figure 2.1 right). The latter is designed to chop two beams in different phases, such that the outer part can be used to chop pump pulses and the inner part can be used to chop probe pulses. In this way, the four different signals can also be generated.

For three pulses measurement, like pump-dump-probe and FSRS, four- or eight-phase data collection is needed in order to eliminate fluorescence contamination and provide appropriate signals needed for data analysis.[6] In these experiments, up to three choppers are needed to chop all three pulses during the measurement. Alternately, we can use one simple chopper to chop the probe pulse and use the second chopper above to chop both excitation pulses (pump and dump pulses in pump-dump-probe experiment and pump and Raman pump pulses in FSRS measurement). Note that the more chopping phases used, beam diameters must be small enough to be transport through the chopper up to 4 times for a given phase. Usually the probe beam is focused tightly enough before the sapphire crystal for white light generation which makes it easy to chop this beam accordingly.

2.4 Sample handling

Regioregular poly-(3-hexylthiophene) (RR-P3HT) (electronic grade, 90-94% regioregular), regioramdom poly-(3-hexylthiophene) (RRa-P3HT) and poly-(3-cyclohexyl, 4-methylthiophene) (PCMT) were purchased from Rieke metals and used after prolonged purging with high purity dry argon. Chlorobenzene and THF were used as solvent and were deaerated by repeated freeze-pump-thaw cycles. All solutions were prepared under an argon atmosphere. For FSRS measurements, the sample concentration was 1 mg/mL, which can guarantee significant Raman signals but without polymer aggregation. For other measurements (transient absorption, three pulses pump-push-probe etc.), the concentration is 0.1~0.2 mg/mL. [6, 7, 8]

In order to prevent the polymer from oxidation, all samples were circulated through a 0.5 mm quartz flowcell with a peristaltic pump during spectroscopic measurements. The sample flow circuit is constructed entirely of PTFE tubing and compression fittings, and has a circulation volume of less than 20 mL. P3HT samples were introduced into the flow circuit under air-free conditions after it was thoroughly purged with dry argon. For FSRS measurement, using a relatively short cell pathlength (0.5 mm) helps to minimize background contributions from non-resonant solvent and polymer ground-state signals.

During our measurements, a red overhead light is used in the lab because ordinary room light can lead to oxidation of some samples. Measurements were usually conducted right after samples were prepared. If not, samples were stored wrapped in foil to prevent

exposure to light.

2.5 References

1. Coherent Inc., Operator's Manual: Mantis, Modelocked Titanium: Sapphire Laser System.
2. Coherent Inc., Operator's Manual: Coherent Legend Elite Ultrafast Amplifier Laser Systems.
3. Light Conversion Inc., User's Manual: The Optical Parametric Amplifier of White-light Continuum.
4. Light Conversion Inc., User's Manual: Traveling-wave Optical Parametric Amplifier.
5. P. Kukura, D. W. McCamant, and R. A. Mathies, *Annu. Rev. Phys. Chem*. **58**, 461, (2007)
6. W. Yu, J. Zhou, and A. E. Bragg, *J. Phys. Chem. Lett*. **3**, 1321-1328 (2012).
7. W. Yu, P. J. Donohoo-Vallett, J. Zhou, A. E. Bragg, *J. Chem. Phys*. **141**, 044201 (2014).
8. W. Yu, T. J. Magnanelli, J. Zhou and A. E. Bragg, *J. Phys. Chem. B*, **120**, 5093-5102 (2016).

Chapter 3. Exciton Conformational Dynamics of poly-(3-hexylthiophene) (P3HT) in Solution from Time-resolved Resonant-Raman Spectroscopy

This chapter describes work previously published [47] in

W. Yu, J. Zhou, and A. E. Bragg. Exciton Conformational Dynamics of Poly(3-hexylthiophene) (P3HT) in Solution from Time-resolved Resonant-Raman Spectroscopy. *J. Phys. Chem. Lett*. **3**, 1321-1328 (2012).

3.1 Abstract

We have used time-resolved resonant-Raman spectroscopy to investigate the picosecond conformational relaxation of regioregular poly-(3-hexylthiophene) (RR-P3HT) in chlorobenzene after 510-nm photoexcitation. Vibrational signatures from modes along and peripheral to the exciton's backbone have been identified according to the time-dependence of excited-state Raman features and from comparisons to Raman spectra of other polymer states. Measured spectral dynamics reflect initial changes in the resonant enhancement of backbone modes on a timescale of 9 ± 1 ps. In contrast, contributions from peripheral modes exhibit time-dependent decay determined only by exciton intersystem-crossing kinetics. Spectral dynamics are interpreted in terms of evolution in bond lengths along the exciton's backbone resulting from increased conjugation allowed by torsional reordering. Possible origins of peripheral features are

discussed, including distorted inter-ring modes at exciton termini. Findings provide a glimpse of the underlying molecular dynamics responsible for the red-shift in the exciton's near-IR transient absorption occurring on the same timescale.

3.2 Introduction

Photovoltaic devices based on conjugated polymers, such as poly(3-hexylthiophene) (P3HT), have held promise as a low-cost solar-cell technology over the last two decades.[1,2] In contrast to the inorganic semiconductors they would replace, the behaviors of these materials are dictated by the dynamics of constituent molecules and their interactions with nearby (and even distant) molecules. Consequently, the initial ultrafast relaxation behaviors of conjugated subunits are critical to the course of subsequent energy and electron transfer that underscore greater material function of these devices.[3-7] A critical step towards understanding dynamics in these complex materials is to elucidate the molecular-level details of photoinduced relaxation in conjugated polymers isolated from electron acceptors.[8-17]

With this focus, the photophysical properties of excited P3HT have been investigated extensively with a variety of time-resolved spectroscopic methods over the last decade – including transient absorption,[18, 19] stimulated emission,[12, 17] fluorescence up-conversion,[11, 16] and non-linear electronic spectroscopies.[13, 15, 16, 20] Much of this work has been carried out with polymer isolated in solution so as to assess intrinsic ultrafast relaxation behaviors of excited polymer segments (or "excitons") without influence from direct interchain or donor-acceptor interactions. Collectively, these studies suggest two primary mechanisms for exciton relaxation that precedes population decay through fluorescence and intersystem crossing:[11-13, 16, 17, 21, 22] Long-range torsional

reorganization on picosecond and sub-picosecond timescales that planarizes and stabilizes the quinoidal bond-order of the excited state;[14, 17, 21, 22] and excitonic energy transfer (EET), through which energy migrates to lower-energy sites characterized by different degrees of planarity and/or conjugation length.[11, 13, 20] These behaviors have been inferred from time-dependent spectral diffusion and anisotropy depolarization of electronic transitions.[11, 16, 17] Given that a spectroscopic signature of both processes is a dynamic red-shift of emission, and that anisotropy depolarization in polythiophenes may originate from mechanisms other than EET,[23] the relative importance of these pathways has been debated in the literature.[12, 17] A recent combination of stimulated emission and 3-pulse pump-dump-probe experiments has shown that relaxation occurs primarily through torsional relaxation on picosecond and sub-picosecond timescales, and not EET.[12] However, even though transient electronic spectroscopies have been able to clarify the primary importance of this pathway, they offer little perspective on the nuclear dynamics that accompany conformational reorganization of the excited state.

In this work we have used time-resolved resonant-Raman spectroscopy to interrogate nuclear conformational relaxation in P3HT excitons that underscores excited-state spectral dynamics observed with transient electronic spectroscopies on picosecond timescales (> 1ps). To our knowledge, time-resolved Raman has not been used to characterize the dynamics of these materials, even though steady-state Raman spectroscopy has been applied extensively to probe structural and morphological

characteristics of conjugated and conducting polymer films.[24-28] Resonantly enhanced Raman scattering, in particular, is highly sensitive to vibrational activity along the totally symmetric modes of conjugated units, as these coincide directly with key structural changes induced by photoexcitation.[29] Processes such as torsional relaxation (and EET) should planarize and/or lengthen an exciton, and thereby induce changes in bond lengths and vibrational frequencies of these same symmetric modes associated with the polymer backbone. Finally, resonantly enhanced Raman spectroscopy is inherently a photo-selective method, permitting the interrogation of structural (and dynamical) variations that underlie inhomogeneously broadened transient-absorption features. Therefore, resonant-Raman spectroscopy is a natural probe for interrogating the conformational relaxation of conjugated polymers at the molecular level, and should provide a new spectroscopic dimension for understanding the excited-state photophysics of this and related systems.

Our work specifically makes use of femtosecond stimulated Raman spectroscopy (FSRS), a method that efficiently captures excited-state Raman gain over a broad frequency range through a 3-pulse measurement:[30, 31] In our experiments, a ~50-fs, 510-nm pulse first excites the polymer solution; subsequently, a combination of a broadband continuum pulse (<100-fs) and a narrow-band Raman-pump pulse (~2-ps) are used to measure stimulated-Raman gain at all inelastically scattered frequencies within the spectral range of the broadband continuum. In this work the Raman-pump pulse is

resonant with a transition between the photoexcited excitonic state and a higher-lying electronic state (specifically at 880 nm), and Raman gain is sampled with a near-IR continuum at longer wavelengths (i.e., through Stokes transitions). FSRS has been shown to yield similar Stokes-shifted features as measured via spontaneous Raman spectroscopy,[32] but with the advantages of increased collection speeds and vastly improved discrimination against excited-state fluorescence. Furthermore, FSRS is experimentally compatible with broadband transient absorption spectroscopy (TA), such that both measurements can be carried out under the same conditions in the lab. Thus, time-dependence of Raman features may be correlated readily with the TA spectral dynamics that are routinely used to characterize photo-excited polymers and polymer-based materials.

3.3 Experimental Methods.

Laser pulses for these experiments were derived from the fundamental output of an amplified Ti:Sapphire laser. 510-nm photoexcitation pulses were generated using an optical parameteric amplifier and were attenuated to 3 μJ/pulse. Narrowband (~10 cm^{-1}) picosecond pulses (2-3 ps) centered at 880 nm were generated with a picosecond OPA. The Raman pump pulse energy was typically 10-15 μJ/pulse. Near-IR white-light probe continuum (850-1100+ nm) was generated by focusing ~80 μJ/pulse into a 2-mm-thick sapphire crystal.

Photoexcitation pulses were collimated to a 4-mm beam diameter before the sample; Raman pump and probe pulses were focused and overlapped within the photoexcited sample volume. Excitation and Raman pump pulses were blocked after the sample with a set of long-pass filters, and probe light was collected and dispersed with a 300-mm spectrograph onto a CCD camera. The camera was configured to collect spectra at the laser's kHz repetition rate, with the Raman (or photoexcitation) beam synchronously chopped at 500 Hz. Transient Raman (or absorption) spectra were then calculated using consecutive pairs of probe spectra. Each Raman spectrum presented is an average of 15000-30000 of these on/off ratios. Transient absorption measurements were made using a low-resolution grating. In contrast, Raman spectra were collected at much higher-resolution, limited by the 10-cm^{-1} bandwidth of the ps-OPA, as well as natural spectral linewidths, spectral congestion, and spectral inhomogeneity.

The photoexcitation pulse delay relative to the Raman pump-probe pulse pair was controlled with a motorized translation stage outfitted with a corner-cube mirror. The relative timing between the Raman pump and probe pulses were optimized according to the spectral shapes of non-resonant features from the solvent, but also to minimize Raman-pump-induced depletion of the excited-state population. Polarizations of all three pulses were kept parallel in the measurements presented here. Excited-state spectra taken with the excitation pulse perpendicular to both the Raman pump and probe pulses produced similar spectral dynamics as that shown in Fig. 3.2 (see supporting information), indicating that these dynamics result from differences in structural relaxation and not due to the reorientation of transition dipoles in excited chromophores.

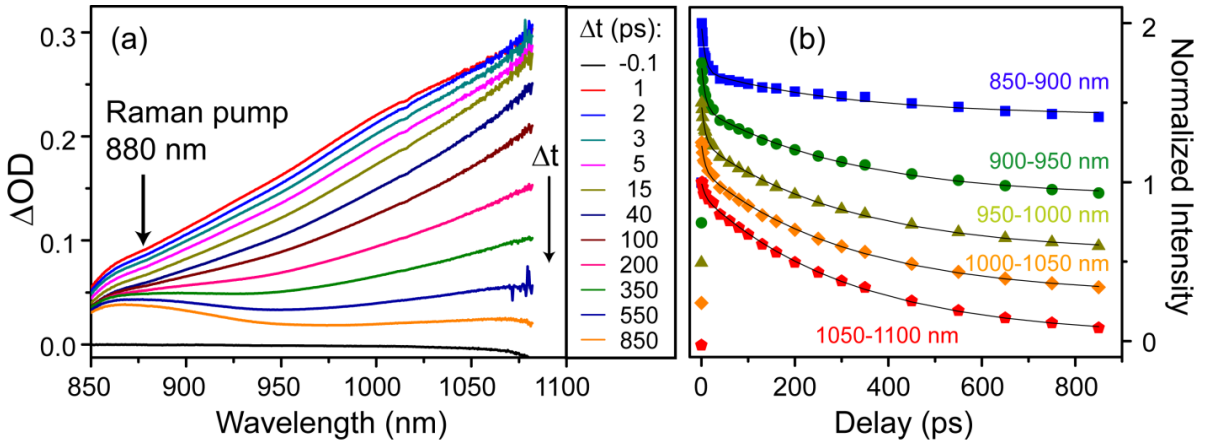

Figure 3.1: Near-IR transient absorption spectroscopy of regioregular poly-(3-hexylthiophene) (RR-P3HT) in chlorobenzene photoexcited at 510 nm. (a) Transient spectra. (b) Normalized integrated intensity from 50-nm wide spectral windows (solid symbols). Spectral evolution in (a) is characterized by a fast spectral red-shift over the first 20-30 ps, followed by a decay in absorbance at longer wavelengths due to exciton decay and triplet formation (triplet absorption peaks below 900 nm). Black lines in (b) represent a constrained biexponential fit with decay timescales of 8 ± 1 and 320 ± 20 ps.

3.4 Results and discussion

Figure 3.1 provides an example of the near-IR TA spectral dynamics measured following 510-nm excitation of regioregular (RR) P3HT dissolved in chlorobenzene. TA spectral dynamics are characterized by a noticeable red-shift that occurs by 15 ps; in contrast, spectral evolution on longer timescales gives rise to a sharp absorption band below 900 nm, consistent with triplet formation from non-fluorescing excitons. These time-dependent behaviors are more clearly illustrated in Fig. 3.1(b), which plots the TA intensity integrated over 50-nm-wide windows within the probed wavelength range (solid symbols). Values for each transient have been normalized at 1 ps, offset for clarity, and fitted using constrained biexponential fitting functions (black lines); a summary of fitting procedures and parameters are provided in the supporting information. These absorption transients exhibit both fast (8 ± 1 ps) and slow (320 ± 20 ps) decay timescales, with fast decay becoming more prominent at shorter wavelengths. The timescale for this faster process is similar to those noted from time-resolved stimulated emission[12] and fluorescence up-conversion measurements,[11, 16] and which have been described as the result of changes in torsional disorder or exciton length resulting from conformational relaxation, EET, or both. The longer timescale corresponds with an apparent exciton population lifetime. These measurements were collected with a parallel pump-probe polarization geometry, and the measured lifetime is faster than the known exciton lifetime due to anisotropy depolarization in the excited state. Similar measurements taken with a

perpendicular pump-probe polarization geometry give an exciton decay lifetime of 490 ± 20 ps, closely matching the known exciton lifetime measured by time-resolved fluorescence.[11, 16]

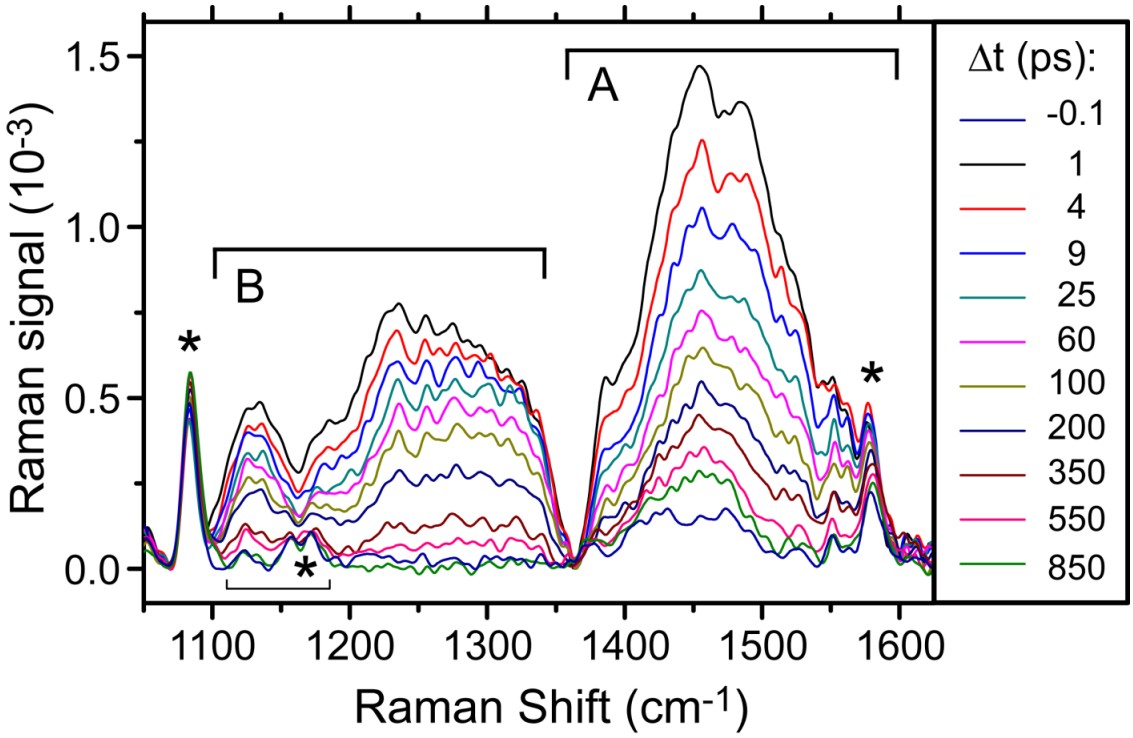

Figure 3.2: Time-resolved resonant-Raman spectra of RR-P3HT in chlorobenzene photoexcited at 510 nm.Spectral dynamics are described in the text. Asterisks denote non-resonantly enhanced solvent bands. Labels "A" and "B" are used in the text in discussing spectral dynamics within their corresponding frequency ranges.

Conformational changes underlying the initial dynamic red-shift in transient absorption can be interrogated directly by applying a resonant-Raman probe. Figure 3.2 presents a progression of baseline-subtracted, resonantly enhanced excited-state Raman spectra collected up to 850 ps after 510-nm excitation. The 880-nm Raman-pump pulse was resonant with the high-energy edge of the exciton's absorption spectrum (indicated with an arrow in Fig. 3.1); this region of the excited-state absorption is most strongly influenced by spectral shifting on the picoseconds timescale, such that resonant-Raman measurements obtained with this wavelength should be most sensitive to underlying relaxation dynamics. Sharp features in Fig. 3.2 marked with asterisks correspond with non-resonantly enhanced Raman modes of the chlorobenzene solvent and have been used to fine-tune frequency calibration of these spectra.[33] Details concerning baseline subtraction methods are outlined in the Supporting Information.

The spectral evolution presented in Fig. 3.2 can be characterized as follows: Spectra collected at time delays preceding arrival of the pump pulse exhibit a broad, weak asymmetric feature peaking near 1470 cm^{-1} that is flanked by a smaller feature near 1390 cm^{-1}. Two broad bands appear at delays following excitation; these features, spanning 1350-1600 cm^{-1} and 1000-1350 cm^{-1}, are labeled A and B, respectively. Each of these bands exhibits evidence of overlapping spectral features: Band A peaks near 1470 cm^{-1}, but has a clear shoulder at lower frequency (~1390 cm^{-1}); in contrast, band B exhibits resolved and partially resolved features at 1130, 1180, and 1220 cm^{-1}. Band A

decays substantially over the first 25 ps; in contrast, band B decays asymmetrically, with intensity below ~1300 cm^{-1} decaying more quickly than the intensity at 1300-1350 cm^{-1}. On longer timescales all excited-state features decay simultaneously. Although the triplet strongly absorbs near 880 nm (c.f. Fig. 3.1), the Raman spectrum measured with the 850-ps delay is much less intense than those measured at earlier times, indicating that the triplet has a significantly reduced resonant-Raman cross-section relative to the singlet exciton.

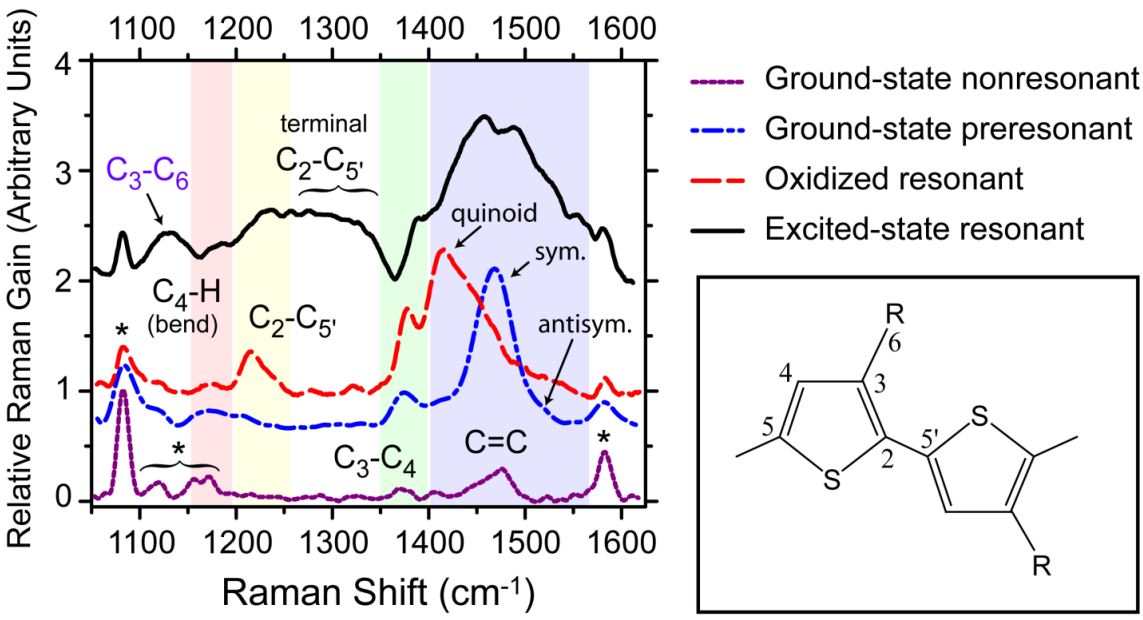

Figure 3.3: Vibrational Raman spectroscopy of RR-P3HT in chlorobenzene solution. Spectra are associated with various polymer states and collected under various resonance conditions. Asterisks denote (non-resonantly enhanced) solvent bands. The preresonant Raman spectrum of the neutral polymer (blue dot-dash line) was collected using a 600-nm Raman-pump wavelength; all other spectra were collected using 880 nm. Spectral assignments are based on those described in Reference 33 and correspond with modes largely described by stretching (and bending where indicated) of bonds between the numbered carbon positions shown at the bottom right. The feature labeled as "terminal" is assigned here to inter-ring stretching in monomers near the ends of the exciton.

Mode-specific assignments for many of these excited-state features can be made through direct comparison with Raman spectra of other polymer states, as presented in Figure 3.3. Valence-bond structures are provided in Chart 3.1 for visualizing structural differences between various polymer states; it is important to note that these structures do not reflect the true electron-density distributions for these states, and are only offered to illustrate qualitative differences in bond-order patterns between states. The non-resonantly enhanced spectrum of the neutral ground-state (purple dotted line) includes features at 1470 and 1380 cm^{-1} that are widely attributed to C=C and C_3-C_4 ring-stretching of thiophene units, respectively.[34] Along with solvent bands (marked with asterisks), these weak non-resonant ground-state features are a background signal in our time-resolved measurements. The C=C stretch has a very large (pre)resonant enhancement (blue dash-dot line), reflecting a significant bond-length displacement between the benzoidal ground state and quinoidal singlet excited states (e.g. Chart 3.1).[34] Weaker features appear in the preresonant spectrum near 1515, 1200, and 1180 cm^{-1}; these have been assigned previously to an antisymmetric (out of phase) C=C ring-stretching mode, C_2-$C_{5'}$ inter-ring stretching, and a combination of inter-ring stretching and C_4-H bending motions.[34] The intensity ratio of these last two features is likely to be related to torsional disorder that inhibits long-range planarity of the polymer backbone, as it has been shown that this ratio correlates with polymer conductivity.[27,28,35]

Oxidation alters the pattern in C-C bond order relative to the neutral (Chart 1),

and changes the steady-state Raman spectrum as follows:[36,37] The photo-oxidized polymer exhibits a marked change in the C=C stretching region, with a peak appearing near 1420 cm^{-1} (often referred to as the "quinoidal stretch"). In contrast, the C_3-C_4 ring (1380 cm^{-1}) and C_2-$C_{5'}$ (1220 cm^{-1}) inter-ring stretches are shifted more weakly from the corresponding features of the ground-state neutral. Two additional weak features appear near 1280 and 1320 cm^{-1}, and have no known mode-specific assignment. These features likely correspond with distortional ("D") or "kink" modes commonly observed in the Raman spectra of oxidized polythiophene;[36, 37] such a feature appears in the Raman spectrum of oxidized poly-(3-decyl-thiopehene) near 1300 cm^{-1}. "Kink" bands are commonly attributed to distorted inter-ring stretching and bending at the interfaces between oxidized and neutral regions of the polymer that are defined by significant changes in polymer conformation.[28, 34, 36-38]

Given the gross similarity in band positions and patterns for the neutral, oxidized, and excited polymer, we believe that the excited-state Raman features measured here correspond with similar modes within the excited polymer: Band A reflects activity in the C=C and C-C ring-stretching modes. Guided by frequency and strength assignments made by Louarn et al. for the unexcited polymer,[34, 39] we tentatively attribute the features in band B to nuclear motions involving inter-ring stretches (1220 cm^{-1}) and a combination of inter-ring stretch and C_4-H bending motions (1185 cm^{-1}). The feature appearing near 1130 cm^{-1} is quite close to a ground-state feature observed previously at 1090 cm^{-1}, and

which Louarn et al. attribute to a mode that involves primarily (pure) C_4-H bending motions. This seems to be the most sensible assignment for the feature appearing at 1130 cm^{-1}, but we note that these authors also attribute a feature near 1020 cm^{-1} to C_3-C_6 stretching in the ground state. We note that both of these features are very weak and obscured by solvent peaks in our ground-state Raman spectrum (Fig. 3.3, blue dot-dash curve).

Bands A and B both extend noticeably to higher frequencies relative to features observed from either the neutral or oxidized ground states. For band A, this breadth likely arises from more than one contribution: Activity in more than one type of C=C stretching mode (specifically, band A spans the range of the quinoidal, symmetric, and antisymmetric stretch frequencies observed in the neutral and oxide); variations in electron density along the length of the exciton; and, to a lesser extent, Raman dispersion due to variation in exciton length.[25, 39] In contrast, the high-frequency (>1300 cm^{-1}) portion of B cannot be attributed to a well-characterized mode feature when compared to the spectrum of either the oxidized or ground-state neutral polymer.

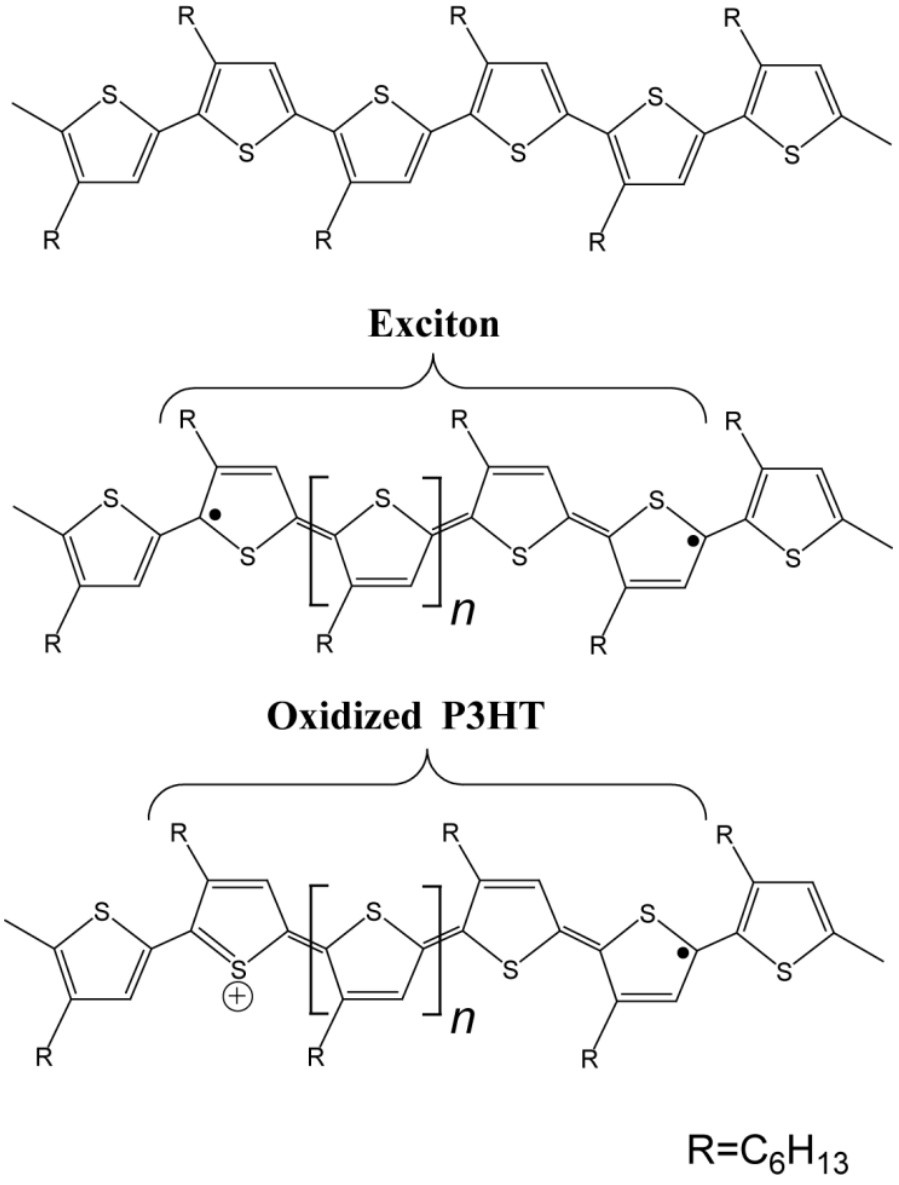

Chart 3.1: Valence-bond structures of the benzoidal ground state (top), quinoidal excited state (middle), and quinoidal oxidized polaron (bottom) of RR-P3HT. The exciton structure has been drawn so as to not imply charge separation, but rather a symmetric redistribution of electron density.

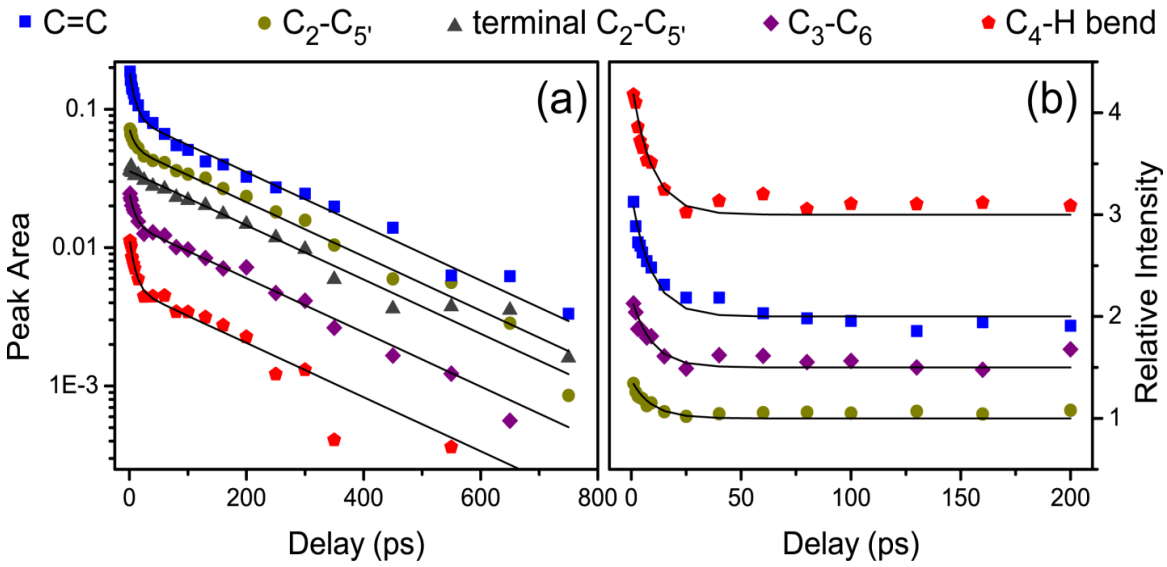

Figure 3.4: Time dependence of Raman features in Figure 3.2 and assigned according to Figure 3.3. (a) Integrated intensities; black lines correspond with biexponential fits with constrained lifetimes of 9 ± 1 and 220 ± 20 ps (fitting amplitudes are provided in the supporting information). The feature assigned to inter-ring stretching at the terminal sites exhibits no decay on the faster timescale (gray triangles). (b) Relative change in feature intensities attributed to torsion-induced exciton conformational relaxation. To make (b), data and fits in (a) were divided by corresponding terminal inter-ring feature intensities, and each time-dependent ratio was scaled to its final value. Each trace in (b) has been offset for clarity.

Time-dependence of the feature at 1300 cm^{-1} helps to illuminate the nature of its corresponding Raman modes. Integrated intensities of each feature are plotted in Figure 3.4(a) (solid symbols), and have been fitted using constrained biexponential functions (solid lines, details of fitting provided in Supporting Information). Non-resonant solvent and polymer background features were carefully removed to determine these intensities. Time-dependent intensities of the assigned excited-state features decay on timescales of 9 ± 1 ps and 220 ± 20 ps. In contrast, the Raman intensity near 1300 cm^{-1} decays only on the longer of these timescales, which must be associated with exciton decay. The apparent contraction in exciton lifetime as determined from our time-dependent Raman intensities likely arises from uncertainties in the baseline shape assumed for subtraction: The baseline primarily reflects a transient bleaching of excited polymer by the 880-nm Raman pump, and therefore gradually changes shape as triplet absorption dominates at the Raman-pump wavelength (similar to the change in absorption features seen in Fig. 3.1(a); see Supporting Information for more details). Corresponding changes in baseline curvature likely leads to a slight systematic over-subtraction at later delays, and thereby influences the best-fit lifetime for exciton decay. Importantly, this change in baseline shape and the related uncertainty in baseline estimation occur on the ISC timescale, and negligibly influences changes in feature intensities associated with the much faster conformation relaxation process.

The faster relaxation timescale apparent from our Raman data closely matches the

initial spectral redshift observed in TA measurements, indicating that the spectral evolution captured in Figs. 3.2 and 3.4(a) is related to the spectral shift apparent in Fig. 3.1(a). Changes to the intensities of all assigned Raman features on this timescale therefore reflect that corresponding vibrational modes are sensitive to exciton relaxation dynamics. In contrast, because the intensity decay near 1300 cm^{-1} occurs only with exciton decay, it must correspond with a mode (or modes) that are insensitive to this faster relaxation process and that are likely to be peripheral to parts of the molecule that are most sensitive to nuclear relaxation.

How conformational relaxation induces changes in the intensities of Raman features can be understood by considering the dominant term of the molecular polarizability under resonant conditions (the Albrecht A term):[29, 40]

$$A_{v'v''} = \frac{1}{\hbar}\sum_{v}\left(\mu_{ge}^{0}\right)_{\rho}\left(\mu_{ge}^{0}\right)_{\sigma}\left[\frac{\langle v'|v\rangle\langle v|v''\rangle}{\omega_{ev,gv'} - \omega_0 - i\Gamma_e}\right] \tag{3.1}$$

Here $\left(\mu_{ge}^{0}\right)_{\rho}$ represents the electronic transition dipole moment in the ρ direction; the *A* term is derived assuming the Franck-Condon Approximation, and these dipole moments are therefore constant. Because the Raman-pump wavelength probes the blue edge of the absorption band in our experiment, time-dependent detuning from resonance with the Raman-pump pulse should be negligible in our measurements (i.e., no change in the denominators of *A* terms). Therefore, the dominant factors controlling Raman intensities are the Franck-Condon overlaps between the initial and intermediate states

($\langle v'|v\rangle$), and the intermediate and final states ($\langle v|v"\rangle$). As TA spectra are sensitive to time-dependent changes in Franck-Condon factors, the spectral shift apparent in Fig. 3.1(a) illustrates the change in overlaps necessary to influence resonant-Raman intensity. Totally symmetric modes that coincide with geometry changes in the molecule are most strongly Franck-Condon active in Equation 1; in P3HT, these include symmetric stretches and bends within monomer rings as well as inter-ring stretches.

Torsion-induced conformational relaxation, specifically, is expected to influence the resonant contributions as follows: Torsional relaxation increases planarity of the exciton's structure, permits increased conjugation, and allows electron density to shift between bonds involving carbon atoms along the backbone. This shift in electron density should induce a corresponding change in bond-length displacement between the potential-energy surfaces for the exciton and the higher-lying state. Therefore, torsional relaxation towards exciton planarization should alter the Franck-Condon overlaps between the initially excited and higher-lying intermediate electronic state in the Raman transition, giving rise to intensity decay for various vibrational modes. Given the general relationship expressed in Equation 1 and the fact that the decay in the feature near 1300 cm^{-1} is controlled only by the time-dependence of the exciton population, this feature must rather correspond with modes that have no time-dependent change in bond-length displacement during exciton relaxation, even though this mode is altered by the initial photoexcitation step.

Within this framework it is possible to consider what modes are likely to contribute the extra intensity at 1300 cm^{-1}. One possibility is that other fingerprint ring modes – such as C-S stretching (1000 cm^{-1}), C-S-C deformation (680 cm^{-1}) and monomer ring deformation (550 cm^{-1})[34] – shift to higher frequency upon excitation and appear within the frequency range probed. Given that all other excited-state features fall roughly at the same frequencies as measured in the ground state, we find it highly unlikely that these other ring modes would shift appreciably (> 300 cm^{-1}) upon polymer excitation. Furthermore, because ab initio calculations have shown that excited-state electron-density also changes at the sulfur site,[41] we expect that these modes should also be sensitive to any redistribution of electron density within and between thiophene rings that occurs during conformational relaxation.

The extra intensity at 1300 cm^{-1} is more likely to arise from additional Raman activity in modes along the pendant hexyl chains. Indeed, various alkyl modes have frequencies near 1300 cm^{-1}, but these modes generally have the wrong symmetry to exhibit significant activity in the resonant-Raman spectrum.[42, 43] Significant enhancement of hexyl modes would imply an appreciable displacement along nuclear coordinates in these pendant groups between the first and second excited states, in contrast with what is observed for the ground and singlet-exciton states (no hexyl modes are observed in the resonant ground-state spectrum). This would further imply that the pendant group has a non-negligible role in supporting this higher-lying excited state of the polymer.

A plausible alternative explanation is that this feature may correspond with distorted modes associated with the ends of excitonic segments, much like the kink bands discussed above that are commonly observed with oxidized polymer. Both states of the polymer take on quasiplanar quinoidal geometries (Chart 3.1), such that they should have similar sensitivity to the presence of large conformational distortions in the polymer:[44] In both states such distortions will strongly limit the extent of conjugation and/or confine conjugation to specific segments of the polymer. Although the characteristics of vibrational modes at these distortions are not well-established, the frequency of distortional modes will be affected by both the relative conformation and charge distribution at these terminal interfaces at the ends of the excitonic or oxidized segment. Ab initio calculations by Benkeen and Pullerits suggest that there is a reduction in electron density (relative to the ground state) at the C_2/C_5 sites at the ends of exciton segments of the polymer,[41] and therefore these modes could be quite similar for excitonic and oxidized regions of the polymer. Importantly, we expect little driving force for reconfiguration of adjacent rings at the boundary of excited and unexcited regions of the polymer, such that there should be little to no change in the Franck-Condon activity (and, thus, resonant enhancement) of these modes during the course of torsion-induced conformational relaxation.

The relaxation behavior captured here with resonant-Raman spectroscopy is consistent with the shifting vibronic structure apparent in stimulated emission[12, 17] and

fluorescence up-conversion[11] measurements. Those measurements reflect changes in overlaps between the exciton and the ground-state vibrational wavefunctions with time. Although the C=C stretch fundamental can be identified from those measurements, those transient electronic bands are otherwise unresolved and overlapped Franck-Condon progressions. Figure 3.2 demonstrates clearly that bond-length changes occur more generally for all bonds associated with carbon atoms along the exciton backbone.

The Raman intensity near 1300 cm^{-1} provides a probe-specific reference for exciton population decay. Thus, the change in intensities of other features due only to conformational relaxation can be isolated by dividing each transient by the intensity decay of this region, as plotted in Fig. 3.4(b). Although some of these features overlap slightly in the integrated ranges, Fig. 3.4(b) illustrates that relaxation affects the intensity of each mode differently. For example, intensities in the C=C stretching and mixed C_4-H bending regions decay by ~50% on this timescale, while the backbone inter-ring and pure C_4-H bend decay by ~25 and 33 %, respectively (the C_3-C_4 ring-stretch has been left out, as it overlaps significantly with the C=C stretches). Qualitatively, we anticipate a significant shift of electron density away from the C=C bonds, and an increase near the C_4-H bend and inter-ring stretch. A more complete and quantitative explanation for these changes will require additional spectral decomposition and modeling of time-dependent bond-length displacements.

Although our measurements highlight evolution in exciton conformation with

time, by themselves they do not imply that torsional relaxation dominates exciton relaxation: EET could involve downhill energy migration between polymer segments with increased planarity, as well as conjugation length, such that both relaxation mechanisms may have the same observables on the picoseconds timescale (i.e., an average change in exciton conformation with time). If EET has an impact on the relaxation of isolated excitons,[13, 20] we expect that Raman spectra will be much more sensitive to this process on faster timescales, as fast EET should dampen the Raman coherence lifetime created through interactions with the Raman-pulse pair, giving rise to broadened spectral shapes. Unfortunately, time-dependent Raman-intensity analysis on sub-ps timescales is complicated by the more favorable fs-pump/ps-repump/fs-continuum probe process that directly competes with the resonant FSRS measurement.[45] However, changes in spectral breadth and relative feature intensities should be identifiable on these faster timescales, and we're currently exploring this faster phase of exciton relaxation.

3.5 Conclusions

In summary, we have used time-resolved resonant-Raman spectroscopy to interrogate the picosecond conformational relaxation dynamics of excitons on RR-P3HT prepared by photoexcitation at 510 nm. We have identified excited-state Raman-active modes associated with carbon atoms along the exciton's conjugated backbone, as well as features associated with peripheral modes that that are insensitive to these dynamics. These peripheral modes likely correspond with vibrations on pendant hexyl groups or distorted ("kink") modes present at the termini of excited segments within the polymer. As resonant-Raman measurements are sensitive to changes in the displacement of nuclear coordinates between potential-energy surfaces, the relative intensity dependence of Raman features indicates the degree to which torsional relaxation alters the bond lengths along the exciton backbone. This data provides a direct structural perspective on the spectral relaxation dynamics observed from transient electronic spectroscopies, and we are currently using this approach to explore correlation between excited-state absorption frequency and degree of torsional disorder in this and related systems

3.6 Supplementary Information

3.6.1. Characterization of polymer solutions using transient absorption spectroscopy.

Polymer concentrations used to make our Raman measurements (~1 mg/mL) are relatively high compared to those typically studied by steady-state or simple pump-probe spectroscopies (typically ~0.1-0.3 mg/mL). Solutions with lower concentrations are generally desired to prevent aggregation of polymers and therefore eliminate the possibility for interchain interactions that can alter exciton relaxation dynamics. Unfortunately, we found that these concentrations were too low for obtaining sufficient signal/noise in our FSRS spectra. Indeed, FSRS is a 5^{th} order spectroscopic measurement, and we typically measure P3HT excited-state Raman gain smaller than 0.25%, even with these more concentrated solutions. Additionally, these small signals are superimposed upon a more intense broad background (described in Section 3.6.2) that must be subtracted in order to isolate spectral dynamics of Raman features alone. For these reasons we found it necessary to push solution concentrations somewhat higher for our measurements.

We note that there is precedent for using higher polymer concentrations in experiments with high-order non-linear spectroscopic methods that suffer from similar signal-to-noise limitations. Nevertheless, in order to ensure that interchain polymer aggregation was not appreciable at this higher polymer concentration (or at least that relaxation dynamics were not affected by polymer concentration), we characterized

solutions with high and low concentrations of P3HT using transient absorption spectroscopy. Figure 3.1S presents typical spectral dynamics of NIR transient absorption features measured after 510-nm photoexcitation of 0.3 and 1 mg/mL P3HT in chlorobenzene. These contour plots have been scaled to their maximum absorbance and given the same intensity contours. Spectral dynamics measured at these two concentrations are remarkably similar, and yield the same exciton lifetime with a perpendicular pump-probe polarization (~500 ps), suggesting that the increased concentration has no appreciable effect on the photophysics of these species. We are therefore confident that our Raman measurements capture relaxation behavior of isolated excitons.

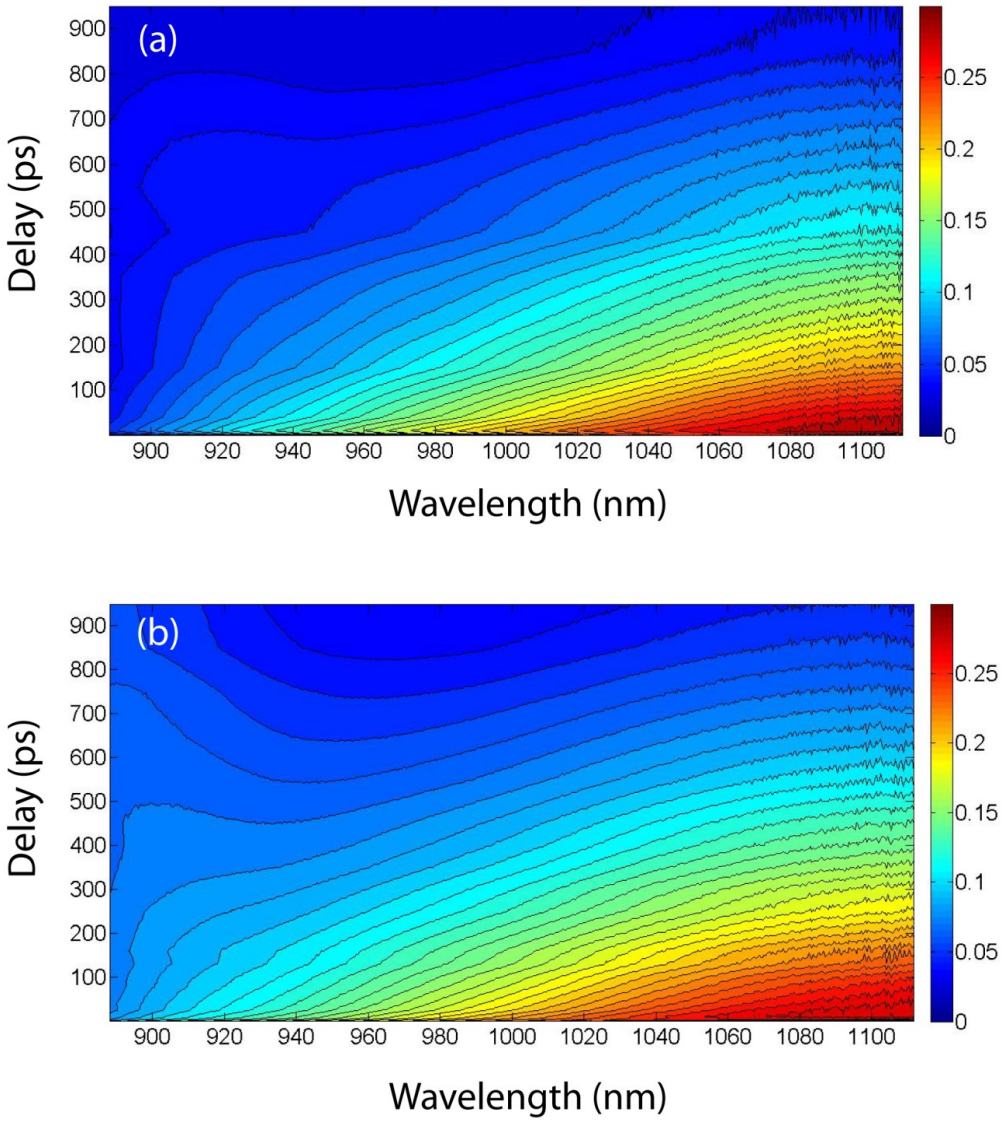

Figure 3.1S: Comparison of near-IR absorption transients collected using (a) low (0.3 mg/mL) and (b) high (1 mg/mL) concentrations of regioregular P3HT in chlorobenzene.

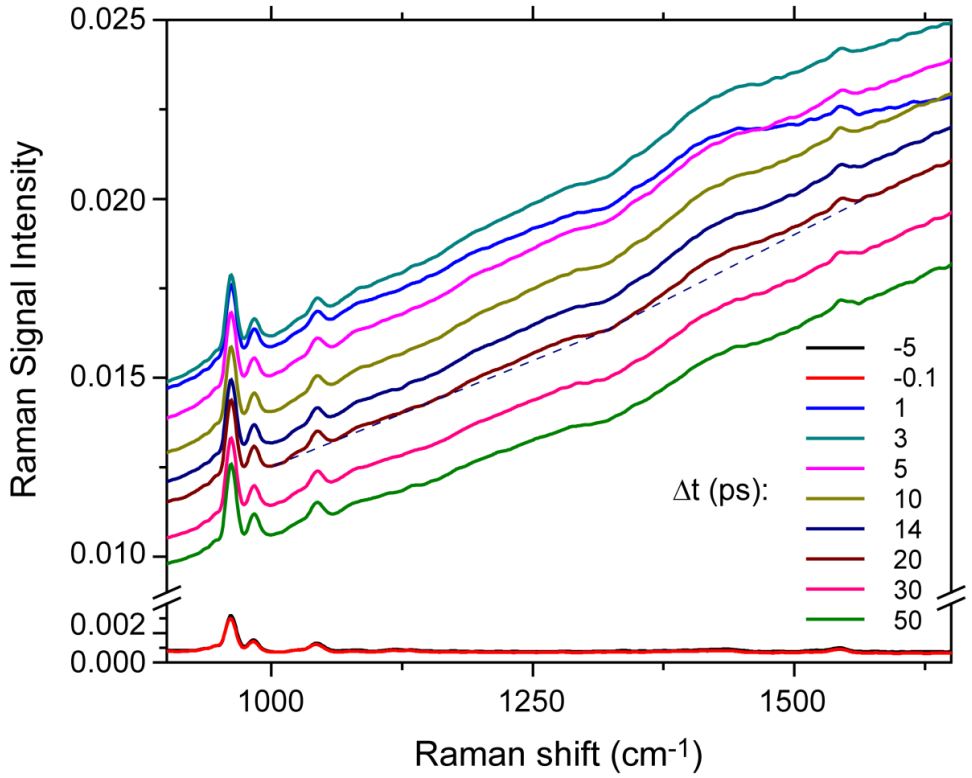

Figure 3.2S: Raw time-resolved resonant-Raman spectra from RR-P3HT in chlorobenzene. Raman features are superimposed on a broad background originating from Raman-pump-induced changes to the optical density of the 510-nm photoexcited sample. Dashed lines illustrate the assumed linear background signal for subtraction, as described in Section 3.6.2.

3.6.2. Background subtraction procedures.

As described in the main text and above, the resonant-Raman signals measured in our experiments are superimposed upon a broad background. This background signal can be described as a transient bleach of the excited-state absorption that is induced by the Raman-pump pulse. This more favorable fs-pump/ps-repump/fs-continuum probe process directly competes with the resonant FSRS measurement. We present an example set of averaged raw transient Raman data in Figure 3.2S that shows that these broad background signals are significant and vary with time.

The background observed here is similar to the broad fluorescence background signals common to spontaneous Raman measurements, and many numerical methods have been developed over the years for removing these contributions. Generally these methods are successful because the Raman and background signals exhibit sharp vs. broad features, respectively, and features that vary only weakly with frequency (fluorescence) can be removed quite reasonably by numerical filtering methods. An obvious problem arises when the breadth of Raman features are comparable to the breadth of background signals (due to broad natural linewidths, spectral congestion, or spectral inhomogeneity). In these cases there is little that can be done to separate these signals other than modeling the shape of the background and subtracting it off.

We've had to take this approach in our data analysis here. Our subtraction procedure was facilitated greatly by the fact that our measured background signals appear

to be roughly linear across the probed wavelength range. We therefore assumed a piece-wise linear background for subtraction: For each spectrum collected, piecewise linear background contributions were estimated according to the intensities measured at three specific frequencies (see dashed lines in Figure 3.2S); these include the dip between solvent bands at 1000 cm^{-1}, the clear dip apparent in the raw data near 1350 cm^{-1}, and at the high-frequency edge of the solvent band apparent near 1600 cm^{-1}. Additional points were also considered between 900 and 1200 cm^{-1}, with the hope that more linear segments would more closely approximate the shape of a non-linear background and provide increased discrimination between Raman and background signals. However, including these points was found to obscure exciton Raman features that overlapped weaker solvent bands around 1000-1200 cm^{-1}, and we therefore chose to use only the two linear background segments described above. Our baseline subtraction procedure appears to be quite robust, as we obtain very similar spectral and temporal behavior from multiple data sets.

An implicit assumption in our subtraction procedure is that the intensity dip at 1350 cm^{-1} reflects an intensity drop in excited-state features towards the Raman baseline from both lower and higher frequencies. It is therefore important to consider (and rule out) other possible origins for this intensity dip. Our measurement reflects the pump-induced excited-state Raman spectrum, and therefore it seems reasonable to consider contributions from a depletion/hole in ground-state Raman features. Such features are

common in time-resolved pump-probe IR measurements; those differential absorption measurements are made by chopping the photoexciting pump, generating spectra that have overlapping signatures from both excited-state absorption and ground-state bleach in the transient IR absorption spectrum. In contrast, only the Raman pump is chopped in our experiment: Although photoexcitation may reduce the size of Raman features from the ground state, a negative bleach contribution will not be measured because the photoexciting beam is not chopped. Therefore this possibility can be ruled out in general by noting that a depletion of the ground-state Raman spectrum will only be apparent after subtracting the spectrum of the un-pumped sample, and not directly from the raw data measured in our experiment.

The possibility that this dip corresponds with a vibrational hole in transient Raman spectra of P3HT can be discounted more specifically by considering the positions and relative intensities of ground-state features measured with this technique. The dip appears at a lower frequency than the C-C and C=C stretching features seen in the (weak) non-resonant Raman spectrum of the ground-state polymer (see Fig. 3.3 of the main text). Because there are no significant background signals at this frequency prior to excitation, an intensity dip at this frequency cannot correspond with a depleted vibrational band of the ground state even after subtraction of the ground-state spectrum measured before "time zero."

Alternative explanations for this dip might include "negative" gain contributions

associated with dispersive and inverse lineshapes possible from FSRS. Dispersive features have been observed in other FSRS measurements, but with lineshapes that are sensitive to the relative Raman pump/probe delay. We note, however, that the size and position of this dip relative to the neighboring positive features does not change appreciably with relative Raman pump-probe pulse delay. Furthermore this dip cannot correspond with an inverse Raman feature, as these occur only at anti-Stokes frequencies with the roles of Raman pump and probe are reversed (our experiment measures Stokes shifts). Therefore we are confident that this dip in the raw data truly occurs due to a gap in excited-state Raman features, and that the minimum in this dip can be used to approximate the Raman baseline.

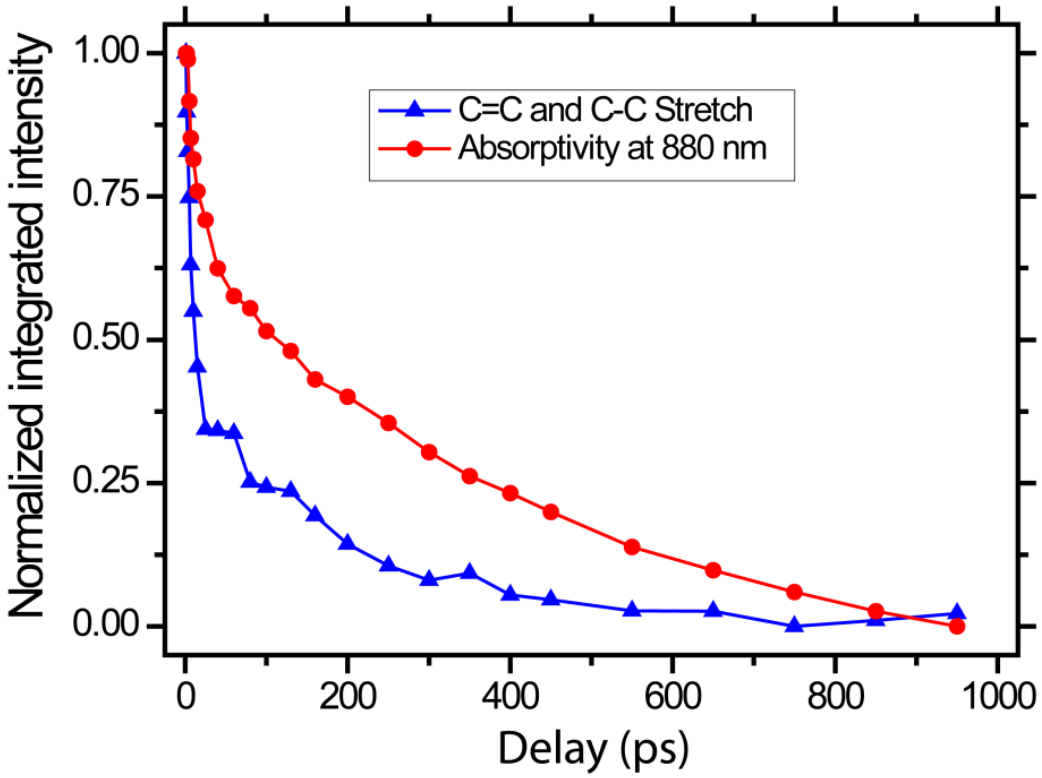

Figure 3.3S: An example of raw signal transients (Raman plus transient bleaching of excited-state absorption) at representative time delays throughout ISC kinetics. Absorption of triplet at 880 nm leads to a change in baseline shape at longer times, and gives rise to slight over-subtraction of Raman feature intensities when approximating the baseline with the linear-spline method. This results in a slightly faster exciton decay lifetime as determined from our Raman-signal intensities.

3.6.3. A note on the accelerated apparent exciton decay lifetime measured via FSRS with an 880-nm Raman pump.

As described in the main text, Raman features measured with the 880-nm Raman pump decay more quickly than the exciton lifetime measured by TA. The possibility for under- or over-subtracting the background has been an important consideration in applying the subtraction routine described above, as in either case the Raman intensity decay observed could be influenced by the time-dependence of the background signal shape. The accelerated decay timescale we obtain from our background-subtracted Raman features likely originates from such baseline shape changes through the ISC process: As illustrated in Figure 3.3S (compare to Fig. 3.1(a) of the main text), the background signal changes from a transient bleach of the excited singlet state to a transient bleach of the triplet; these two spectral shapes differ in curvature (negative vs. positive) across the probed spectral range. We expect that this change in background curvature, specifically, gives rise to a slight over-subtraction of Raman feature intensities at longer delays where the triplet absorption dominates.

Figure 3.4S compares the integrated intensity in the C=C stretch region measured using both 880-nm and 950-nm Raman pump pulses. The signal collected at 950 nm decays with the expected timescale (315 ps ± 40 ps). As this Raman pump wavelength falls far from the triplet absorption, the background signal in these measurements was dominated by a transient bleaching of the singlet excited state only and no baseline shape

changes occur during the ISC process. This comparison clarifies that the effect of the baseline uncertainty influences the extracted signal intensity at long delays where the triplet absorption at 880-nm dominates.

It is important to note, however, that this over-subtraction in the 880-nm data only occurs at time delays much longer than those during which the initial conformational relaxation takes place. Therefore, baseline shape uncertainties that influence the apparent exciton decay lifetime do not influence extraction of Raman spectra that capture the initial excited-state relaxation process. As demonstrated in Figure 3.2S above, the spectral baseline maintains roughly the same shape during this faster phase of evolution, such that baseline uncertainties should be of little concern at these much earlier delays. Over-subtraction at these later delays could likely be eliminated by modeling changes in baseline shape. However, given the spectral congestion in the exciton fingerprint region, we believe that the linear-spline background subtraction is the most honest approach for extracting Raman features from our data as it does not require a subjective guess of the baseline shape.

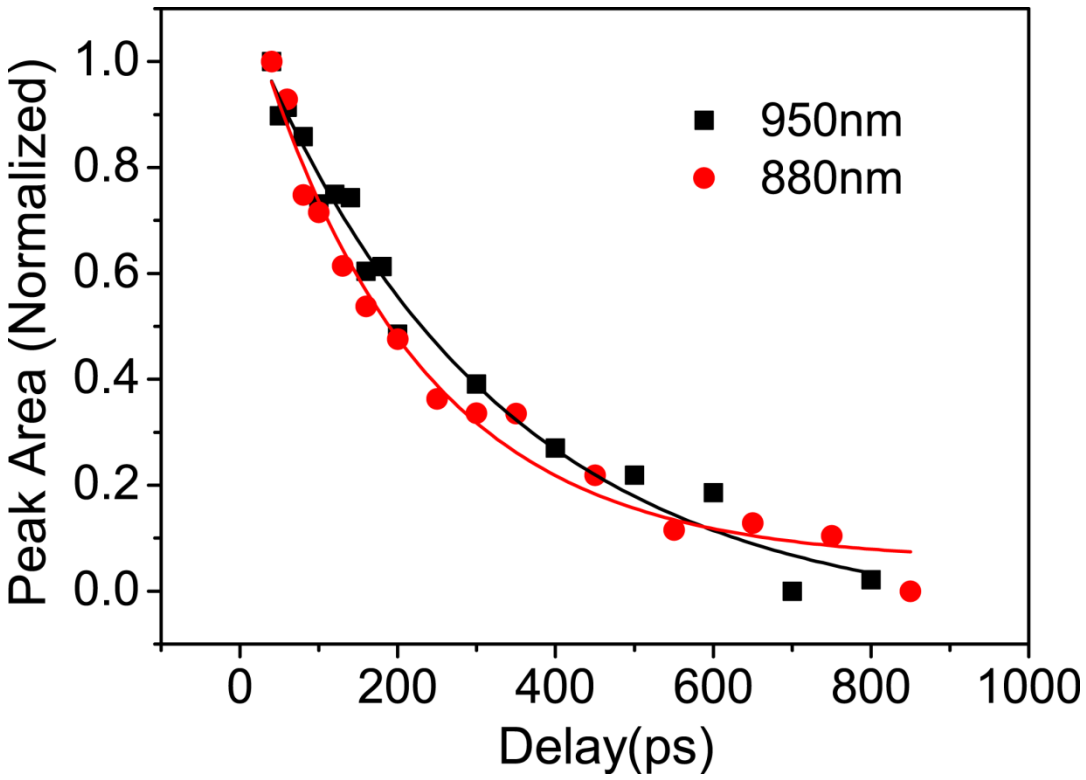

Figure 3.4S: Long-time decay (> 40 ps) of Raman intensity in the C=C ring stretch region (~1450 cm^{-1}) as measured using 950 and 880-nm Raman pump pulses. Integrated peak intensities have been normalized at 40 ps. Raman intensity probed via 880-nm occurs with a lifetime of 220 ± 20 ps. Raman intensity probed via 950-nm decays with a timescale of 315 ± 40 ps, similar to the exciton decay lifetime measured by transient absorption spectroscopy.

3.6.4. Measurement of resonant Raman spectrum of oxidized P3HT

As described above, P3HT can readily photo-oxidize in solution, and oxidized P3HT exhibits a broad absorption band in the NIR. Consequently, resonant Raman features from the oxidized byproduct can interfere with excited-state Raman measurements if the sample is not appropriately managed during measurements (using a flow cell or sample rastering).

For the purposes of preparing Fig. 3.3 of the main text, we exposed a cuvette of P3HT at 510 nm for a prolonged period and subsequently measured the Raman spectrum with the photoexcation source blocked. A resonant Raman spectrum of the oxidized polymer was extract by a scaled subtraction of non-resonant features (solvent and polymer). Features apparent in this spectrum closely match those measured via electrochemical oxidation of P3HT films.

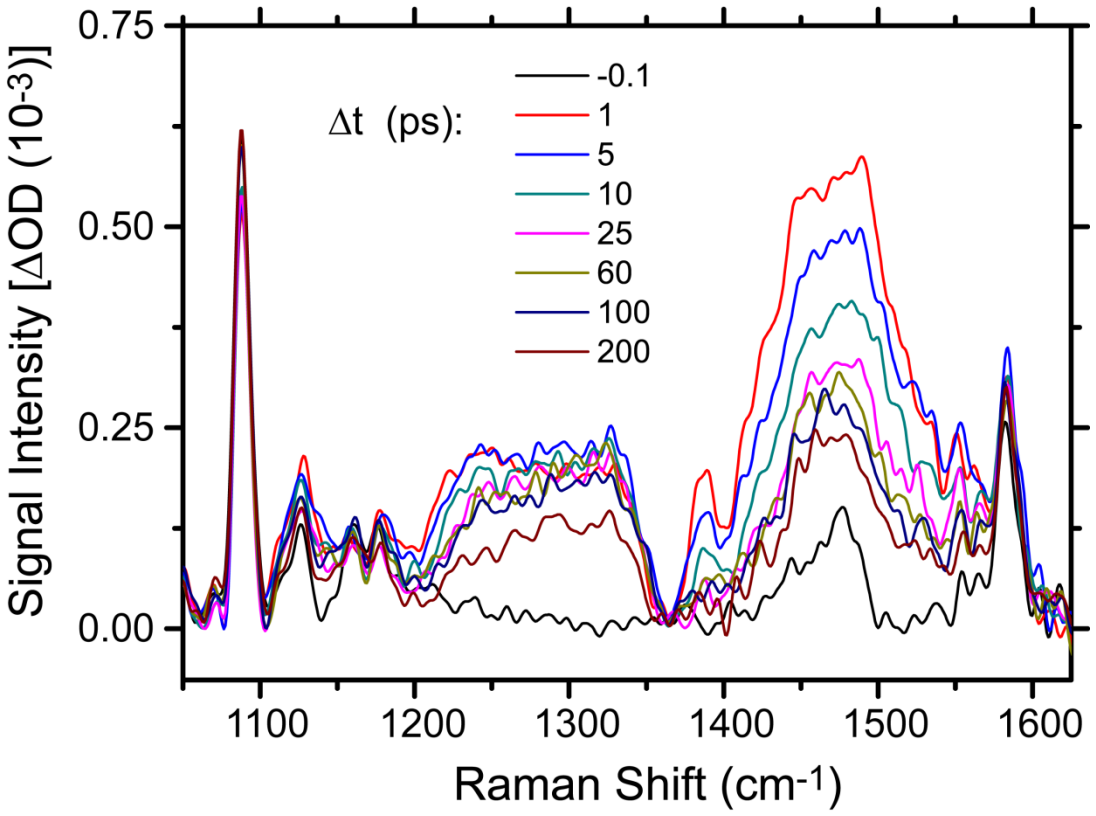

Figure 3.5S: Time-resolved Raman spectra of RR-P3HT collected with perpendicular relative polarization between the 510-nm excitation pulse and the Raman probing pulses. Although the signal level is much smaller, spectral dynamics observed are similar to those seen in Fig. 3.2 of the main text.

3.6.5. Influence of relative pulse polarization on transient Raman signals.

The data presented in Figure 3.2 of the main text was collected using a parallel relative polarization between the actinic pump and probing Raman pulses. Figure 3.5S illustrates the same measurements collected over the 200-ps time window but with the actinic pump polarization perpendicular to that of the Raman probing pulses. This progression exhibits the same behavior as that seen in the Figure 3.2 of the main text: Features associated with carbon atoms along the exciton backbone decay appreciably over the initial timescale, while the intensity at 1275-1350 cm^{-1} remains fairly constant. Although we anticipate the anisotropy decay may have some significance in the relative sizes of our measured signals, the similarity in spectral dynamics indicates that the Raman intensity decay reflects changes in resonant enhancement that are *not* induced by anisotropy depolarization.

3.6.6. Data fitting procedures.

TA and time-resolved Raman intensities presented in the text were fitted with biexponential functions, each with a common (i.e. constrained) set of relaxation and population decay lifetimes:

$$I(t) = A_1 \exp\left(-\frac{t}{T_R}\right) + A_2 \exp\left(-\frac{t}{T_D}\right) + y_0 \qquad (3.2)$$

As we have no quantitative model (as of yet) to connect the relative changes in spectral intensity between various spectral regions in either measurement, amplitudes (A_1, A_2) and an offset (y_0) for each transient were nominally treated as free parameters for these fits, but with additional constraints imposed for fitting each transient.

Our fitting procedure can be summarized as follows: All transients were first fit separately (no constraints) in order to obtain initial guesses for these parameters for constrained fitting. As we scaled all TA transients according to their intensity at 1 ps, we used the constraint that the sum of the amplitudes and offset for each trace equals 1. For Raman data, the offset parameters determined from individual fits were subtracted from each transient in order to reduce the number of free parameters necessary to fit each trace. Each of these sets was then fit using constrained relaxation and decay timescales. On average, each trace in Fig. 3.1(a) and Fig. 3.4(a) is fit with <2.2 parameters (9-10 amplitudes + 2 timescales for each set of 5 transients). Fit parameters for TA and Raman data are provided in Tables 3.1S and 3.2S, respectively.

Table 3.1S: Best fit amplitudes for fitting of TA intensities (Fig. 3.1(b) of main text). Constrained decay timescales determined from fit are 8 ± 1 and 320 ± 20 ps.

	850-900 nm	**900-950 nm**	**950-1000 nm**	**1000-1050 nm**	**1050-1100 nm**
A_1	0.307	0.288	0.254	0.181	0.086
A_2	0.274	0.556	0.689	0.779	0.884

Table 3.2S: Best fit amplitudes for fitting of TA intensities (Fig. 3.1(b) of main text). Constrained decay timescales determined from fit are 9 ± 1 and 220 ± 20 ps.

	C=C	**C_2-C_5'**	**Term. C_2-C_5'**	**C_4-H**	**C_3-C_6**
A_1	0.104	0.0199	—	0.0102	0.00664
A_1	0.086	0.0524	0.0255	0.0148	0.00504

3.7 References

(1) Gunes, S.; Neugebauer, H.; Sariciftci, N. S. Conjugated Polymer-based Organic Solar Cells. *Chem. Rev.* **2007**, *107*, 1324-1338.

(2) Facchetti, A. π-conjugated Polymers for Organic Electronics and Photovoltaic Cell Applications. *Chem. Mater.* **2011**, *23*, 733-758.

(3) Scharber, M. C.; Muhlbacher, D.; Koppe, M.; Denk, P.; Waldauf, C.; Heeger, A. J.; Brabec, C. J. Design Rules for Donors in Bulk-Heterojunction Solar Cells - Towards 10 % Energy-Conversion Efficiency. *Adv. Mater.* **2006**, *18*, 789-794.

(4) Bredas, J. L.; Norton, J. E.; Cornil, J.; Coropceanu, V. Molecular Understanding of Organic Solar Cells: The Challenges. *Acc. Chem. Res.* **2009**, *42*, 1691-1699.

(5) Barbour, L. W.; Hegadorn, M.; Asbury, J. B. Watching Electrons Move in Real Time: Ultrafast Infrared Spectroscopy of a Polymer Blend Photovoltaic Material. *J. Am. Chem. Soc.* **2007**, *129*, 15884-15894.

(6) Cook, S.; Ohkita, H.; Durrant, J. R.; Kim, Y.; Benson-Smith, J. J.; Nelson, J.; Bradley, D. D. C. Singlet Exciton Transfer and Fullerene Triplet Formation in Polymer-Fullerene Blend Films. *Appl. Phys. Lett.* **2006**, *89*, 101128.

(7) Guo, J.; Ohkita, H.; Benten, H.; Ito, S. Near-IR Femtosecond Transient Absorption Spectroscopy of Ultrafast Polaron and Triplet Exciton Formation in Polythiophene Films with Different Regioregularities. *J. Am. Chem. Soc.* **2009**, *131*, 16869-16880.

(8) Bjorklund, T. G.; Lim, S. H.; Bardeen, C. J. Dependence of Poly(p-Phenylene Vinylene) Morphology and Time-resolved Photophysics on Precursor Solvent. *Synth. Met.* **2002**, *126*, 295-299.

(9) Schwartz, B. J. Conjugated Polymers as Molecular Materials : How Chain Conformation and Film Morphology Influence Energy Transfer and Interchain Interactions. *Annu. Rev. Phys. Chem.* **2003**, *54*, 141-172.

(10) Hayes, G. R.; Samuel, I. D. W.; Phillips, R. T. Ultrafast Dynamics of Photoexcitations in Conjugated Polymers. *Synth. Met.* **1997**, *84*, 889-890.

(11) Banerji, N.; Cowan, S.; Vauthey, E.; Heeger, A. J. Ultrafast Relaxation of the Poly(3-hexylthiphene) Emission Spectrum. *J. Phys. Chem. C* **2011**, *115*, 9726-9739.

(12) Busby, E.; Carroll, E. C.; Chinn, E. M.; Chang, L.; Moulé, A. J.; Larsen, D. S. Excited-state Self-trapping and Ground-state Relaxation Dynamics in Poly(3-hexylthiophene) Resolved with Broadband Pump-Dump-Probe Spectroscopy. *J. Phys. Chem. Lett.* **2011**, *2*, 2764-2769.

(13) Hwang, I.; Scholes, G. D. Electronic Energy Transfer and Quantum-coherence in p-conjugated Polymers. *Chem. Mater.* **2011**, *23*, 610-620.

(14) Tretiak, S.; Saxena, A.; Martin, R. L.; Bishop, A. R. Conformational Dynamics of Photoexcited Conjugated Materials. *Phys. Rev. Lett.* **2002**, *89*, 097402.

(15) Wells, N. P.; Blank, D. A. Correlated Exciton Relaxation in Poly(3-hexylthiophene). *Phys. Rev. Lett.* **2008**, *100*, 086403.

(16) Wells, N. P.; Boudouris, B. W.; Hillmyer, M. A.; Blank, D. A. Intramolecular Exciton Relaxation and Migration Dynamics in Poly(3-hexylthiophene). *J. Phys. Chem. C* **2007**, *111*, 15404-15414.
(17) Westenhoff, S.; Beenken, W. J. D.; Friend, R., H.; Greenham, N. C.; Yartsev, A.; Sundström, V. Anomalous Energy Transfer Dyanmics due to Torsional Relaxation in a Conjugated Polymer. *Phys. Rev. Lett.* **2006**, *97*, 166804.
(18) Cook, S.; Furube, A.; Katoh, R. Analysis of the Excited States of Regioregular Polythiophene P3HT. *Energy Env. Sci.* **2008**, *1*, 294-299.
(19) Piris, J.; Dykstra, T. E.; Bakulin, A. A.; van Loosdrecht, P. H. M.; Knulst, W.; Trinh, M. T.; Schins, J. M.; Siebbeles, L. D. A. Photogeneration and Ultrafast Dynamics of Excitions and Charges in P3HT/PCBM Blends. *J. Phys. Chem. C* **2009**, *113*, 14500-14506.
(20) Collini, E.; Scholes, G. D. Coherent Intrachain Energy Migration in a Conjugated Polymer at Room Temperature. *Science* **2009**, *323*, 369-373.
(21) Westenhoff, S.; Beenken, W. J. D.; Yartsev, A.; Greenham, N. C. Conformational disorder of conjugated polymers. *J. Chem. Phys.* **2006**, *125*, 154903.
(22) Parkinson, P.; Müller, C.; Stingelin, N.; Johnston, M. B.; Herz, L. M. Role of Ultrafast Torional Relaxation in the Emission from Polythiophene Aggregates. *J. Phys. Chem. Lett.* **2010**, *1*, 2788-2792.
(23) Yang, A.; Hughes, S.; Kuroda, M.; Shirashi, Y.; Kobayashi, T. Stationary and Time-Resolved Spectra of 2,2':5',2"-terthiophene. *Chem. Phys. Lett.* **1997**, *280*, 475-480.
(24) Miller, S.; Fanchini, G.; Lin, Y. Y.; Li, C.; Chen, C. W.; Su, W. F.; Chhowalla, M. Investigation of Nanoscale Morphological Changes in Organic Photovoltaics During Solvent Vapor Annealing. *J. Mater. Chem.* **2008**, *18*, 306-312.
(25) Tsoi, W. C.; James, D. T.; Kim, J. S.; Nicholson, P. G.; Murphy, C. E.; Bradley, D. D. C.; Nelson, J. The Nature of In-Plane Skeleton Raman Modes of P3HT and Their Correlation to the Degree of Molecular Order in P3HT:PCBM Blend Thin Films. *J. Am. Chem. Soc.* **2011**, *133*, 9834-9843.
(26) Gao, Y. Q.; Martin, T. P.; Thomas, A. K.; Grey, J. K. Resonance Raman Spectroscopic- and Photocurrent Imaging of Polythiophene/Fullerene Solar Cells. *J. Phys. Chem. Lett.* **2010**, *1*, 178-182.
(27) Sauvajol, J. L.; Chenouni, D.; Lére-Porte, J. P.; Chorro, C.; Moukala, B.; Petrissans, J. Resonant Raman Spectra and Photoluminescence in Polythiophene. *Synth. Met.* **1990**, *38*, 1-12.
(28) Furukawa, Y.; Akimoto, M.; Harada, I. Vibrational Key Bands and Electrical Conductivity of Polythiophenes. *Synth. Met.* **1987**, *18*, 151-156.
(29) Albrecht, A. C. On the Theory of Raman Intensities. *J. Chem. Phys.* **1961**, *34*, 1476-1484.
(30) Kukura, P.; McCamant, D. W.; Mathies, R. A. Femtosecond Stimulated Raman Spectroscopy. *Annu. Rev. Phys. Chem.* **2007**, *58*, 461-488.
(31) Yoshizawa, M.; Kurosawa, M. Femtosecond Time-resolved Raman Spectroscopy using Stimulated Raman Scattering. *Phys. Rev. A* **1999**, *61*, 013808.
(32) Lee, S. Y.; Zhang, D. H.; McCamant, D. W.; Kukura, P.; Mathies, R. A. Theory of Femtosecond Stimulated Raman Spectroscopy. *J. Chem. Phys.* **2004**, *121*, 3632-3642.

(33) Pein, B. C.; Seong, N.-H.; Dlott, D. D. Vibrational Energy Relaxation of Liquid Aryl-Halides X-C_6H_5 (X = F, Cl, Br, I). *J. Phys. Chem. A* **2010**, *114*, 10500-10507.
(34) Louarn, G.; Trznadel, M.; Buisson, J. P.; Laska, J.; Pron, A.; Lapkowski, M.; Lefrant, S. Raman Spectroscopic Studies of Regioregular Poly(3-alkylthiophenes). *J. Phys. Chem.* **1996**, *100*, 12532-12539.
(35) Akimoto, M.; Furukawa, Y.; Takeuchi, H.; Harada, I.; Soma, Y.; Soma, M. Correlation Between Vibrational Spectra and Electrical Conductivity of Polythiophene. *Synth. Met.* **1986**, *15*, 353-360.
(36) Shi, G.; Xu, J.; Fu, M. Raman Spectroscopic and Electrochemical Studies on the Doping Level Changes of Polythiophene Films During their Electrochemical Growth Processes. *J. Phys. Chem. B* **2002**, *106*, 288-292.
(37) Chen, F.; Shi, G.; Zhang, J.; Fu, M. Raman Spectroscopic Studies on the Structural Changes of Electrosynthesized Polythiophene Films During the Heating and Cooling Processes. *Thin Solid Films* **2002**, *424*, 283-290.
(38) Sauvajol, J. L.; Poussigue, G.; Benoit, C.; Lére-Porte, J. P.; Chorro, C. Sample Dependence of Raman Spectrum on Polythiophene Films. *Synth. Met.* **1991**, *41-43*, 1237-1242.
(39) Louarn, G.; Buisson, J. P.; Lefrant, S. Vibrational Studies of a Series of a-oligothiophenes as Model Systems of Polythiophene. *J. Phys. Chem.* **1995**, *99*, 11399-11404.
(40) McHale, J. L. *Molecular Spectroscopy*; Prentice-Hall Inc.: Upper Saddle River, NJ, 1999.
(41) Beenken, W. J.; Pullerits, T. Spectroscopic Units in Conjugated Polymers: A Quantum Chemically Founded Concept? *J. Phys. Chem. B* **2004**, *108*, 6164-6169.
(42) Cates, D. A.; Strauss, H. L.; Snyder, R. G. Vibrational Modes of Liquid *n*-Alkanes: Simulated Isotropic Raman Spectra and Band Progressions for C_5H_{12}-$C_{20}H_{42}$ and $C_{16}D_{34}$. *J. Phys. Chem. A* **1994**, *98*, 4482-4488.
(43) Mirkin, N.; Krimm, S. *Ab Initio* Studies of the Conformational Dependence of the Spectra of Stable Conformers of *n*-Pentane and *n*-Hexane. *J. Phys. Chem.* **1993**, *97*, 13887-13895.
(44) Barford, W.; Lidzey, D. G.; Makhov, D.; Meijer, J. H. Exciton Localization in Disordered Poly(3-hexylthiophene). *J. Chem. Phys.* **2010**, *133*, 044504.
(45) Weigel, A.; Dobryakov, A.; Klaumunzer, B.; Sajadi, M.; Saalfrank, P.; Ernsting, N. P. Femtosecond Stimulated Raman Sepctroscopy of Flavin after Optical Excitation. *J. Phys. Chem. B* **2011**, *115*, 3656-3680.
(46) Chen, T. A.; Rieke, R. D. The First Regioregular Head-to-Tail poly(3-hexylthiophene-2,5,-diyl) and a Regiorandom Isopolymer: Nickel versus Palladium Catalysis of 2(5)-bromo-5(2)-(bromozincio)-3-hexylthiophene Polymerization. *J. Am. Chem. Soc.* **1992**, *114*, 10087-10088.
(47) Yu, W., Zhou, J., Bragg, A. E. Exciton Conformational Dynamics of Poly(3-hexylthiophene) (P3HT) in Solution from Time-solved Resonant-Raman Spectroscopy. *J. Phys. Chem. Lett.* **2012**, 3, 1321-1328

Chapter 4. Ultrafast photo-induced nuclear relaxation of a conformationally disordered conjugated polymer probed with transient absorption and femtosecond stimulated Raman spectroscopies

This chapter describes work previously published[35] in

W. Yu, P. J. Donohoo-Vallett, J. Zhou, and A. E. Bragg. Ultrafast Photoinduced Nuclear Relaxation of a Conformationally Disordered Conjugated Polymer Probed with Transient Absorption and Femtosecond Stimulated Raman Spectroscopies. *J. Chem. Phys*. **141**, 044201 (2014).

4.1 Abstract

A combination of transient absorption (TAS) and femtosecond stimulated Raman (FSRS) spectroscopies were used to interrogate the photo-induced nuclear relaxation dynamics of poly(3-cyclohexyl,4-methylthiophene) (PCMT). The large difference in inter-ring dihedral angles of ground and excited-state PCMT make it an ideal candidate for studying large-amplitude vibrational relaxation associated with exciton trapping. Spectral shifting in the S_1 TA spectra on sub-ps timescales (110 ± 20 and 800 ± 100 fs) are similar to spectroscopic signatures of excited-state relaxation observed with related photoexcited conjugated polymers and which have been attributed to exciton localization and a combination of resonant energy transfer and torsional relaxation, respectively. Measurements made with both techniques reveal fast PCMT S_1 decay and triplet formation (τ_{S1} =25-32 ps), which is similar to the excited-state dynamics of short oligothiophenes and highly twisted polyconjugated molecules. On ultrafast timescales

FSRS of S_1 PCMT offers a new perspective on the nuclear dynamics that underlie localization of excitons in photoexcited conjugated polymers: Spectral dynamics in the C=C stretching region (1400-1600 cm^{-1}) include a red-shift of the in-phase C=C stretching frequency, as well as a change in the relative intensity of in-phase and out-of-phase stretch intensities on a timescale of ~100 fs. Both changes indicate an ultrafast vibrational distortion that increases the conjugation length in the region of the localized excitation and are consistent with exciton self-localization or trapping. Wavelength-dependent excited-state FSRS measurements further demonstrate that the C=C stretching frequency provides a useful spectroscopic handle for interrogating the degree of delocalization in excited conjugated polymers given the selectivity achieved via resonance enhancement.

4.2 Introduction

Conjugated polymers have become a common component in organic electronic materials[1,2] and there is continued interest in characterizing properties and dynamics of the electronic states that underlie their material behaviors.[3-13] On a fundamental level conjugated polymers raise interesting questions regarding the nature of localized states in disordered, highly inhomogeneous systems and also regarding what structural changes are responsible for trapping these states along an extended π-conjugated framework.[14-16] The structural complexity of these systems leads naturally to many questions: How does one accurately describe delocalized states on a disordered polymer backbone?[14] How are the properties of polymer excitations determined by both the polymer's torsional conformation and other structural variations along the polymer backbone? What structural relaxation dynamics following photoexcitation are responsible for exciton trapping and how can we observe such nuclear evolution directly?[7,17] Addressing these questions experimentally requires methods that can differentiate amongst structural variations within an ensemble of localized excited states and track excited-state structural relaxation directly in time.[7,12] Here we specifically demonstrate the use of femtosecond stimulated Raman spectroscopy (FSRS)[18] in combination with ultrafast transient absorption spectroscopy (TAS) to characterize the nuclear relaxation associated with exciton trapping in the conjugated polymer poly(3-cyclohexano,4-methylthiophene), or PCMT.

The photoinduced dynamics and spectroscopy of conjugated polymers in solution have been examined extensively over the last decade using various transient electronic spectroscopies in order to address the questions listed above.[3-13] From these studies it has been concluded that the dynamics underlying various phases of excited-state relaxation include: (1) Exciton self-trapping or localization, associated with transient spectral evolution over timescales of ~100 fs or less;[3-5,7,9,10] (2) Resonant excitonic energy transfer (EET)[3,6,11,19] through which energy migrates to lower-energy sites characterized by different degrees of delocalization and/or (3) local, long-range torsional relaxation, both occurring on timescales ranging from sub-ps to 10s of ps;[4,5,9,10,12] and (4) singlet exciton decay by emission and intersystem crossing (ISC), occurring on timescales of 100s of picoseconds.[3,12,13] ISC is readily identified by the appearance of a triplet absorption band at slightly higher transition energies, analogous to the spectral dynamics of conjugated oligomers.[12,20,21] Signatures of EET have been identified through measurements of both time-dependent spectral diffusion[8] and anisotropy depolarization;[3,8,11] the latter have revealed very fast and appreciable randomization of the stimulated emission (or fluorescence) polarization after excitation, which models predict to occur primarily via energy transfer between sites.[11,22,23] The relative importance of EET and torsional relaxation has been debated for some time, but pump-probe (transient absorption and time-resolved fluorescence),[4,11] multi-pulse,[4] and photon-echo spectroscopies[9] have shed new light on the relaxation dynamics of

polythiophenes in recent years, revealing that local relaxation contributes significantly to the stabilization of excited poly(3-alkylthiophenes). Although nuclear relaxation associated with exciton self-trapping is the most plausible explanation for transient evolution in the electronic spectroscopy of excited polymers on ultrafast timescales,[4,9] there is little information about what occurs during this process directly from experiment. This can be attributed to the very fast timescale on which localization occurs, as well as the fact that clear spectroscopic interrogation of this localization requires a sensitive probe of ultrafast nuclear dynamics out of the Franck-Condon region in the excited state.[9]

Raman spectroscopy has been used extensively to characterize conjugated polymers and polymer-based materials,[24-31] and is a promising complement to electronic spectroscopies for interrogating the structural characteristics and dynamics of conjugated polymers in their excited states.[7,12] Conjugated polymers and oligomers exhibit very large ground-state Raman cross-sections, with spectra dominated by totally symmetric modes that coincide with the change in molecular geometry that accompanies polymer excitation.[32] Furthermore, vibrational frequencies of various Raman-active modes (most notably the in-phase C=C stretching frequency) are directly sensitive to the extent of delocalization along an oligomer or polymer backbone.[32,33] Given that excited states of conjugated oligomers and polymers are highly delocalized by nature, we anticipate that C=C stretching frequencies of excited states should be highly sensitive to variations or evolution in the excited-state delocalization length. Thus, time-resolved excited-state

Raman spectroscopy could be used as a direct method for interrogating evolution in conformation and delocalization length that occurs through the course of excited-state relaxation of photoexcited conjugated polymers and oligomers.[12]

In previous work we used time-resolved resonant FSRS to investigate the picosecond structural relaxation dynamics of regio-regular poly(3-hexylthiophene) (RR-P3HT) following photoexcitation at 510 nm.[12] Time-dependent evolution in the excited-state Raman spectrum on a timescale of 9 ps was attributed to the influence of conformational relaxation on the resonant enhancement of modes that involve moieties within the conjugated backbone; this behavior was explained to result from torsion-induced changes to the Franck-Condon overlap between the excited and probing states, and occurs on a similar timescale as spectral relaxation in near-IR absorption transients. Raman measurements also revealed a feature between 1300 and 1350 cm^{-1} that only evolved with the population decay of the excited state; we attributed this feature to vibrations peripheral to the conjugated backbone that effectively spectate conformational relaxation, and we postulated that this feature corresponds with modes localized around polymer defects or distortions that demarcate the boundaries of localized excited states. Thus, this work demonstrated that excited-state Raman spectroscopy can offer new and more detailed perspective on the structural properties and dynamics of photoexcited polymers and complements what can be gleaned from transient electronic spectroscopies.

Here we further explore the use of FSRS for interrogating the vibrational

spectroscopy and dynamics of conjugated polymers, and specifically those of PCMT. We use the ultrafast evolution in the frequencies and band-shapes in the C=C stretching region as a probe of the initial nuclear relaxation dynamics associated with exciton trapping, making use of the high time resolution available with FSRS.[18] The substitution pattern along the conjugated backbone in PCMT gives rise to very large inter-ring dihedral angles compared to other polythiophenes in their ground states, and we expected that TAS and FSRS should be particularly sensitive to large-amplitude twisting or deformation along these angles as PCMT relaxes out of the Franck-Condon region in the S_1 state. We have also interrogated the structural dependence of intersystem crossing (ISC) on longer picosecond timescales. Finally, the spectroscopic selectivity of wavelength-dependent resonantly enhanced FSRS enables characterization of the variations in delocalization that underlie broad transient electronic absorption bands of the excited polymer.

4.3 Experimental Methods

4.3.1 Sample preparation.

PCMT and RR-P3HT (electronic grade, molecular weight 50-70 kD) were purchased from Rieke metals and used "as-is" after prolonged purging with high-purity dry argon. Chlorobenzene (CB, Fisher Scientific, >99% purity) and unstabilized tetrahydrofuran (THF, Sigma Aldrich, >99.9% purity) were deaerated through repeated freeze-pump-thaw cycles using liquid nitrogen. Under an argon atmosphere, solutions of PCMT in THF and

RR-P3HT in CB were prepared in vials and transferred into the reservoir of a sample flow loop. Spectroscopic measurements were made on sample solutions as they passed through a flow cell with a 0.5 mm pathlength and fused-silica windows (Spectrocell). The sample flow circuit was constructed entirely of PTFE tubing and compression fittings to ensure chemical compatibility with the solvents used and has a circulation volume of less than 30 mL. Samples were circulated at 15 mL/min with a peristaltic pump during the course of spectroscopic measurements, and no signs of photoproduct were observed after many hours of exposure to laser pulses.

Higher sample concentrations (1 mg/mL) were necessary for conducting excited-state Raman measurements, whereas lower sample concentrations (0.2 mg/mL) were used for transient absorption measurements and ground-state Raman measurements with P3HT. We have previously demonstrated that the photophysics of P3HT does not change within this concentration range.[12] We likewise observe no differences in the photophysics of PCMT at low and high sample concentrations. PCMT samples used for TAS measurements had an OD of 0.5 at the excitation wavelength; the OD used for FSRS measurements was much higher (> 2).

Steady-state UV-Vis spectra of sample solutions were measured using a diode-array spectrometer fiber-optically coupled to incandescent deuterium and tungsten light sources (Stellarnet). Samples used for measurements of steady-state absorption spectra were diluted to have OD < 1 in a 0.5 mm cuvette at the peak absorption wavelength.

4.3.2 Laser instrumentation and measurements.

Steady-state resonant Raman measurements with ground-state polymer in solution were conducted using FSRS.[18] Excited-state polymer spectroscopy and dynamics were examined using broadband TAS and time-resolved FSRS. All measurements utilized ultrafast laser pulses, which were derived from the fundamental output of an amplified Ti:Sapphire laser (Coherent Legend Elite, 4.5 mJ/pulse, 1 kHz rep. rate, 35-fs pulse duration, 800-nm peak wavelength). Half of this output was used to pump an optical parameteric amplifier (Coherent OperaSolo) that generates photoexcitation pulses (or actinic pulses) at 320 nm through second harmonic generation of the second harmonic of the OPA signal at 1280 nm; excitation pulses were attenuated to an energy of 3 μJ/pulse for these measurements. Another portion of the amplifier output (~1 mJ/pulse) was used to pump a second-harmonic bandwidth compressor (SHBC, Light Conversion), which generates narrowband (~12 cm^{-1}) pulses with 2-3 ps duration at 400 nm. Pulses derived from the SHBC were used either directly for ground-state stimulated Raman measurements or to pump a white-light-seeded OPA (TOPAS-400, Light Conversion) in order to generate tunable narrowband Raman-excitation (or Raman-pump) pulses for wavelength-dependent excited-state and transient Raman experiments (600 nm or 840 nm). The Raman-pump pulse energy was typically 10-15 μJ/pulse. A few μJ of amplifier output at 800 nm was focused into a 2-mm-thick sapphire crystal to generate a broadband

probe continuum used in all measurements (420-720 nm or 850-1100 nm).

Photoexcitation pulses (or actinic pulses, at 320 nm) were focused to a 2-mm beam diameter on the sample. Raman-excitation pulses were focused towards the sample with a 1-meter focal-length lens, with the focus located behind the sample; the Raman-excitation beam had a 500 mm diameter at the position of the sample and crossed at the center of the larger beam profile of the actinic pump. White-light probing pulses were focused to the center of the Raman-pump beam on the sample with a ~50 μm diameter using an off-axis parabolic mirror. The sizes, pulse energy and overlap of the three beams guarantee the collection of three-pulse signals, and specifically excited-state Raman spectra via FSRS.

Photoexcitation and Raman-pump pulses were blocked after the sample with a set of long-pass filters, and probe pulses were collected and dispersed with a 300-mm spectrograph (Acton-2360) onto a CCD camera (Pixis-100BR). The camera was configured to collect spectra at the laser's repetition rate, with the photoexcitation beam and Raman beam chopped (or blocked) accordingly for each type of measurement. The output reference signals from both the camera and the choppers were used to correlate chopper phases with each exposure.

Multiple types of measurements were made using this optical configuration:[34]

(1) Broadband TAS probing at visible (420-750 nm) and near-IR wavelengths (830-1100 nm) was conducted by blocking the Raman excitation beam and chopping the

photoexcitation beam at one half of the laser repetition rate. Transient spectra were computed with white-light spectra (photoexcitation on vs. off) from consecutive laser shots dispersed across the detector array using a low-resolution grating (800-nm blaze, 150 lines/mm).

(2) Ground-state Raman (GSR) measurements were made by blocking the photoexcitation beam and chopping the Raman-excitation beam. GSR spectra were likewise computed from a comparison of consecutive white-light spectra (Raman excitation on vs. off) dispersed at much higher resolution (grating: 1000-nm blaze, 600 lines/mm). Linewidths in these measurements were limited predominantly by the bandwidth of the Raman excitation source (15-20 cm^{-1}), as well as natural transition linewidths, spectral congestion, and spectral inhomogeneity.

(3) Three-pulse transient and excited-state Raman measurements were conducted using a four-phase chopping sequence, with the photoexcitation and Raman excitation beams chopped at one-fourth and one-half of the laser repetition rate, respectively (Photoexcitation/Raman-excitation sequences: on/on; on/off; off/on; off/off). Multiple signals were derived simultaneously with this approach, including: TAS covering the spectral region probed in Raman measurements (on/off vs. off/off); GSR (off/on vs. off/off); and three-pulse signals collected in the presence of the photoexcitation pulse (on/on vs. on/off). For brevity, we refer to the third signal as Raman-excitation chopped (RC), although GSR and other (non-Raman) three-pulse signals also appear in these

spectra (see Section 2.3 below). A complementary three-pulse signal can be obtained by synchronously chopping (SC) both beams (on/on vs. off/off).

Each of these spectra was calculated from the measurement sequence as follows:

$$TAS = \log(I_{pu+pr}/I_{pr}) \quad (4.1a)$$

$$GSR = \log(I_{r+pr}/I_{pr}) \quad (4.1b)$$

$$RC = \log(I_{pu+r+pr}/I_{pu+pr}) \quad (4.1c)$$

$$SC = \log(I_{pu+r+pr}/I_{pr}) \quad (4.1d)$$

Subscripts in Eqn. 1 correspond with photoexcitation (pu), Raman excitation (r) and white light probe (pr) pulses, respectively. As described in Section 2.3, we make use of these various signals to isolate excited-state Raman features in our spectral analysis. Each Raman spectrum presented here is an average of 15000-30000 measurements cycles (2- or 4-phase).

Timings of the photo- and Raman-excitation pulses relative to the probe pulse were controlled with two motorized translation stages (Newport ESP301-2N and Newport MFA-PPD, respectively). The stages controlling the photoexcitation and Raman time delays were outfitted with a protected silver or aluminum retroreflecting mirrors to ensure that the path of the excitation beam was parallel to the stage. Positioning of the stages, rotation of the spectrograph gratings, collection of spectra, synchronization with choppers, and calculation of transient spectra were all coordinated through a data acquisition program written in LabView.

TAS measurements were conducted with a magic-angle pump-probe polarization. In contrast, polarizations of all three pulses were kept parallel for Raman measurements. For ground-state Raman measurements, the relative Raman pump-probe pulse delay was timed such that the probe pulse arrived near the middle of the Raman pump pulse duration, as it was determined that this gave the best Raman line shapes from the solvent. For excited-state Raman spectra the probe pulse was timed to arrive slightly earlier in the Raman excitation pulse in order to minimize excited-state population depletion induced by the Raman-pump when on resonance.

The time-dependent, two-photon (pump-probe) solvent response of neat THF was used for correcting the influence of temporal chirp from the continuum probe in transient measurements. An example of the time-dependent solvent response and a brief description of chirp correction procedures are provided in the supplemental material.[35] Wavelength-dependent cuts through the solvent response were used to determine the effective time-resolution of the experiment, which was found to range between 100 and 150 fs from the near UV to the near IR.

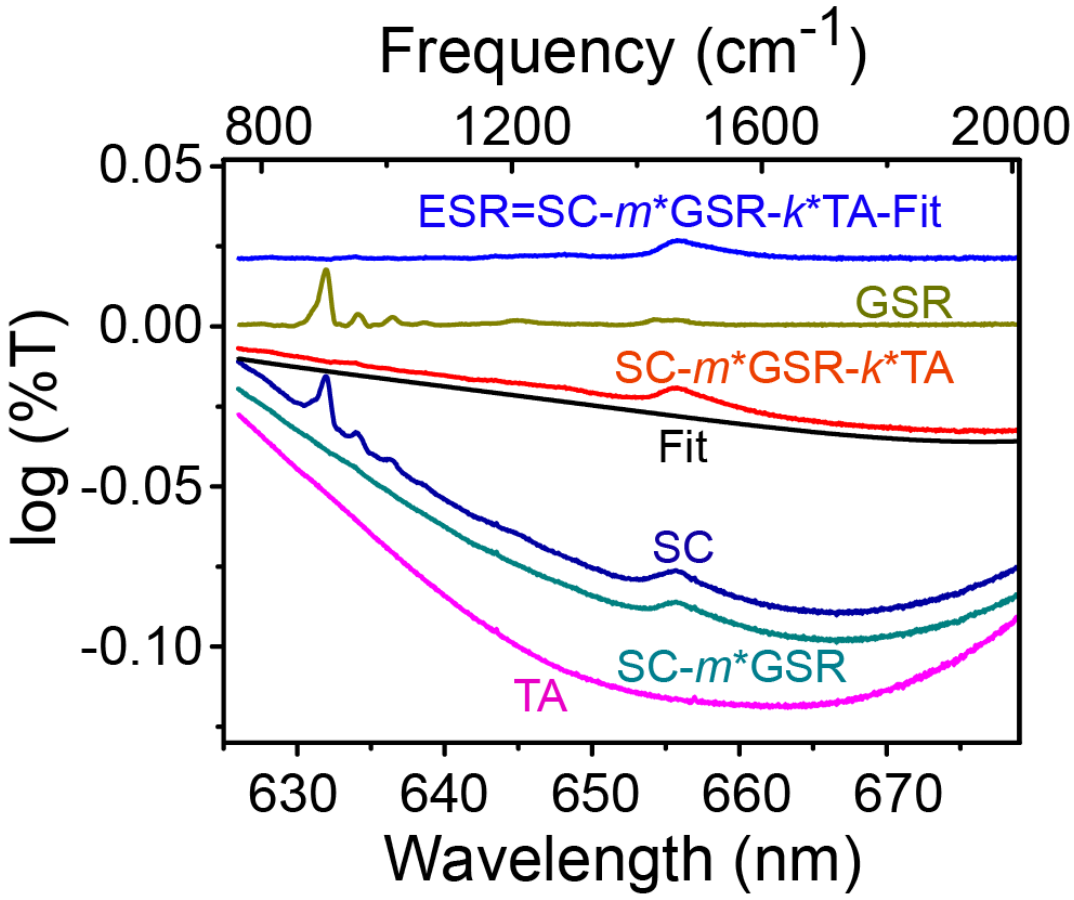

Figure 4.1: Representative FSRS data acquired with PCMT and an illustration of spectral analysis for isolating excited-state Raman features. Spectra have been offset for clarity.[35] Transient absorption (TA), ground-state Raman (GSR) and synchronously chopped (SC) signals are obtained experimentally as described in the text. *m* and *k* are scalars for subtraction of GSR and TA signals contributing to SC, and "Fit" refers to a polynomial baseline fit applied to account for low-frequency base-line modulation. Procedures for isolating excited-state Raman (ESR) features are outlined in the text.

4.3.3 FSRS signal analysis procedures.

Three-pulse FSRS spectra contain contributions from multiple spectroscopic signals.[36,37] Steps involved in processing spectra to isolate excited-state Raman features are described below and are illustrated graphically in Figure 4.1.

Our analysis begins with the synchronously chopped (SC) spectrum (dark-blue curve, Fig. 4.1), which contains five signal contributions: Solvent and polymer GSR, polymer ESR, Raman-pump induced modulations in transient absorption (TA), and other signals from nonlinear processes. In a first step we remove ground-state Raman signal contributions (dark-yellow curve, Fig. 4.1). Formally, these should include non-resonant GSR from both solvent and polymer. GSR signals from PCMT are negligible compared to solvent bands at the Raman-excitation wavelengths used in transient measurements,[35] and we therefore assume that pump induced changes in the non-resonant polymer GSR is negligible compared to ESR contributions. We remove GSR contributions from the SC spectra through scaled subtraction; the scaling factor, *m*, is optimized in order to remove the THF solvent peak appearing at 914 cm^{-1}, specifically.

The difference spectrum (SC-*m**GSR, light-blue curve in Fig. 4.1) obtained through this procedure contains primarily ESR and broad background signal. Most of the latter originates from Raman-pump-induced depletion of the excited-state transient absorption;[36,37] thus, the TA signal collected simultaneously in this optical window provides a first-order approximation for the shape of the broad baseline and can be used

to remove much of the baseline by scaling with an appropriate factor (denoted as k). The result of scaled subtraction of the TA signal is shown in red in Fig. 4.1. From here we assume that the contribution to the background from other nonlinear processes can be approximated with a polynomial. In total, excited-state Raman spectra were obtained using the formula:

$$\mathrm{ESR} = \mathrm{SC} - m*\mathrm{GSR} - k*\mathrm{TA} - \mathrm{Fit} \qquad (4.2)$$

Spectral regions where there are no significant ESR signals (below 1150 cm^{-1} or above 1650 cm^{-1}) were utilized to arrive at the best polynomial fit for the residual baseline. The values of k and polynomial parameters that yield the minimum sum of residual squares in these regions were deemed to provide the best baseline correction.

The time-dependent value of m provides an internal standard for the effective Raman-pump intensity and can be used to correct the intensities of ESR features after their isolation. Values of m were found to range between 0.7 and 1 at both Raman probe wavelengths and were used to correct time-resolved FSRS intensities on picosecond timescales. The time-dependent values of k provide a measure of excited-state depopulation induced by interactions with the Raman-excitation pulse. At 840 nm the value of k was found to be roughly constant near 0.85. At 600 nm k started at ~1 and dropped through actinic pump-probe delays that are within the duration of the Raman-excitation pulse, but held between 0.4 and 0.5 on delays of picoseconds to tens of picoseconds. As variation in k suggests variation in excited-state population available to

probe by FSRS, we have only examined the time-dependence of FSRS signal intensities for $\Delta t > 2$ps where k is relatively constant and have only examined the time-dependence of peak positions and shapes on faster timescales. A plot of time-dependent values m and k is provided in the supplemental materials.[35]

Our primary concern in this work is the wavelength- and time-dependent frequency of the C=C stretching band, the most intense band observed in the excited-state Raman spectra. It is important to note that alternate analysis procedures were also used to double-check that time-dependent frequency shifts in Raman spectra were not artifacts from the procedure described above.[35] Importantly, all methods applied give comparable results, with absolute peak positions negligibly affected by choice of analysis procedure and revealing the same wavelength- and time-dependent trends. These similarities indicate that quantitative conclusions we draw from our data are robust and are not tied to details of our analysis procedures.

4.3.4 Computational Methods.

A small set of DFT calculations were performed to support interpretation of spectra. All calculations were carried out in the Gaussian 09 software package.[38] All geometry optimizations were performed without symmetry constraints and utilized the 6-31g(d) basis set[39,40] along with the range-corrected CAM-B3LYP density functional.[41] Range-corrected functionals are necessary to correctly describe the Raman dispersion

effect with increasing oligomer length.[42] All calculations were performed in vacuum. Stable geometries were verified by vibrational analysis that returned zero normal modes with imaginary frequencies. Reported vibrational frequencies are unscaled. The in-phase and out-of-phase C=C backbone stretches were identified by the distinctive intense Raman signal of the in-phase mode in conjunction with visual inspection of the normal mode motions using the Jmol software package.[43] Vertical electronic excitation energies and geometry-relaxed (optimized) excited singlet states were determined using time dependent density functional theory (TD-DFT), although vibrational analysis of the geometry optimized excited states could not be performed analytically or numerically as a result of the computational cost. Images of optimized geometries were generated using the Molekel version 5.4.0.8 software package.[44]

4.4 Results

4.4.1 Steady-state spectroscopy of PCMT.

To our knowledge, the photophysics and spectroscopy of PCMT have not been characterized, and we therefore present the steady-state absorption and Raman spectroscopy of this polymer – with instructive comparisons to related oligomers and polymers – prior to presenting results of time-resolved absorption and Raman measurements.

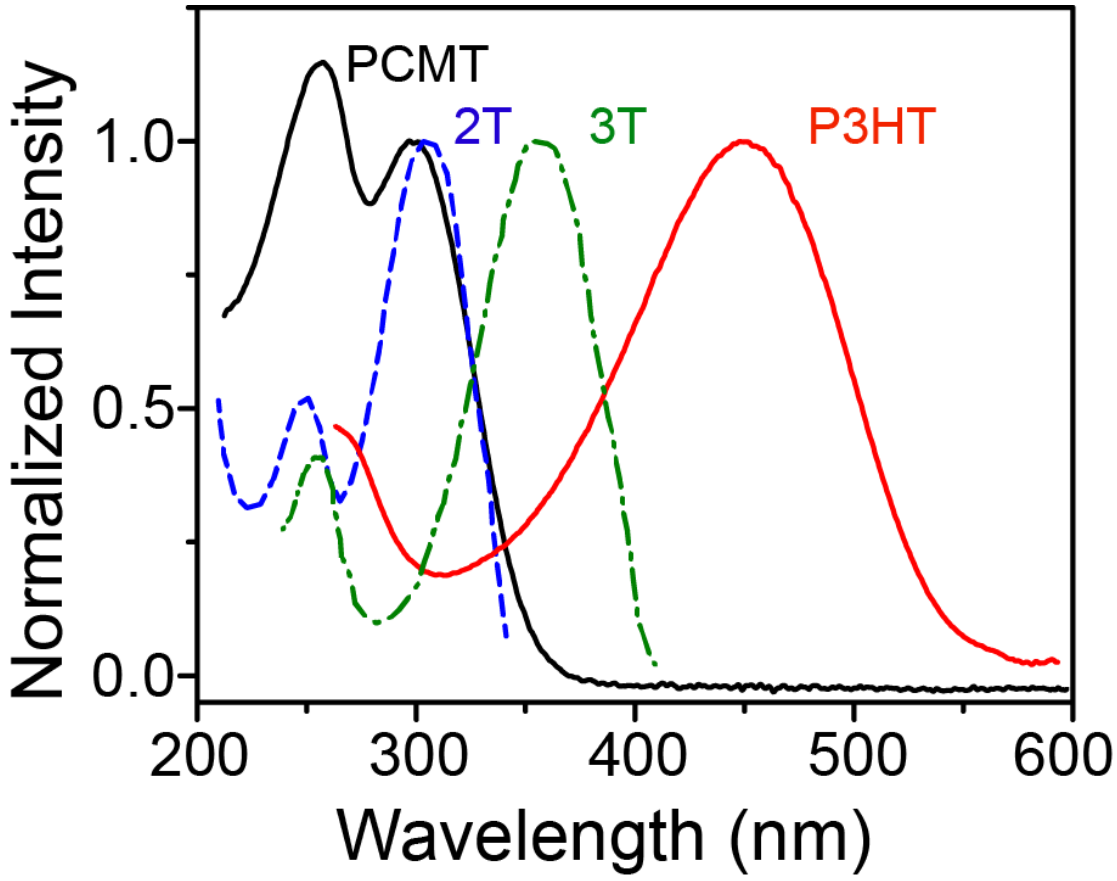

Figure 4.2: Steady-state absorption spectra of poly-(3-cyclohexyl-4-methylthiophene) (PCMT) in THF, dithiophene (2T) and terthiophene (3T) in dioxane, and regioregular poly-(3-hexylthiophene) (RR-P3HT) in chlorobenzene. 2T and 3T spectra were taken from reference [20]. Spectra are normalized to the peak of the lowest-energy transition for clarity.

Figure 4.2 compares the steady-state UV/Vis absorption spectrum of PCMT dissolved in THF with spectra of dithiophene (2T) and terthiophene (3T) in dioxane, as well as RR-P3HT in chlorobenzene. UV-Vis data for the oligothiophenes were digitized from reference.[20] Two features can be identified in the spectrum of each species; these include a low-energy band with a peak position dependent on the identity of the species, and a high-energy feature that appears near 250 nm for all systems. The lower-energy feature corresponds with the lowest energy π-π^* (S_0-S_1) transition.[20,45] The peak positions of the low-energy transition (ground-state absorption, or GSA) for these species are summarized in Table 1 together with GSA peak positions for quaterthiophene (4T), quinquethiophene (5T) and sexithiophene (6T).[20] It is well known that the GSA red-shift with oligomer length can be rationalized using a free-electron model,[20,45,46] which treats the π electrons of the conjugated systems as a one-dimensional free-electron gas (i.e. "particle in a box") that extends along the length of the oligomer chain. Based on the size-dependence of the electronic band gap of oligothiophenes, it has been estimated that the effective chromophore or conjugation length (the dominant segment length prepared via excitation) of RR-P3HT is ~7-10 monomers.[20] On the contrary, a similar comparison based only on length dependence of the chromophore (Fig. 4.2 and Table 4.1) suggests that the effective conjugation length of PCMT is on the order of 2 -3 monomers.

Table 4.1: Peak positions for ground-state absorption (GSA), ground-state Raman (GSR, singlet transient absorption (STA), and triplet transient absorption (TTA) of PCMT, P3HT, and various oligothiophenes in solution.

	2T	3T	4T	5T	6T	P3HT	PCMT
GSA/nm	306	355	392	414	435	455	298
GSA/eV	4.05	3.49	3.16	3.00	2.85	2.73	4.16
GSR (C=C)/cm^{-1}	-----	1463	1465	1467	1469	1475	1506
STA/nm	495	600	710	845	900	>1100	660
TTA/nm	-----	460	560/595	630	680	885	580

GSA, STA, and TTA peak positions for 2T-6T were taken from reference.[20] The STA and TTA peak positions of RR-P3HT is taken from reference.[12] GSR peak positions of oligothiophenes are from reference.[47]

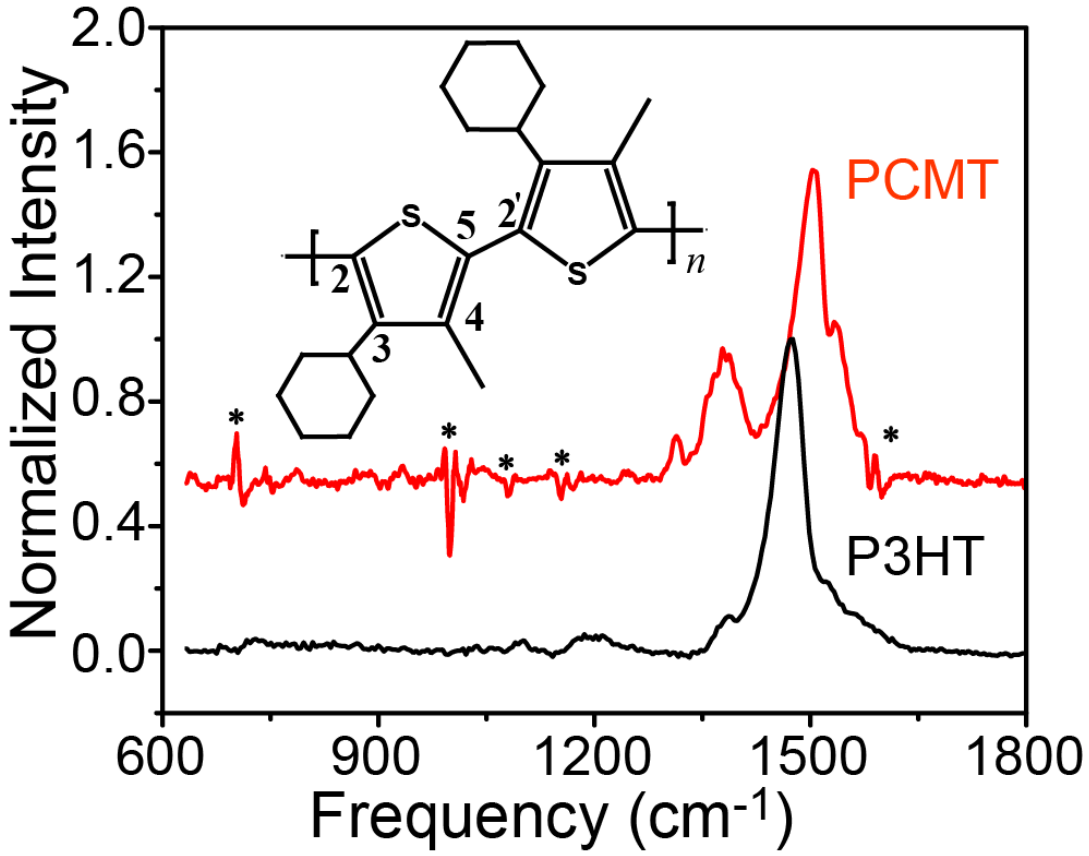

Figure 4.3: Ground-state Raman (GSR) spectra of PCMT and RR-P3HT. Spectra were collected using 400 nm and 480 nm Raman excitation for PCMT and RR-P3HT, respectively. Asterisks denote artifacts from the subtraction of solvent bands. Spectra have been normalized to the peak of the in-phase C=C stretching feature and the GSR spectrum of PCMT is offset for clarity. The inset shows the structure of a dimeric unit of PCMT with labeled carbon sites.

Figure 4.3 compares the ground-state Raman spectra of PCMT and RR-P3HT. Mode-specific assignments for features in both spectra are based on those described in references.[12,26] The dominant feature at 1475 cm^{-1} for RR-P3HT is assigned to the in-plane, in-phase C=C ring stretching mode, whereas the weaker features at 1380 and 1525 cm^{-1} correspond with C_3-C_4 intra-ring and out-of-phase C=C stretching of thiophene units (see Fig. 4.3 inset for carbon positions). For PCMT, features associated with the C=C in-phase and out-of-phase stretching modes appear at 1506 and 1534 cm^{-1}, respectively, as does an intra-ring C-C stretch at 1380 cm^{-1}. A weak feature appears near 1200 cm^{-1} for P3HT and corresponds with the inter-ring C_2-$C_{5'}$ stretch; in contrast, no clear feature can be distinguished from the baseline in this region for PCMT in light of features from solvent-subtraction appearing in the same region and the lower signal-to-noise ratio.

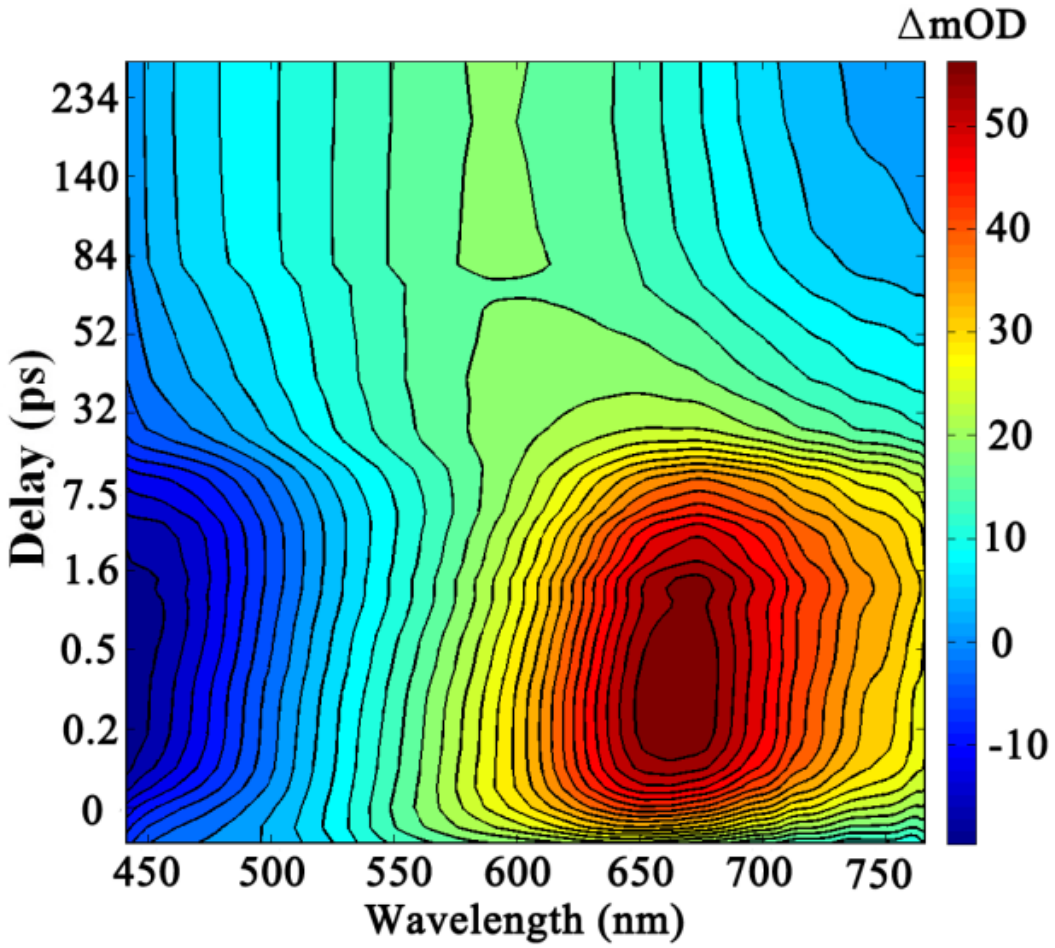

Figure 4.4: Transient absorption spectroscopy (TAS) of PCMT in THF probed at visible wavelengths following photo-excitation at 320 nm.

4.4.2 Excited-state dynamics of PCMT probed with broadband TAS.

Transient spectral dynamics of PCMT were initiated with a photoexcitation (actinic) wavelength of 320 nm in order to cleanly excite only the lowest-energy electronic transition of the polymer (see Fig. 4.2). Figure 4.4 illustrates the transient spectral dynamics of PCMT as probed via absorption at visible wavelengths; this plot shows spectral evolution against a non-linear time axis in order to highlight the spectral evolution that dominates each time regime of excited-state relaxation.

Throughout the first 20 ps that follow photoexcitation the transient spectrum of PCMT can be characterized as the superposition of a negative feature below 520 nm and a positive band that peaks around 660 nm. Because the ground-state absorption of PCMT falls much further to the blue (Figure 4.2, solid black line), the negative band appearing in the transient spectrum must correspond with stimulated emission (SE) from the transient excited state rather than a bleach of the ground-state absorption. On the other hand, the positive band corresponds with a transition to a higher-lying excited state of the polymer. Two distinct spectral dynamics associated with these features are apparent from Figure 4.4: (1) Disappearance of these features with the concomitant appearance of a broad and weaker absorption peaking at 600 nm on a 10s of picoseconds timescale, which signals decay out of the initially prepared excited state; and (2) an initial shift in the transient spectrum of the photoprepared excited state on sub-ps to picosecond timescales.

4.4.2.1 Intersystem crossing dynamics.

The spectral evolution occurring on longer timescales (process 1 listed above) is similar to what has been observed previously in picosecond time-resolved studies of excited oligothiophenes:[20,48-50] For oligomers, spectral evolution over tens to hundreds of picoseconds is dominated by the disappearance of the singlet transient absorption (STA) and SE bands and the appearance of a broad absorption centered at shorter wavelengths that is attributed to a triplet transient absorption (TTA); assignment of this weaker band to a triplet state is predicated on its sensitivity to the presence of common triplet quenchers.[20] Peak wavelengths for STA and TTA of various oligothiophenes are listed in Table 1 along with the peak positions of transient spectra observed for PCMT in Fig. 4.4. This similarity with the spectral dynamics of oligothiophenes indicates that the photophysics of the lowest singlet excited state of PCMT is dominated by intersystem crossing to a longer-lived triplet level.

To further characterize these dynamics we have analyzed the excited-state spectral evolution over time delays > 4 ps using principle component (PCA) and global target analysis.[51,52] Figure 4.5(a) plots spectral cuts from Fig. 4.4 at selected delays after 4 ps (solid lines). Spectra collected on times below 4 ps were excluded from this analysis in order to eliminate the influence of fast spectral shifting (process 2 above) on these analyses. PCA was used to determine that only two significant components contribute to the spectral evolution over this time regime, which is consistent with the presence of

the isosbestic point at 585 nm in Fig. 4.5(a). Global target analysis was then applied using a sequential, two-state kinetic interconversion model (S_1 triplet) in order to obtain the S_1 lifetime, t_{S1}, and spectra of the two photophysical species. Importantly, only t_{S1} was adjusted to fit the data in a least-squares minimization of the differences between the model and data. The spectra of the two photophysical components obtained from global target analysis are plotted in Figure 5(b). Dashed lines in Fig. 5(a) plot the reconstructed time-dependent spectra obtained using this simple kinetic model, the associated component spectra, and the value of t_{S1} that minimizes the sum of squared residuals with the experimental data. Time-dependent intensities at selected probe wavelengths are plotted in Figure 5(c), along with curves corresponding with the kinetic interconversion model applied (solid lines); we have plotted these on a logarithmic time axis to highlight the quality of the fits over the entire range of delays. The fit to the data on these timescales is quite good, and yields an S_1 lifetime of 25.6 ps. The component spectra of the singlet and triplet obtained are similar to corresponding spectra for oligomers.[35]

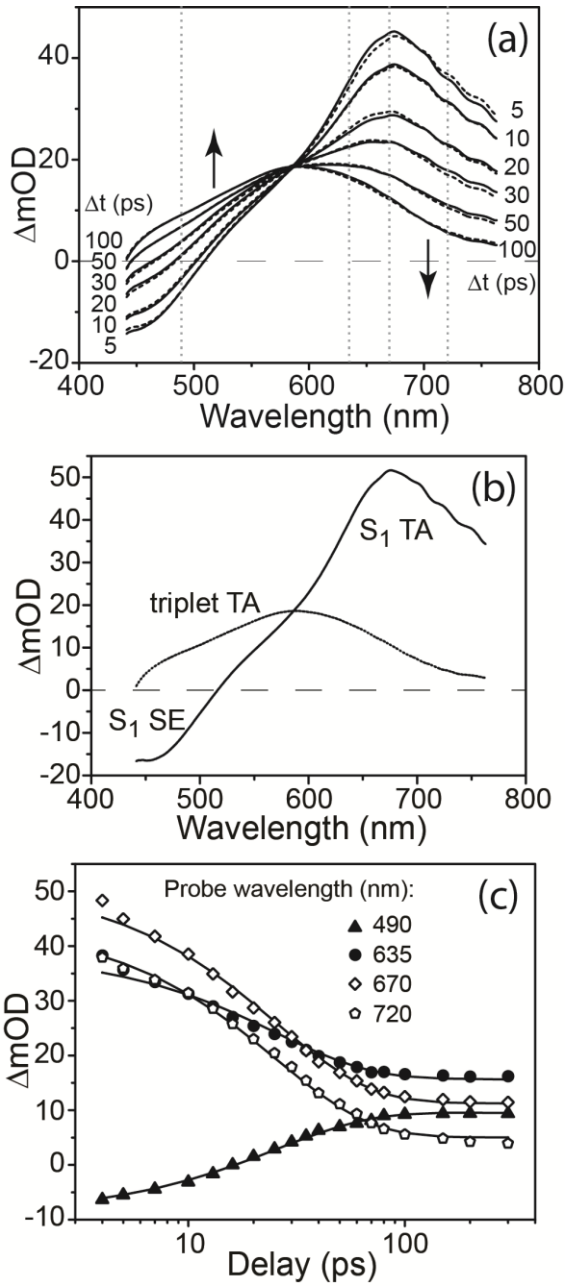

Figure 4.5: Global target analysis of PCMT transient absorption on times > 4 ps. (a) Experimental spectra (solid lines) compared to spectra obtained via fitting to a kinetic interconversion model (black dashed lines). (b) Component spectra obtained from global target analysis: S_1 transient absorption and stimulated emission, and triplet transient absorption. (c) Transient absorption (symbols) with fits to kinetic model (solid lines) at the selected wavelengths denoted with gray dotted lines in panel (a); data are plotted logarithmically with time to demonstrate the quality of the kinetic fit over all timescales.

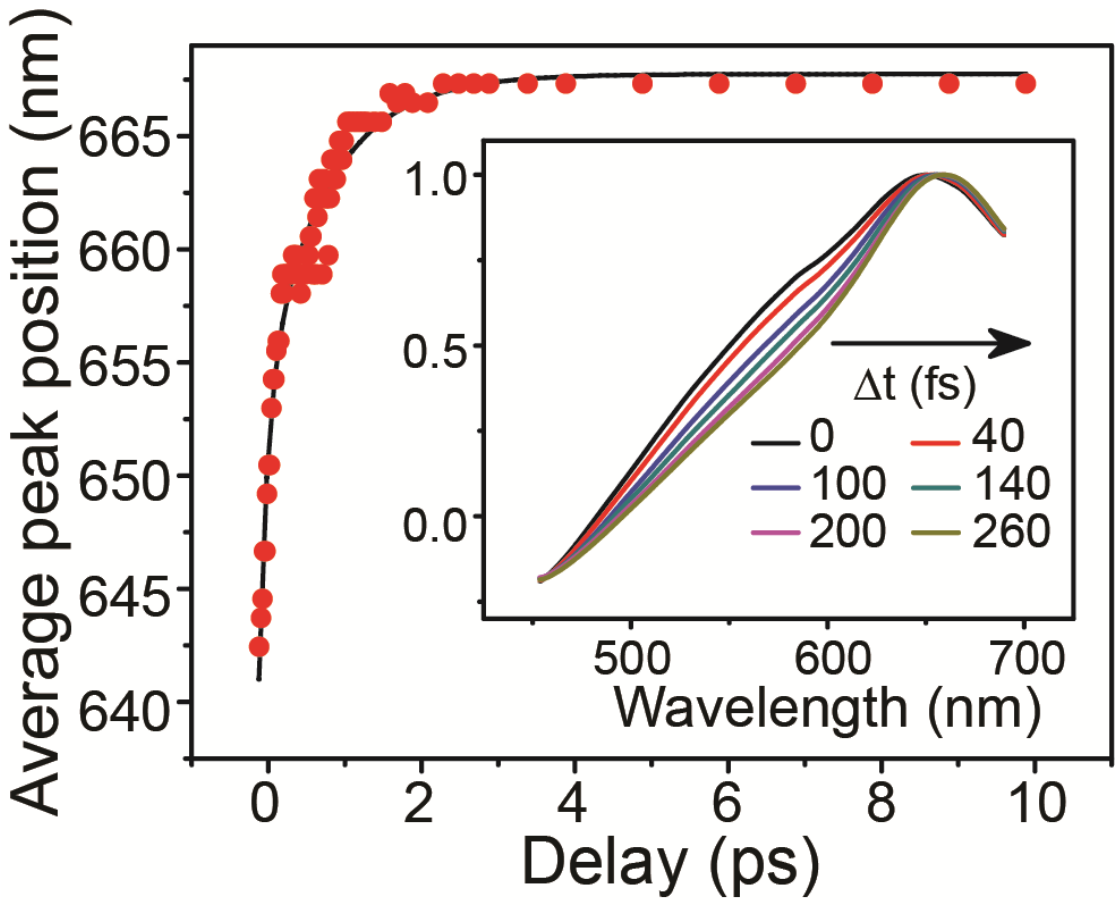

Figure 4.6: Time-dependent shift in the S_1 transient absorption peak position; the solid line corresponds with a biexponential fit to the peak position explained in the text (t_1=110 ± 20 fs, t_2=800 ± 100 fs). (*inset*) Peak-normalized pump-probe spectra of PCMT illustrate spectral evolution occurring over the first few hundred fs.

4.4.2.2 Ultrafast TA spectral relaxation.

On much shorter timescales, transient spectral features from the photoprepared singlet excited state are observed to red-shift by ~25 nm during the first several hundred femtoseconds after excitation. This fast evolution is most apparent in Figure 4.6 (inset), in which the transient singlet spectra measured over the first 260 fs have been normalized such that they have the same peak intensity. The time-dependent peak position of the singlet absorption band is plotted up to the first 10 ps after excitation. Experimental data has been fitted using a bi-exponential function with two relaxation timescales:

$$\lambda_{peak}(t) = \Delta\lambda_1 \exp\left(-\frac{t}{\tau_1}\right) + \Delta\lambda_2 \exp\left(-\frac{t}{\tau_2}\right) + \lambda_{peak}^{final}. \qquad (4.3)$$

A fit to this function yields two relaxation timescales, 110 ± 20 fs and 800 ± 100 fs (fit shown with a dashed line).

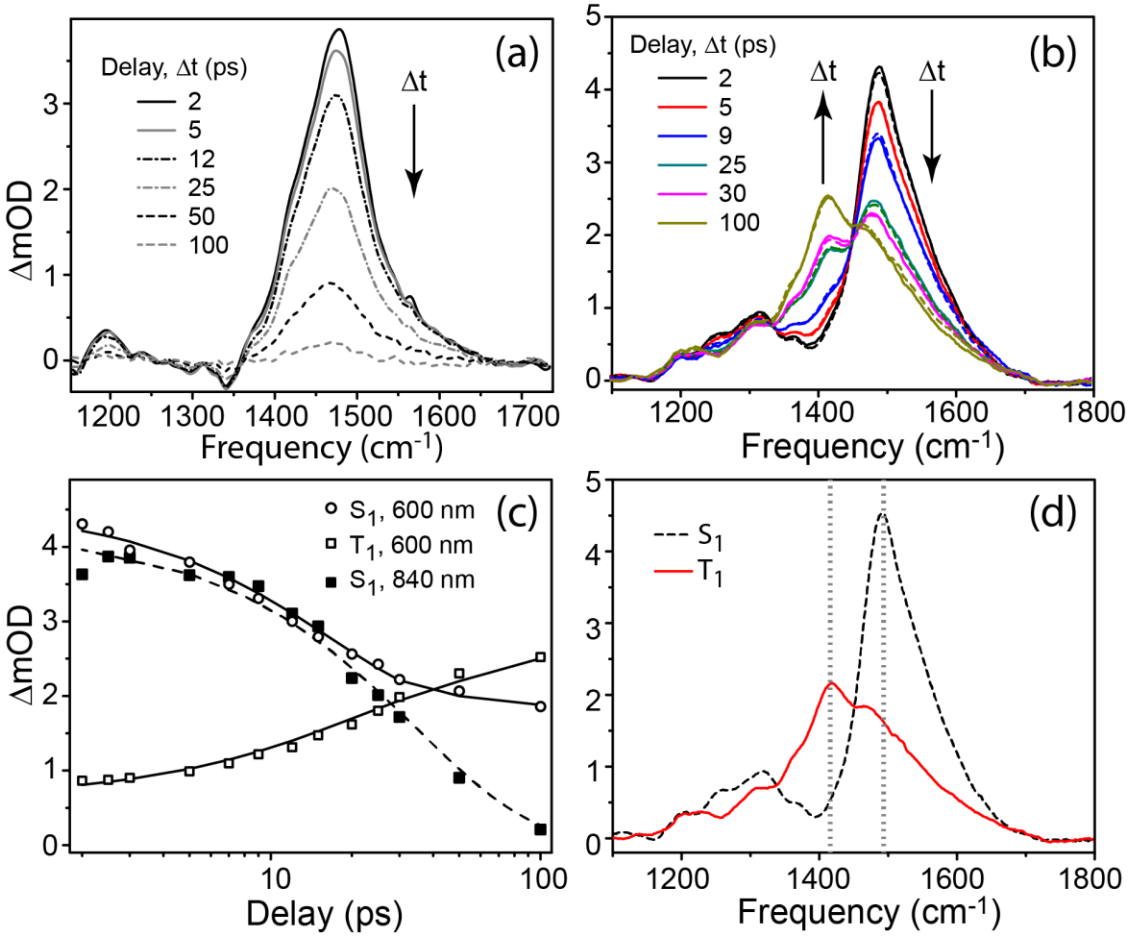

Figure 4.7: Time-resolved resonant-Raman spectroscopy of PCMT in THF. (a) 840-nm Raman excitation selectively probes S_1 PCMT. (b) 600-nm Raman excitation probes both the S_1 and triplet states: Data, solid lines; fits from global analysis, dashed lines. (c) Time-dependence of peak intensity of S_1 and triplet features. Solid lines correspond with best-fit kinetic model obtained by global target analysis of data in (b); the dashed line corresponds with a single-exponential fit of Raman signal decay at 840-nm excitation. (d) Component S_1 and triplet Raman spectra obtained from global analysis of transient Raman probed via 600-nm Raman excitation.

4.4.3 Excited-state relaxation of PCMT probed with FSRS.

4.4.3.1 Intersystem crossing.

On longer time delays (t > a few picoseconds), excited-state Raman spectroscopy provides a complementary probe of ISC that follows the photoexcitation of PCMT.

Figure 4.7 presents time-dependent excited-state Raman spectra obtained with (a) 840 and (b) 600 nm Raman-excitation pulses following 320-nm excitation of PCMT. Transient absorption of the singlet extends into the near IR (not shown in Figs. 4.4 and 5(a)),[35] whereas the TTA band is limited to the visible region of the spectrum; thus Raman excitation at 840 nm enables state-selective interrogation of the photoprepared singlet state via resonance enhancement. Figure 4.7(a) demonstrates that the resonance enhanced Raman at 840 nm gives rise to a single set of Raman features that decay with delay following the photopreparation of the excited singlet state. In contrast, Raman excitation at 600 nm enables resonance enhancement with both the STA and TTA bands, and thus probes vibrational signatures of both the singlet and triplet states through the course of ISC. Spectra collected with 600-nm Raman excitation for representative delays > 2ps are plotted in Figure 4.7(b) (solid lines). Much like absorption transients shown in Figure 4.5, Raman transients exhibit signatures of a kinetic interconversion, with an isosbestic point appearing near 1460 cm^{-1}.

We have applied global target analysis to the time-dependent Raman spectra obtained with 600-nm resonant excitation; the kinetic model applied here was identical to that used

in our analysis of TAS data. Dashed lines in Fig.7(b) correspond with the reconstructed time-dependent spectra obtained with a two-component model, with Raman spectra for the singlet and triplet states plotted in Figure 4.7(d). Minimizing the sum of residuals squared resulted in a t_{S1} of 18 ps, which is somewhat faster than that obtained from TAS data. Temporal cuts through the time-dependent spectra taken near the peaks of the singlet and triplet features at 1493 and 1421 cm^{-1}, respectively, are plotted in Figure 4.7(c) (open symbols) along with the best fit curves obtained through global target analysis. The time-dependent intensity of the singlet vibrational spectrum obtained using 840-nm Raman excitation is also plotted in this panel (solid circles); fitting these to an exponential decay gives a singlet decay timescale of 33 ± 2 ps.

The discrepancies in intensity-dependent decay amongst all three measurements (1 TAS and 2 FSRS) could be associated with inaccuracies in the estimation and subtraction of baseline contributions to regions congested with broad Raman features or variations in the excited-state population available to probe due to interactions with the Raman-pump pulse. One might also expect that an all-parallel FSRS geometry would result in faster decay lifetimes compared to magic angle TAS, as the FSRS geometry will be sensitive to time-dependent evolution in polarization anisotropy. This could explain the faster decay of FSRS signal at 600 nm, and the differences between the decay rates observed at the two Raman excitation wavelengths could be due in part to energy transfer between low- and high-energy sites along the polymer (see Discussion). However, we also anticipate

that the ensemble of S_1 PCMT created via 320-nm photoexcitation should be characterized by a distribution in delocalization lengths (see Discussion), such that this discrepancy in lifetimes quite likely reflect the selectivity with which resonance Raman interrogates sub-populations characterized by different conjugation lengths and ISC rates. Indeed, the S_1 lifetime measured using only near-IR TAS (830-1100 nm) is 32 ± 1 ps, compared to 25.6 ps in the visible region.[35] Nevertheless, these various pieces of time-dependent data provide a consistent picture of the excited-state relaxation of the initially prepared excited singlet of PCMT via intersystem crossing.

The spectra plotted in Figure 4.7(a,b,&d) share many similarities with Raman spectra of polythiophenes in their ground and excited states. Feature assignments can be made through comparisons with the PCMT ground-state Raman spectrum, the P3HT excited-state Raman spectrum, and the Raman spectra of oxidized thiophenes.[12,26,53] For the singlet excited-state, the feature at 1490 cm^{-1} can be attributed to C=C stretching; this feature is quite broad and asymmetric in shape, and likely includes contributions also from intra-ring C-C stretching at frequencies slightly to the red of the peak and (intra-ring) out-of-phase C=C stretching at slightly higher frequencies (see Fig. 4.3). Raman features near 1200 cm^{-1} are attributed to inter-ring stretches. Raman intensity also appears near 1300 cm^{-1}; the relative intensity appears to decrease when probing via low-energy Raman excitation, although this may be (in part) due to differences in quality of the baseline removal in this region of the spectrum. The C=C stretching region of the triplet

is red-shifted considerably relative to that of the singlet. Peak positions are consistent with so-called "quinoidal" stretching frequencies observed in the Raman spectra of oxidized polythiophenes.[53]

4.4.3.2 Ultrafast nuclear dynamics.

Whereas time-dependent Raman spectra measured on time delays of picoseconds provide a complementary perspective on the ISC dynamics captured via TAS, evolution of Raman spectra on ultrafast timescales provide a new perspective on the nuclear dynamics that accompany the initial relaxation of the polymer after excitation. Figure 4.8 plots Raman spectra collected at delays within the first 200 fs after photoexcitation for the two Raman excitation wavelengths. Spectra have been normalized to the peak of the C=C stretching feature in order to directly compare peak positions and feature shapes. At both excitation wavelengths the peak position of the Raman features is observed to redshift over the first 150 fs. Furthermore, the band in the C=C stretching region is observed to narrow considerably on this same timescale when probing via resonance at 600 nm (Figure 4.8(a)).

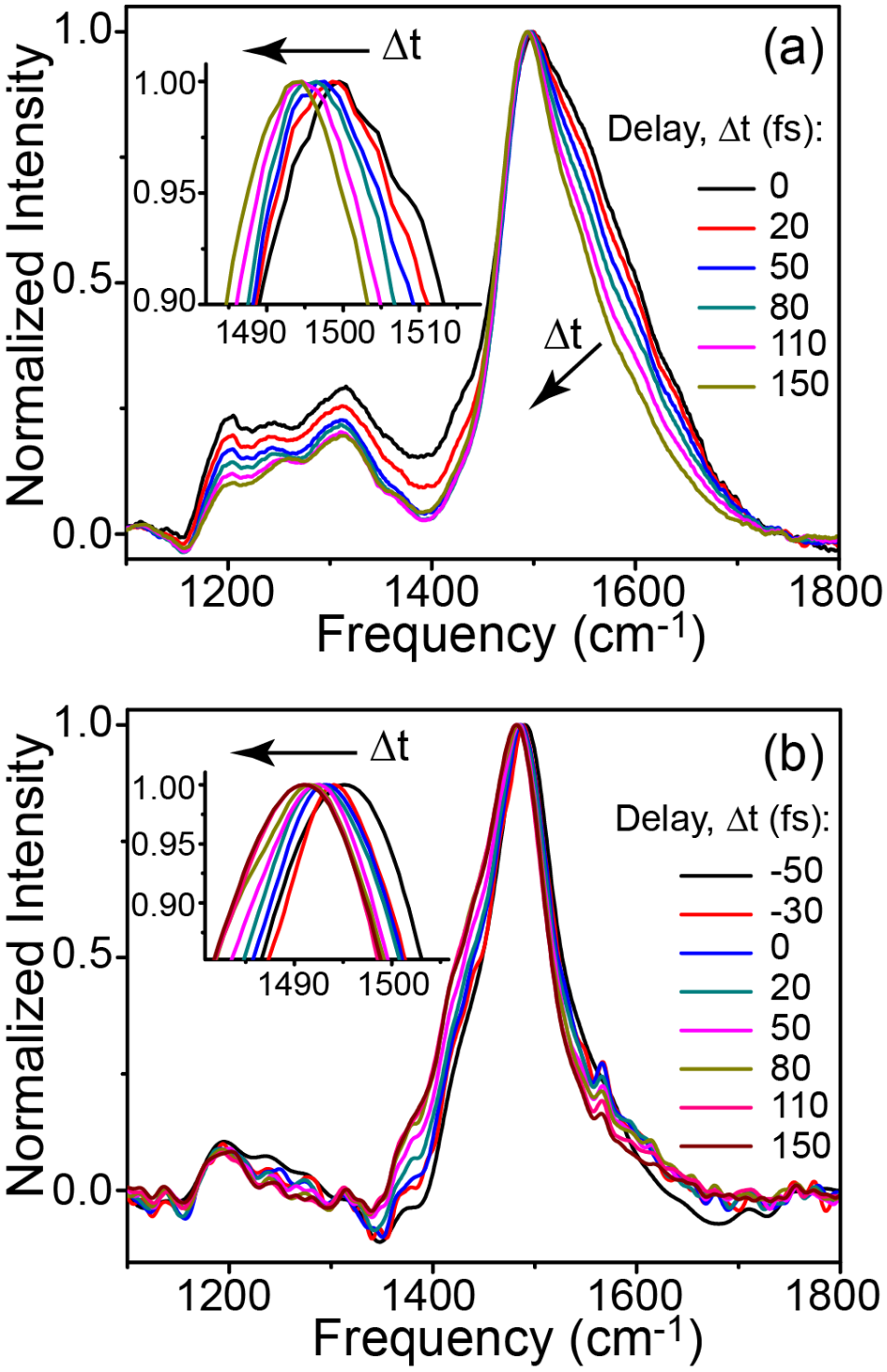

Figure 4.8: Ultrafast evolution in Raman features of S_1 PCMT after 320-nm excitation. (a) 600-nm and (b) 840-nm Raman excitation. (*insets*) Blow-up of the C=C peak-shift with delay.

Figure 4.9(a) summarizes the time-dependence in the peak positions of C=C stretching bands measured at the two Raman-excitation wavelengths. In order to rule out the possibility that the specifics of the baseline subtraction procedure influences the extracted peak positions, we have verified that these trends are still observed when minimal data processing is applied.[35] Results obtained using both methods are almost identical, demonstrating that spectral manipulations required for analysis do not affect the position assignments. In fact, the trends in peak position are discernible directly from raw FSRS data.

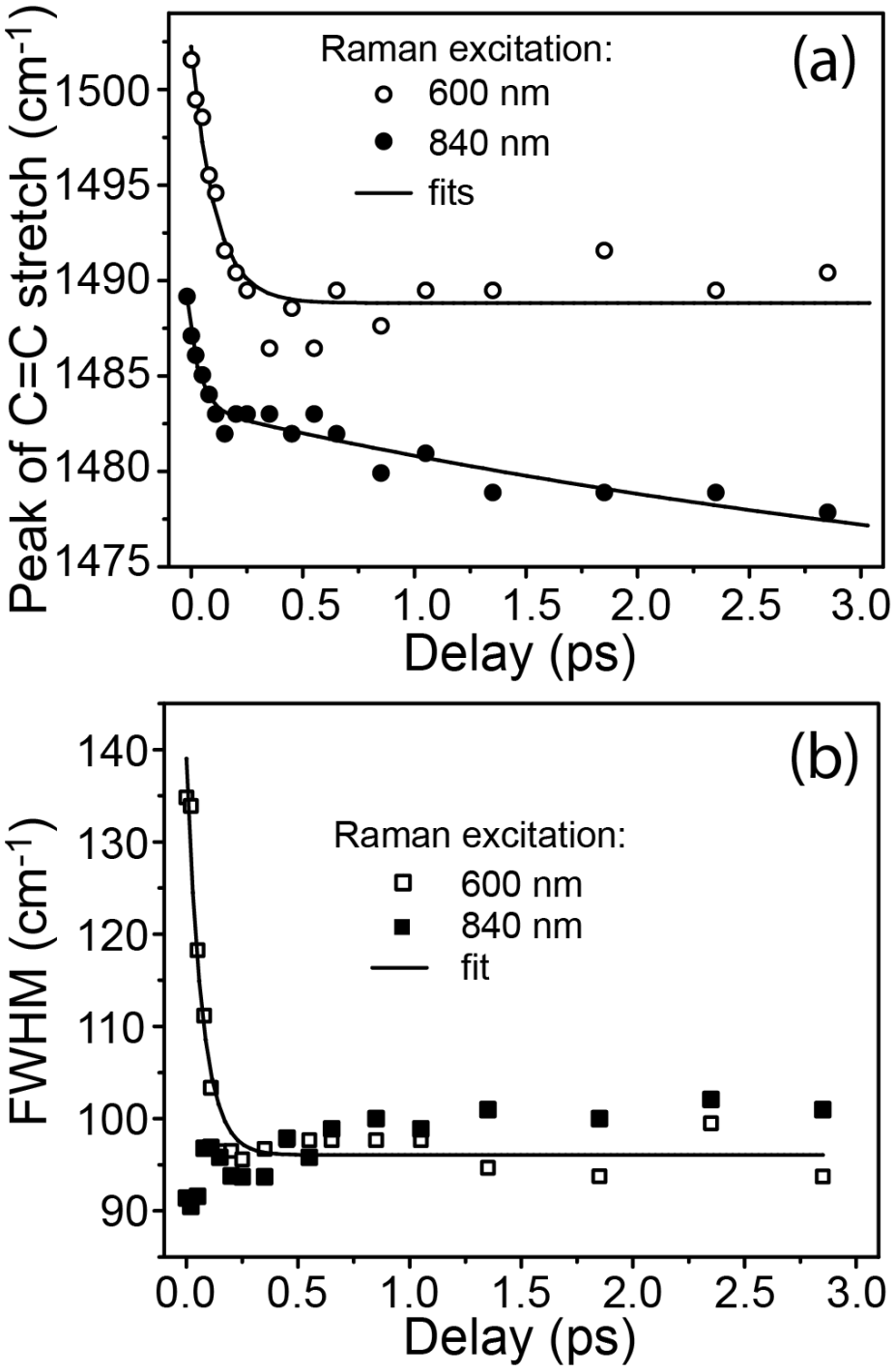

Figure 4.9: Spectral evolution in the C=C stretching region for S_1 PCMT after 320-nm excitation. (a) Time-dependent Raman peak position as probed via 600 nm and 840 nm Raman excitation. (b) FWHM of the C=C stretching region.

The excited-state Raman peak positions presented in Figure 4.9(a) exhibit two behaviors. Firstly, a shift in the C=C stretching frequency is identified between spectra collected at the two Raman excitation wavelengths at any given delay, with the stretching frequency falling ~10-15 cm^{-1} lower when probing with a lower Raman-excitation energy. A second observation is that the peak positions shift to lower frequency with time at both Raman excitation energies. The Raman frequency probed via 600-nm Raman excitation exhibits a 110 ± 10 fs shifting timescale while the C=C frequency probed with 840 nm shifts on two timescales at 80 ± 20 fs and 2.2 ± 0.5 ps; these timescales were determined by fitting the peak position to mono- and biexponential shifting function similar to Equation 5.

Figure 4.9(b) plots the time-dependent evolution in the width of the band in the C=C stretching region. Time-dependence in the FWHM of the C=C stretching bands shows contrary behavior at the two excitation wavelengths: The bandwidth decreases over the first ~200 fs when probed via a 600-nm excitation pulse, but is roughly constant under 840-nm Raman excitation. In order to verify that these changes are real and not an artifact of baseline subtraction, spectra were analyzed with an alternative baseline-correction method.[35] The evolution in feature bandwidth measured with 600-nm Raman excitation occurs on a timescale of 90 ± 10 fs timescale (fit with a solid line in Fig. 4.9(b)), which is similar to timescales obtained for the shift in peak position. Figure 4.8(a) demonstrates that this evolution in bandwidth occurs from changes to the band

shape on the blue side of the spectrum between 1500 and 1650 cm^{-1}, which overlaps the region of the C=C in-plane out-of-phase stretching mode.

4.5 Discussion

4.5.1 Steady-state spectroscopy and the ground-state geometry of PCMT.

A comparison of the absorption spectrum of PCMT in its ground state with the spectra of oligothiophenes (Fig. 4.1 and Table 4.1) predicts an effective delocalization length for its ground state of 2-3 monomer units. A critical caveat about this comparison is that the substituents and associated steric interactions between monomer units in the polymer can be expected to influence ring-to-ring dihedral angles and should give rise to a larger vertical gap to the potential-energy surface of the quasi-planar excited-state in the Franck-Condon region when compared to unsubstituted oligothiophenes.[54,55] Explained at the level of the free-electron model, an increase of dihedral angle will increase the energetic asymmetry between the limiting valence-bond structures and thus the periodic potential that describes the degree of bond-length alteration.[46]

In order to qualify how much the dihedral angle influences the vertical excitation energy, we have calculated the lowest vertical transition energy for bithiophene at various dihedral angles. The ground state geometry was first optimized in the gas phase and a dihedral angle (C_3-C_2-$C_{5'}$-S, following the labels in Figure 4.3) of 26.1° was obtained at the minimum-energy geometry, which is very close to published experimental and theoretical results.[56-58] Constrained optimizations were then performed with the dihedral angle fixed to several different values, with corresponding energy gaps ($S_1 \leftarrow S_0$) determined at the TD/CAM-B3LYP/6-31G(d) level of theory. Results of these

calculations are summarized in Table 4.2 and illustrate that the band gap of 2T increases by ~1eV when the dihedral angle is modified from 0 to 75°. This dependence on torsion dihedral is comparable to the difference in energy gap between oligomers in this size regime (e.g. 2T vs. 3T),[20] and thus we can conclude that an effective conjugation length of 2-3 monomers is not highly dependent on the torsional order of the polymer. Compared with oligothiophenes and P3HT, the dihedral angle of PCMT can be expected to be larger due to large steric interactions between the substituents on adjacent thiophene rings. Indeed, a ground-state geometry optimization of a 3-cyclohexyl,4-methylthiophene dimer (2-CMT) using these same calculation methods predicts a torsional dihedral of 82°. Such an extreme dihedral angle for PCMT would explain the slightly larger transition energy for PCMT (4.16eV) compared to 2T (4.05eV).

Table 4.2:. S_1 vertical transition energy of 2T as a function of inter-ring dihedral angle.

Dihedral	$S_1 \leftarrow S_0$ (eV)
0°	4.353
26.1°	4.507
50°	4.836
75°	5.353

Steady-state Raman measurements reveal a significant shift in the in-phase C=C stretching frequency between PCMT and P3HT. Another critical difference is the relative intensity of the in-phase and out-of-phase C=C stretching features. DFT calculations were undertaken with simple oligomer analogues of P3HT and PCMT in order to relate these observations to differences in molecular structure. These analogues included a tetramer of 3-methylthiophene (3′,3″,3‴,3‴-tetramethyl-2,2′:5′,2″:5″,2‴-quaterthiophene, herein referred to as 4-MT), serving as a computationally tractable model of P3HT, and a tetramer of 3,4-dimethylthiophene (3,3′,3″,3‴,4,4′,4″,4-octamethyl-2,2′:5′,2″:5″,2‴-quaterthiophene, herein referred to as 4-DMT), serving as a model for PCMT. Key results from these calculations are reported in Table 4.3.

Table 4.3: DFT-calculated inter-ring dihedral angle (θ), in-phase C=C stretching frequency, and out-of-phase/in-phase C=C stretch intensity ratios for quaterthiophene analogues of P3HT and PCMT.

	Θ	**C=C stretch (cm^{-1})**	**$I_{out\text{-}of\text{-}phase}/I_{in\text{-}phase}$**
4-MT	32°	1568	0.114
4-DMT	73°	1605	0.197

The effect of the second methyl substituent on the ground-state tetramer structure is readily apparent, with the average inter-ring dihedral angle (θ) increasing by 40° from 4-MT to 4-DMT. The large dihedral angle for 4-DMT is also consistent with the large dihedral for 2-CMT mentioned above. Comparing the calculated Raman spectra of 4-DMT to 4-MT, the in-phase C=C stretch blue-shifts by ~40 cm^{-1} and the relative intensities of the out-of-phase to the in-phase C=C stretching mode increases from ~10% to ~20% with the introduction of the second methyl group on each monomer. Both findings are consistent qualitatively with Raman spectra previously calculated for 7T at various dihedral angles.[27] These calculated trends agree qualitatively with differences in the ground-state Raman spectroscopy of P3HT and PCMT. This implies that the larger steric interactions in PCMT increases the ground-state dihedral angle relative to P3HT and is responsible for both the increase in the in-phase C=C stretching frequency and the intensity increase in the out-of-phase C=C mode relative to the in-phase stretch.

We have also calculated the optimized geometries for the S_1 excited states of 4-MT and 4-DMT in order to determine the magnitude of planarization that should be expected upon photoexcitation. For 4-MT the dihedral angle decreases from 32° to fully planar 0.0°, while for 4-DMT the dihedral angle decreases from 73° to 23°.[35] This implies that the magnitude of geometric relaxation after excitation in PCMT is considerably greater than in P3HT, and any experimental features arising from this relaxation should be more pronounced in PCMT as compared to P3HT.

4.5.2 Intersystem crossing in PCMT.

The relatively fast ISC kinetics observed here following photoexcitation of PCMT are similar to the electronic relaxation dynamics of short oligothiophenes,[20,50,59-61] but contrast with the much slower ISC kinetics for P3HT and other polyalkylthiophenes with substituents only located at the C_3 location.[12] For oligothiophenes the rate of ISC has been observed to decrease substantially as the oligomer length is increased.[20] This variation in rate has been attributed to length-dependence in the relative energetics of states in the triplet and singlet manifolds modulated by state-to-state spin-orbit couplings between the S_1 and triplet levels:[45,61] At very short oligomer lengths (2T and 3T), the S_1 state lies relatively close energetically to higher-lying triplet states ($>T_1$) that couple strongly to the excited singlet, giving rise to correspondingly faster ISC rates. ISC occurs on a timescale of ~50 ps for 2T, for which the lowest-lying excited singlet state is roughly isoenergetic with the T_2 level. In contrast, the S_1 level falls below the T_2 level for terthiophene.[61] Excitation-dependent ISC lifetimes were measured for 3T, decreasing from 126 to 51 ps between 400 and 374 nm,[60] as were energy-dependent triplet yields;[50] these results suggest increased singlet-triplet coupling as excitation tunes towards the higher-lying triplet level.[50] As the oligomer length is increased further (>4), the S_1 level drops even further below these triplet levels, and ISC rates occurring over several hundred ps or longer.[20,59] These variations in ISC rate with oligomer length may also be intimately tied to a length dependence of the intermonomer dihedral angle, which is

thought to increase at smaller oligomer lengths. Such a relationship is well-known and supported by recent work with substituted phenylthiophenes that has demonstrated that ISC rates are directly sensitive to torsional dihedral angle.[62]

The ISC lifetime measured for PCMT is somewhat shorter than that of 2T in solution, further suggesting that the effective delocalization length of the relaxed exciton in PCMT is on the order of 2-3 monomer units. More importantly, the substantially faster rate relative to other polythiophenes reflects that the relative energetics and/or coupling between singlet and triplet manifolds are highly sensitive to the torsional dihedral angle. Although the concept of an "effective conjugation length" provides a zeroth-order picture of localized states along conjugated polymers, delocalization length and energetics in polymers is not by nature limited by the physical length of the molecule as it is for oligomers. Thus, the observation of fast ISC dynamics in PCMT is a strong indicator that torsional conformation truly plays a significant role on ISC dynamics in oligo- and polythiophenes.

4.5.3 Variations in excited-state delocalization observed with transient absorption and wavelength-dependent Raman spectroscopies

Comparisons of transient absorption spectra obtained for PCMT with those of oligothiophenes in their relaxed excited states enables consideration of the extent of delocalization in polymer excited states. Excited-state peak positions of oligomer and

polymer transient bands are summarized in Table 4.1.[20,35] For oligomers the STA peak position shifts from 495 nm to 900 nm and the TTA peak position shifts from 460 nm to 680 nm as the chromophore length is increased from 2 to over 6 monomers. STA and TTA spectra of PCMT overlap with spectra of oligothiophenes over a range of lengths. Using a band-gap argument similar to that applied to the ground-state absorption spectrum of PCMT, one would estimate an effective conjugation length for relaxed singlet PCMT to be 2-5 monomers at 1 ps and a triplet conjugation length of 3-6 monomers at 1 ns. This comparison suggests that an ensemble of delocalization lengths are created after photoexcitation of PCMT, although the precise distribution in delocalization length for the ensemble of photoexcited PCMT cannot be assessed quantitatively from comparisons with unsubstitued thiophene oligomers for the same reasons described above in Section 4.1.

As illustrated in Figures 4.8 and 4.9(a), the C=C stretching frequency measured for the relaxed PCMT excited state is dependent on the Raman-excitation wavelength. This likewise reflects that a distribution of excited-state delocalization lengths is prepared via photoexcitation, as C=C stretching frequencies and intensities are known to be directly sensitive to the extent of delocalization along the backbone of conjugated oligomers and polymers.[32,33,47,63] The most general explanation for length-dependent Raman frequencies is given by the Effective Conjugation Coordinate (ECC) Theory,[32,63] which describes how delocalization across multiple monomers influences the frequency of the

so-called "conjugation coordinate," $\mathit{Я}$, which corresponds with the change in molecular geometry between limiting valence structures (such as benzoidal and quinoidal resonance structures for oligo- and polythiophenes) and which also coincides with C=C in-phase stretching. The vibrational force constant along the conjugation coordinate (and hence the C=C stretch) is influenced by coupling of modes and is thus sensitive to delocalization of electron density between monomer units: Delocalization gives rise to vibrational coupling between monomers both locally and non-locally, and has the net effect of softening the force constants for vibration along the conjugation coordinate, thus reducing the vibrational frequency of the C=C stretch.

Raman frequency "dispersion" amongst oligothiophenes of various lengths in their ground states is virtually non-existent,[47] as monomer aromaticity effectively pins electron density locally and limits delocalization in the ground state.[33] However, we expect that there should be considerable Raman frequency dispersion with variation in the effective delocalization length of excited states as these states are highly delocalized by nature. In polymers, excited states are effectively localized within finite segments of the extended polymer framework that may vary in length, conformation, or structure at different sites.[16] Thus, wavelength-dependent resonant Raman frequency dispersion provides a probe of the relative delocalization of excitons within an ensemble of excited polymers.

Based on the wavelength-dependence of the C=C stretching frequency from our

measurements, it is clear that 600-nm and 840-nm Raman excitation interrogate excited-state sub-populations characterized by somewhat different degrees of delocalization. Furthermore, the direction of the shift in Raman frequency is consistent with the variation in effective conjugation that can be deduced from comparisons to the vertical excitation energies of oligomers: Higher-energy Raman excitation probes sub-populations characterized by shorter effective conjugation length and low energy Raman excitation probes excitons with longer conjugation lengths. Thus, our Raman measurements indicate that the excited-state population of PCMT exhibits a distribution of conjugation lengths that underlie the broad width of the transient absorption.

Probe-dependent S_1 decay rates measured with TAS and FSRS are yet another reflection of the distribution in excited-state delocalization generated via excitation of an ensemble of PCMT in solution: A somewhat longer lifetime of 32 ± 1 ps is obtained from the decay of near-IR absorption transients compared to the findings from TAS data obtained by probing at visible wavelengths (Fig. 4.5);[35] this slightly longer lifetime matches that obtained from decay of Raman signals probed via 840-nm excitation. As described above, ISC rates are highly sensitive to delocalization length amongst small thiophene oligomers. Given the similarities between PCMT and oligothiophene photophysics, we expect that a distribution of delocalization lengths within PCMT would exhibit a corresponding variation in S_1 decay rate via ISC. As longer probe wavelengths (or Raman excitation wavelengths) interrogate longer conjugation lengths, we expect that

the observed ISC rate should be slower when measured in these regions relative to a region of shorter wavelengths, explaining the wavelength-dependent ISC rates obtained from both our Raman and TAS measurements.

Finally, we note that the distribution in effective delocalization lengths in PCMT and the potential for energy transfer between them may explain differences observed in the FSRS signal decay measured at 600 and 840 nm using an all-parallel polarization geometry: Raman excitation at 600 nm presumably interrogates shorter conjugation lengths from which energy transfer would originate; thus the somewhat faster FSRS signal decay relative to the magic angle TAS may reflect contributions from both population and polarization anisotropy decays. The 840-nm FSRS signal decays much more slowly with the same all-parallel polarization geometry, with a lifetime that matches the NIR decay measured by TAS at magic angle to within experimental error. This may reflect that the polarization anisotropy has been randomized at longer probing wavelengths as a consequence of energy transfer to these sites.

4.5.4 Ultrafast relaxation of S_1 PCMT from TA and Raman spectral dynamics.

The ultrafast TA spectral dynamics apparent in Figure 4.4 and 4.6, through which both the transient SE and absorption bands red-shift on sub-ps timescales, indicate that PCMT in its S_1 state undergoes fast nuclear relaxation following photoexcitation into its Franck-Condon region. The dynamic shift in the STA peak position is similar to the

spectral shifting dynamics observed with other polythiophenes shortly after photoexcitation,[3,4,10-12] although the overall timescale observed for PCMT is considerably faster, with no apparent relaxation on timescales of picoseconds. Nevertheless these spectral dynamics are consistent with both the resonant energy transfer and localized torsional relaxation mechanisms that have been invoked to explain relaxation on the picoseconds timescale. Given the highly twisted structure of the polymer noted above, we expect that there is likely to be a higher driving force for relaxation through both mechanisms, and thus a larger relaxation rate, for PCMT relative to less twisted polymers assembled from monosubstituted monomer units (e.g., P3HT).[11,23]

Spectral shifting on timescales ~100 fs also appears in our TAS data (within our experimental time-resolution), although it is difficult to ascribe this to specific nuclear relaxation mechanisms using the TAS data alone, although reports on other conjugated polymers attribute dynamics on similar timescales to torsional conformational relaxation out of the Franck-Condon region.[3,4,9] The ultrafast Raman data presented in Figures 4.8 and 4.9 provide a new experimental perspective on the nuclear dynamics that occur in the first 200 fs after photoexcitation: On the earliest time delays probed, C=C stretching frequencies are observed to red-shift at both Raman-excitation wavelengths on a timescale of ~100 fs (also comparable with our experimental time resolution). The direction of this frequency shift is consistent with the evolution expected as the inter-ring dihedral angle is reduced, as demonstrated through the ground-state C=C stretching

frequencies of variously substituted oligothiophenes in Table 4.3. Additionally, the change in spectral bandwidth (and shape) observed when probing via 600-nm Raman excitation is consistent with a time-dependent change in the relative intensities of the C=C out-of-phase and in-phase stretching bands over the first 150 fs following photoexcitation. The decrease in the relative intensity of the out-of-phase stretching band likewise indicates an evolution in the dihedral angle between monomers following photoexcitation in the direction of a more planar excited-state geometry along the polymer backbone. Given these observations, we believe that the ultrafast vibrational dynamics observed here are reflections of the nuclear distortions that enable ultrafast self-localization of the excited-state after photoexcitation. The trigger for self-localization is the relaxation from the ground-state geometry to a more planar configuration within a specific segment of the polymer.

It is interesting to note that the C=C stretching frequency as probed via 840 nm continues to evolve on a 2-ps timescale, whereas the frequency measured at 600 nm does not. Furthermore we do not observe the same evolution in band-shape at 840 nm as we do at 600 nm. These differences are most likely tied with the size and/or conformational selectivity of resonant Raman spectroscopy: As noted above, high-energy Raman excitation (600 nm) will selectively probe excitons characterized by a large vertical excitation gap, which would be associated with a shorter delocalization length and great degree of conformational disorder; lower Raman excitation energies, on the other hand,

interrogate excited regions characterized by greater delocalization and/or higher conformational order. The lack of significant changes in the band-shape at 840 nm indicates that this excitation wavelength already probes highly ordered states. On the other hand, as the vertical energy gaps for various effective conjugation lengths overlaps more appreciably at longer wavelengths,[35] the C=C stretching frequency probed via Raman excitation at 840-nm will be more sensitive to the slower phases of nuclear relaxation apparent in TAS data.

4.6 Conclusions

We have used a combination of transient absorption (TAS) and femtosecond stimulated Raman (FSRS) spectroscopies to interrogate the electronic and nuclear relaxation of excited-states of poly(3-cyclohexyl,4-methylthiophene), or PCMT. TAS measurements have revealed similar spectroscopic signatures to those previously attributed to exciton localization, relaxation, and singlet exciton decay in related photoexcited conjugated polymers and oligomers. On the other hand, ultrafast Raman measurements present new experimental signatures of ultrafast nuclear dynamics: Specifically, ultrafast shifting of the C=C stretching frequency and the relative intensity of in-phase and out-of-phase C=C stretching intensities provide a sensitive vibrational reporter on ultrafast (~100 fs) vibrational distortion associated with exciton self-localization or trapping. We have also demonstrated that the in-phase C=C stretching frequency provides a spectroscopic handle for interrogating the degree of delocalization in an ensemble of relaxed conjugated polymers in their S_1 excited state given the selectivity achieved via resonance enhancement. In sum, we have shown that time-resolved resonance enhanced Raman spectroscopy can be utilized as a sensitive probe of structural dynamics and structural variation within an ensemble of photoexcited conjugated polymers.

4.7 Supplementary Information

4.7.1 Chirp correction procedure for TAS

For chirp correction of TAS, chirp signals from the pure solvent samples (THF) are used as reference. The detailed steps are as follows: For each spectrum collected at a specific time delay, the highest and lowest peak positions are measured. The middle point between them from the rising edge (the long wavelength side of the peak) is the point that we need. Then we fit all the points of different delays using a polynomial, which will be used as the chirp correction line.

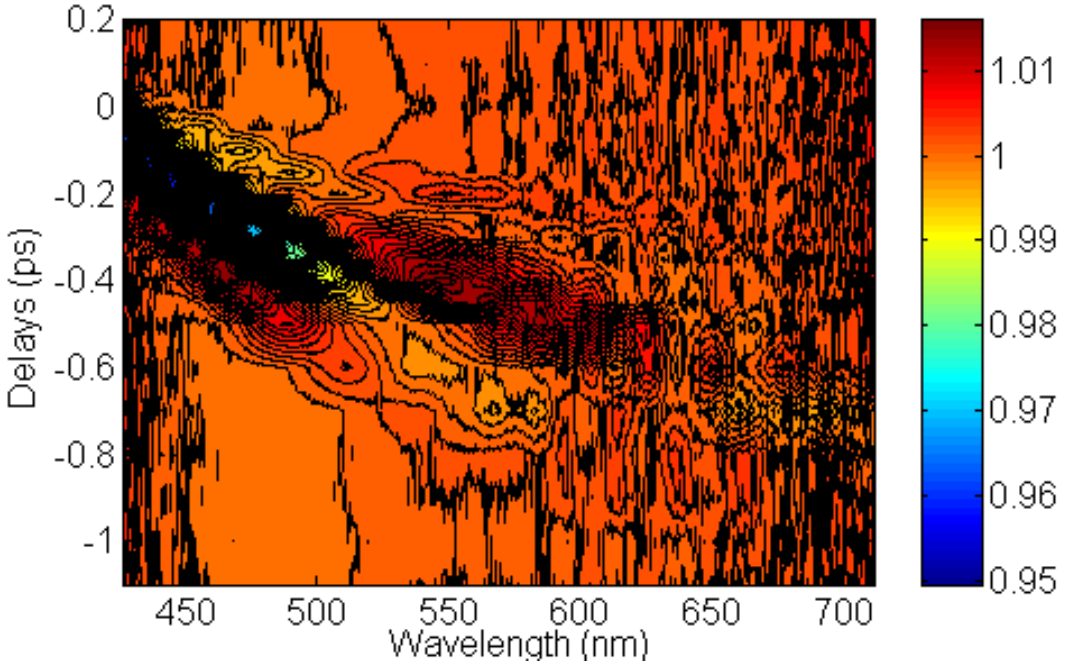

Figure 4.1S: Chirp signals collected under the same laser conditions as TAS. The sample is pure solvent (THF) and the path length is chosen to be the same as TAS.

4.7.2 Processing procedures for raw FSRS data

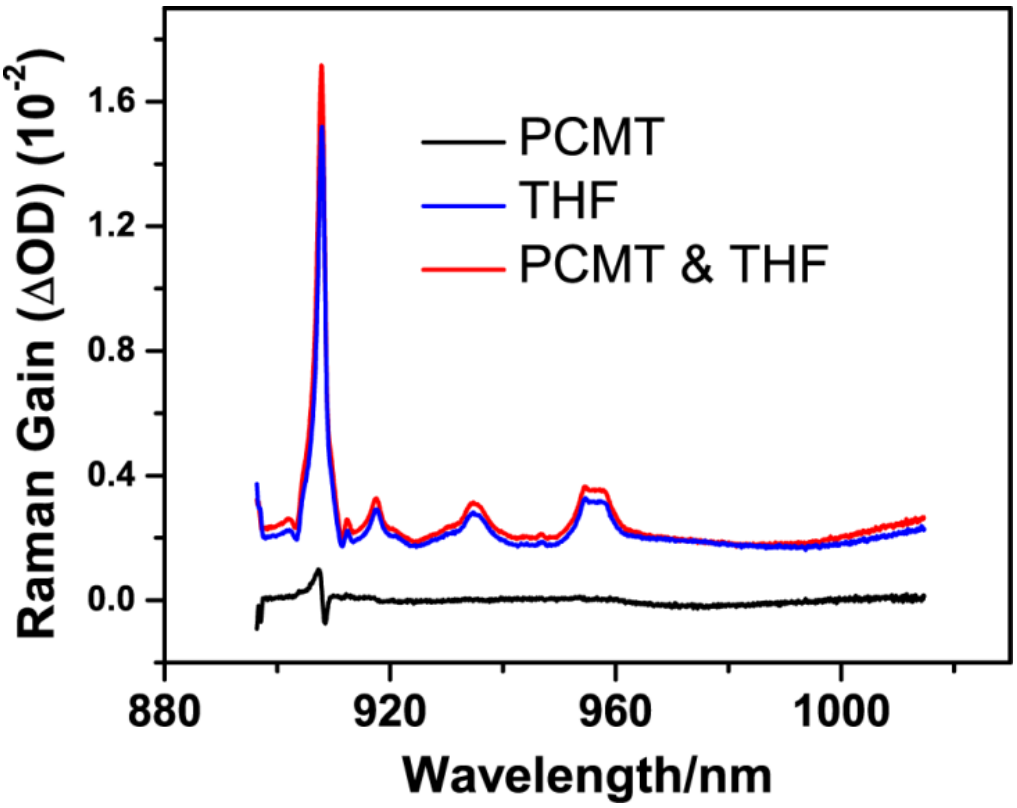

Figure 4.2S: Ground-state Raman spectra of PCMT and THF collected with 840-nm Raman excitation. As stated in the manuscript, ground-state Raman signals from the polymer are negligible compared to the GSR signal of the solvent.

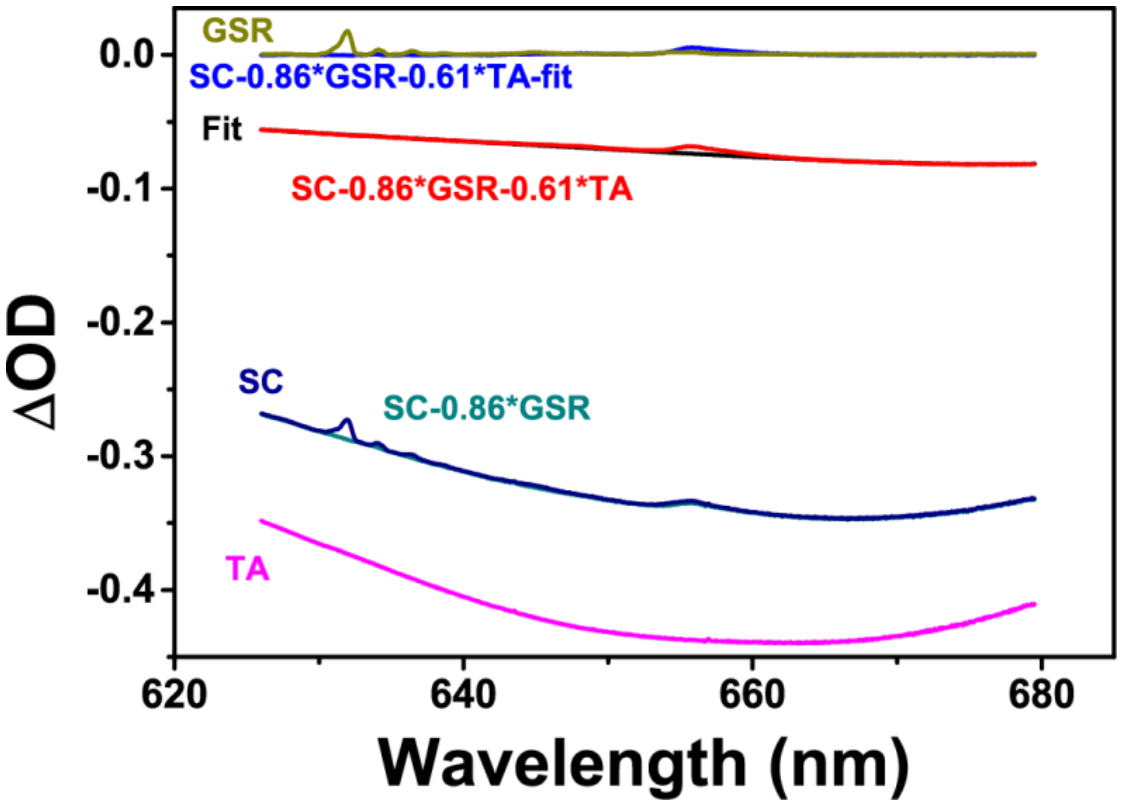

Figure 4.3S: Example of Raw signals obtained during FSRS measurements, including transient absorption (TA), ground-state Raman (GSR) and synchronously chopped signals (SC). Other labels refer to specific steps in the extraction of excited-state polymer Raman features from measured signals (see text).

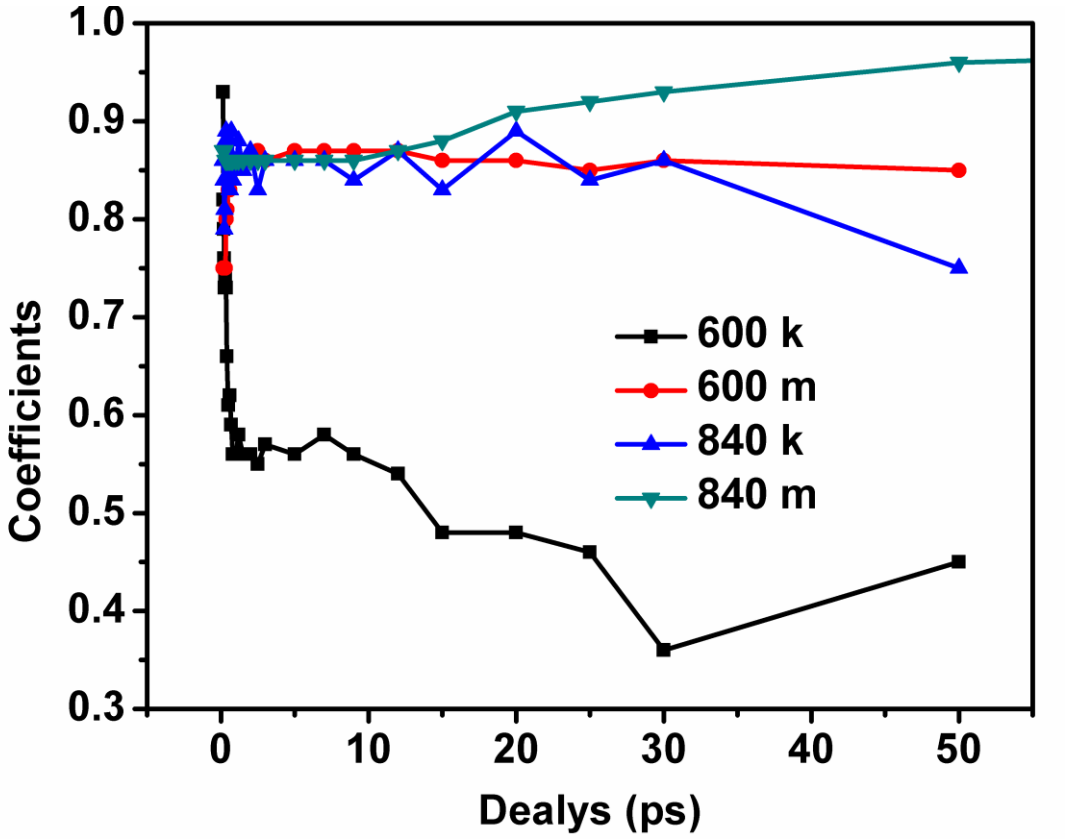

Figure 4.4S: The m and k values plotted for different delays. In the case of Raman signals collected using 840 nm Raman pump pulses, ESR signals are scaled by m for each delay in order to eliminate the change of effective Raman intensity.

Here we provide an explicit example of FSRS signal processing (refer to Figure 4.3S). Firstly, the GSR signal is removed from SC through scaled subtraction; the scaling factor, *m*, is optimized in order to remove the THF solvent peak appearing at 914 cm^{-1}. In Figure 4.3S, the scaling factor is $m = 0.86$. The resulted spectrum (SC-0.86*GSR) has a broad baseline due to Raman-pump modulation of the transient absorption as well as other nonlinear signals in addition to the desired ESR signal. Contributions due to modulation of TAS are removed through scaled subtraction of the TA signal. We change the TA scaling factor *k* from 0 to 1 with a step of 0.01 and fit the residual signal (SC-0.86*GSR-*k**TA) using a second order polynomial. The sum of squared residuals is calculated for each *k* and the best fit corresponds to the least sum in the regions of the spectrum that lack significant Raman features. Here $k = 0.61$. The final ESR spectrum is given by SC – 0.86*GSR – 0.61*TA – Fit. (Fit stands for the fitted second order polynomial).

4.7.3 Verification of time-dependent Raman frequency shifts with alternative spectral processing methods.

Procedurally, solvent Raman features were first removed by subtracting an attenuated ground-state Raman (GSR) spectrum from the synchronized chopped (SC) spectrum (this step is the same for the two methods) A scaled transient absorption (TA) spectrum was then subtracted from the each spectrum using the same scaling factor for each delay. The difference between these two methods is that the alternative signal processing method doesn't fit or subtract a polynomial baseline and the scaling factors for removing TA contributions are the same at all delays. Thus, variations in peak positions cannot be attributed to systematic errors in baseline subtraction.Peak positions were calculated after smoothing the spectra using fast Fourier transform (FFT) filter with a 6 points window. A comparison of time-dependent frequencies determined with both methods at the two excitation wavelengths are given in Figure 4.6S.

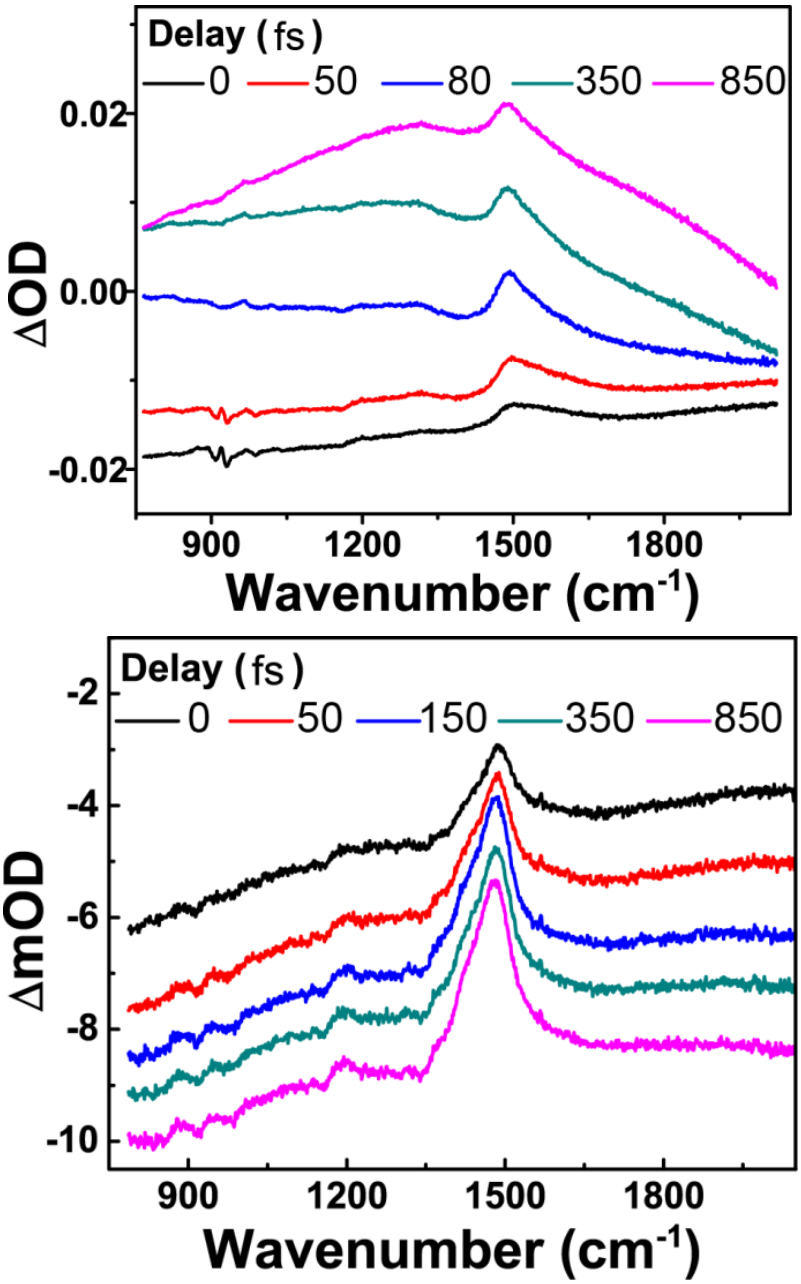

Figure 4.5S: Excited-state Raman spectra with minimal spectral decomposition. Spectra are offset for clarity. (Left) 600 nm Raman excitation. Spectra presented here are calculated according to formula: SC-GSR-TA*0.8, without smoothing. (Right) 840 nm Raman excitation. Spectra presented here are calculated according to formula: SC-GSR-TA*0.9, without smoothing.

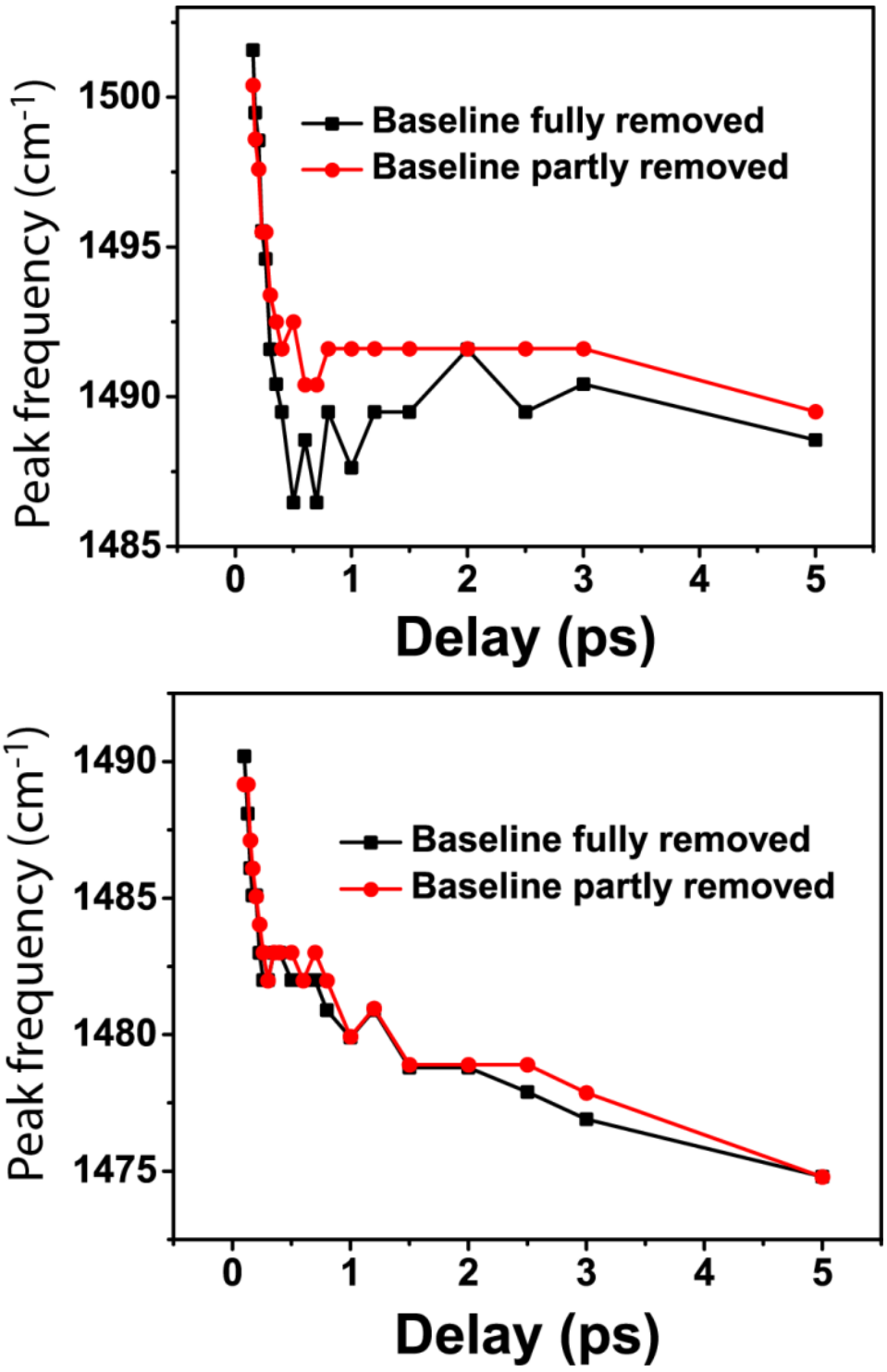

Figure 4.6S: Excited states Raman peak positions comparison between spectra with baseline fully removed (Figure 4.7, main text) and partly removed (Figure 4.5S).
(Left) Peak positions obtained with 600-nm Raman excitation. (Right) Peak positions obtained with 840-nm Raman excitation.

4.7.4 Ultrafast spectral dynamics in the C=C stretching region.

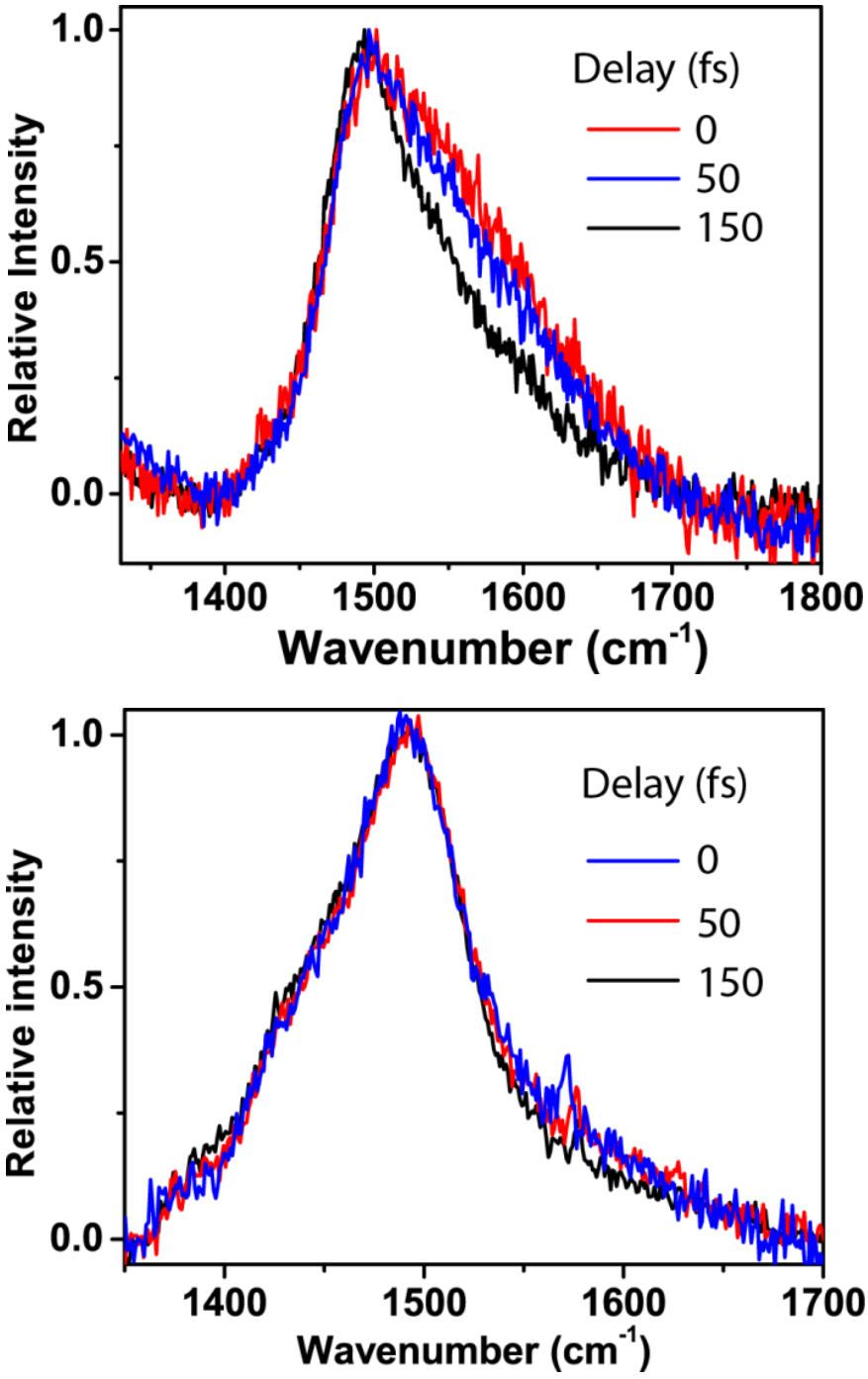

Figure 4.7S: Normalized Raman spectra focused on C=C stretching region using 600 nm (Left) and 840 nm (Right) Raman excitation. No spectral smoothing has been applied to demonstrate that variation in spectral bandwidth on the left is well-beyond measurement noise.

4.7.5 Comparison of PCMT and oligomer excited singlet and triplet TA spectra.

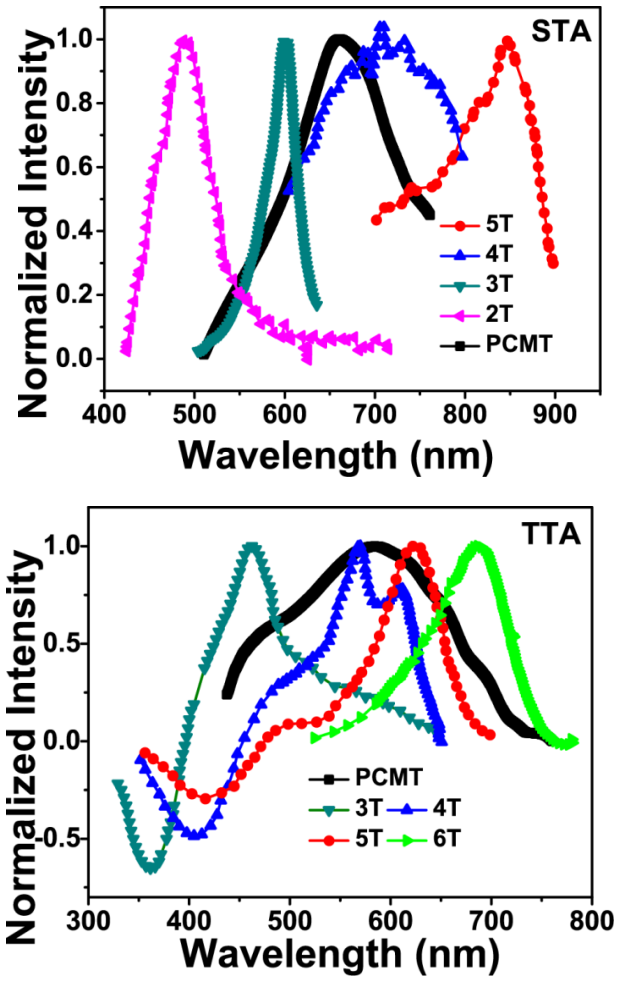

Figure 4.8S: STA and TTA spectra of PCMT, 2T, 3T, 4T and 5T. Oligothiophene spectra were taken from Reference 18 of the main text.

4.7.6 PCMT S_1 relaxation probed by TAS at 840 nm

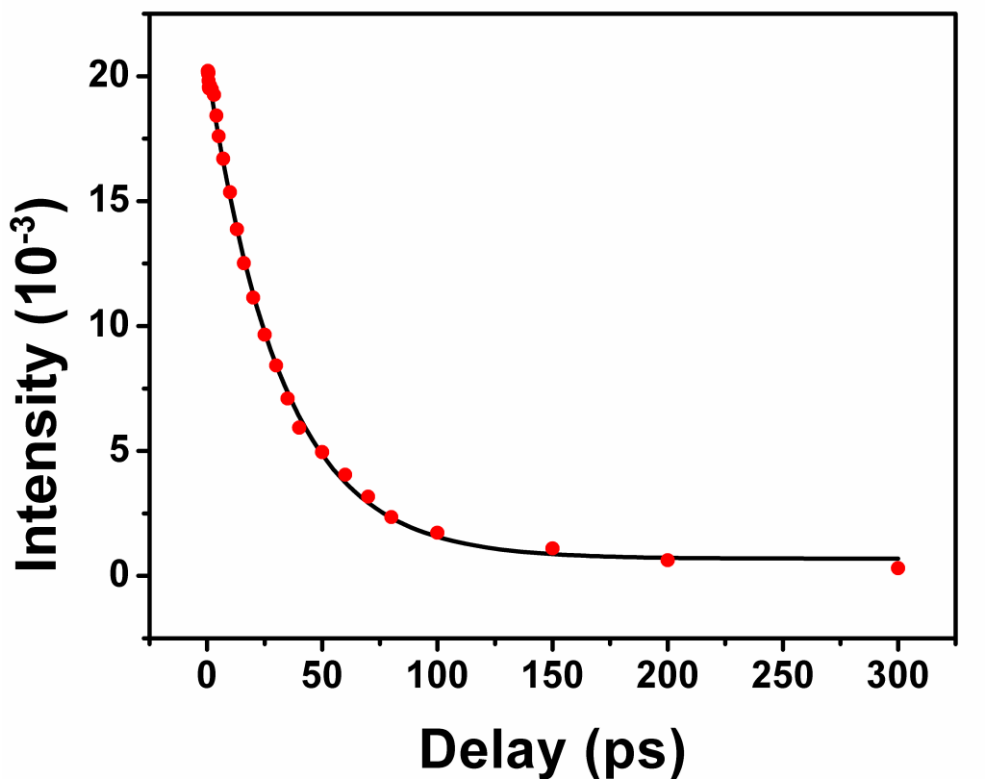

Figure 4.9S: PCMT S_1 decay probed via TAS at 840 nm. The solid line is an exponential fit with a decay timescale at 32± 1 ps.

4.7.7 Raman spectrum of PCMT's triplet states collected at 200 ps delay.

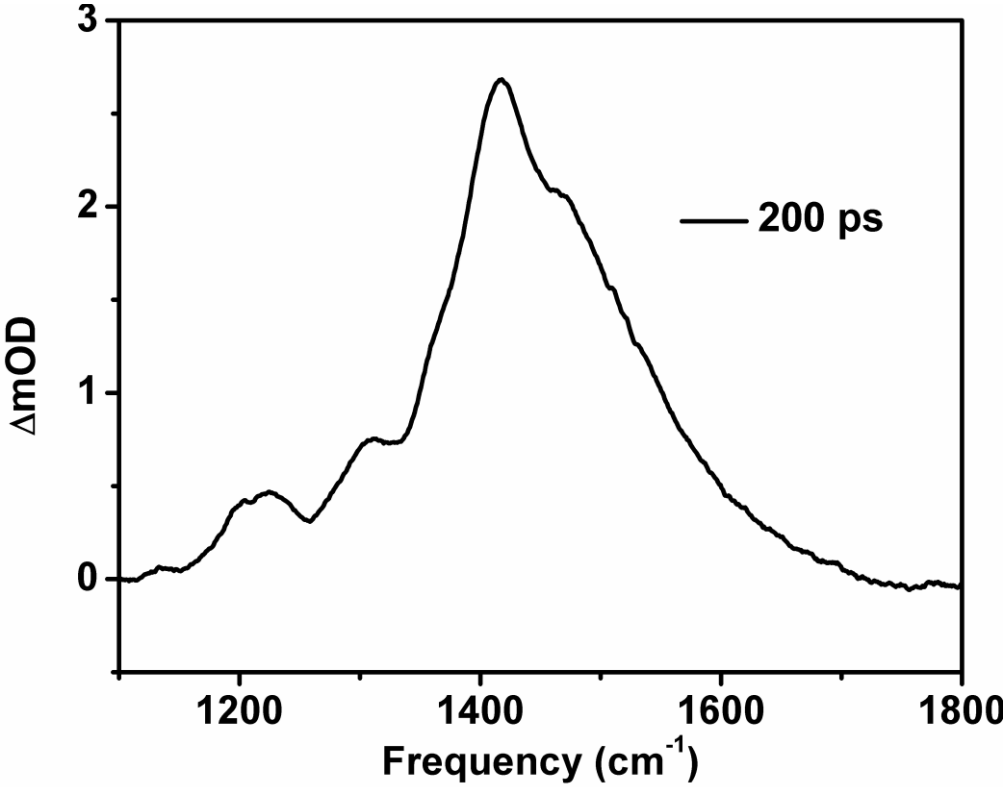

Figure 4.10S: Raman spectrum of PCMT's triplet states collected at 200ps delay. This spectrum is almost identical as what we get from global fit in Figure 4.7(d).

4.8 References

(1) A. Facchetti, *Chem. Mater*. **23**, 733-758 (2011).

(2) S. Gunes, H. Neugebauer, and N. S. Sariciftci, *Chem. Rev*. **107**, 1324-1338 (2007).

(3) N. Banerji, S. Cowan, E. Vauthey, and A. J. Heeger, *J. Phys. Chem. C* **115**, 9726-9739 (2011).

(4) E. Busby, E. C. Carroll, E. M. Chinn, L. Chang, A. J. Moulé, and D. S. Larsen, *J. Phys. Chem. Lett*. **2**, 2764-2769 (2011).

(5) J. Clark, T. Nelson, S. Tretiak, G. Cirmi, and G. Lanzani, *Nature Physics* **8**, 225-231 (2012).

(6) E. Collini and G. D. Scholes, *Science* **323**, 369-373 (2009).

(7) J. Du, Z. Wang, W. Feng, K. Yoshino, and T. Kobayashi, *Phys. Rev. B* **77**, 195205 (2008).

(8) I. Hwang and G. D. Scholes, *Chem. Mater*. **23**, 610-620 (2011).

(9) N. P. Wells and D. A. Blank, *Phys. Rev. Lett*. **100**, 086403 (2008).

(10) N. P. Wells, B. W. Boudouris, M. A. Hillmyer, and D. A. Blank, *J. Phys. Chem. C* **111**, 15404-15414 (2007).

(11) S. Westenhoff, W. J. D. Beenken, R. Friend, H., N. C. Greenham, A. Yartsev, and V. Sundström, *Phys. Rev. Lett*. **97**, 166804 (2006).

(12) W. Yu, J. Zhou, and A. E. Bragg, J. *Phys. Chem. Lett*. **3**, 1321-1328 (2012).

(13) S. V. Frolov, Z. Bao, M. Wohlgenannt, and Z. V. Vardeny, *Phys. Rev. Lett*. **85**, 2196-2199 (2000).

(14) W. J. Beenken and T. Pullerits, *J. Phys. Chem. B* **108**, 6164-6169 (2004).

(15) B. J. Schwartz, *Nature Physics* **7**, 427-428 (2008).

(16) S. N. Yaliraki and R. J. Silbey, *J. Chem. Phys*. **104**, 1245-1253 (1996).

(17) W. Barford, D. G. Lidzey, D. Makhov, and J. H. Meijer, *J. Chem. Phys*. **133**, 044504 (2010).

(18) D. W. McCamant, P. Kukura, S. Yoon, and R. A. Mathies, *Rev. Sci. Instrum*. **75**, 4971-4980 (2004).

(19) E. Collini and G. D. Scholes, *J. Phys. Chem. A* **113**, 4223-4241 (2009).

(20) D. Grebner, M. Helbing, and S. Rentsch, *J. Phys. Chem*. **99**, 16991-16998 (1995).

(21) J. Guo, H. Ohkita, H. Benten, and S. Ito, *J. Am. Chem. Soc*. **132**, 6154-6164 (2010).

(22) G. D. Scholes, Annu. Rev. Phys. Chem. **54**, 57-87 (2003).

(23) W. Westenhoff, C. Daniel, R. H. Friend, C. Silva, V. Sundström, and A. Yartsev, *J. Chem. Phys*. **122**, 094903 (2005).

(24)J. L. Sauvajol, D. Chenouni, J. P. Lére-Porte, C. Chorro, B. Moukala, and J. Petrissans, *Synth. Met*. **38**, 1-12 (1990).

(25) S. Miller, G. Fanchini, Y. Y. Lin, C. Li, C. W. Chen, W. F. Su, and M. Chhowalla, *J. Mater. Chem*. **18**, 306-312 (2008).

(26) G. Louarn, M. Trznadel, J. P. Buisson, J. Laska, A. Pron, M. Lapkowski, and S. Lefrant, *J. Phys. Chem*. **100**, 12532-12539 (1996).

(27) W. C. Tsoi, D. T. James, J. S. Kim, P. G. Nicholson, C. E. Murphy, D. D. C. Bradley, and J. Nelson, *J. Am. Chem. Soc*. **133**, 9834-9843 (2011).

(28) Y. Q. Gao, and J. K. Grey, *J. Am. Chem. Soc*. **131**, 9654-9662 (2009).

(29) M. Baibarac, M. Lapkowski, A. Pron, S. Lefrant, and I. Baltog, *J. Raman Spectrosc*. **29**, 825-832 (1998).
(30) S.-A. Chen and J.-M. Ni, *Macromolecules* **25**, 6081-6089 (1992).
(31) Y. Furukawa, *J. Phys. Chem*. **100**, 15644-15653 (1996).
(32) C. Castiglioni, M. Del Zoppo, and G. Zerbi, *J. Raman Spectrosc*. **24**, 484-494 (1993).
(33) V. Hernandez, C. Castiglioni, M. Del Zoppo, and G. Zerbi, *Phys. Rev. B* **50**, 9815-9823 (1994).
(34) S. Laimgruber, H. Schachenmayer, B. Schmidt, W. Zinth, and P. Gilch, *Appl. Phys. B* **85**, 557-564 (2006).
(35) W. Yu, P. J. Donohoo-Valett, J. Zhou, and A. E. Bragg *J. Phys. Chem*. **141**, 044201
(36) M. Kloz, R. van Grondelle, and J. T. M. Kennis, *Chem. Phys. Lett*. **344**, 94-101 (2012).
(37) A. Weigel and N. P. Ernsting, *J. Phys. Chem. B* **114**, 7879-7893 (2010).
(38) M. J. Frisch, G. W. Trucks, H. B. Schlegel, G. E. Scuseria, M. A. Robb, J. R. Cheeseman, G. Scalmani, V. Barone, B. Mennucci, G. A. Petersson *et al*, *Gaussian 09, Revision B.01* Gaussian, Inc., Wallingford CT (2010).
(39) J. S. Binkley, J. A. Pople, and W. J. Hehre, *J. Am. Chem. Soc*. **102**, 929-947 (1980).
(40) M. S. Gordon, J. S. Binkley, J. A. Pople, W. J. Pietro, and W. J. Hehre, *J. Am. Chem. Soc*. **104**, 2797-2803 (1982).
(41) T. Yanai, D. P. Tew, and N. C. Handy, *Chem. Phys. Lett*. **393**, 51-57 (2004).
(42) P. J. Donohoo-Vallett, and A. E. Bragg, *in preparation* (2014)
(43) *Jmol: an open-sourced Java viewer for chemical structures in 3D.*, 12.2.33, (2012). http://www.jmol.org/.
(44) U. Varetto, *Molekel*, 5.4.0.8, Swiss National Supercomputing Centre, Manno, Switzerland (2010).
(45) D. Beljonne, Z. Shuai, G. Pourtois, and J. L. Bredas, *J. Phys. Chem. A* **105**, 3899-3907 (2001).
(46) H. Kuhn, *J. Chem. Phys.* **17**, 1198-1212 (1949).
(47) A. Milani, L. Brambilla, M. Del Zoppo, and G. Zerbi, *J. Phys. Chem. B* **2007**, 1271-1276 (2007).
(48) G. Lanzani, M. Nisoli, S. De Silvestri, and R. Tubino, *Synth. Met*. **76**, 39-41 (1996).
(49) W. Paa, J.-P. Yang, and S. Rentsch, *Appl. Phys. B* **71**, 443-449 (2000).
(50) J.-P. Yang, W. Paa, and S. Rentsch, *Chem. Phys. Lett*. **320**, 665-672 (2000).
(51) J. J. Snellenburg, S. P. Laptenok, R. Seger, K. M. Mullen, and I. H. van Stokkum, M, *J. Stat. Softw.* **49** (2012).
(52) I. H. M. Stokkum, D. S. Larsen, and R. van Grondelle, *Biochim. Biophys. Acta* **1657**, 82-104 (2004).
(53) F. Chen, G. Shi, J. Zhang, and M. Fu, *Thin Solid Films* **424**, 283-290 (2002).
(54) T. Benincori, G. Bongiovanni, C. Botta, C. Cerullo, G. Lanzani, A. Mura, L. Rossi, F. Sannicolò, and R. Tubino, *Phys. Rev. B* **58**, 9082-9086 (1998).
(55) W. J. Beenken and H. Lischka, *J. Chem. Phys*. **123**, 144311 (2005).
(56) M. Takayanagi, T. Gejo, and I. Hanazaki, *J. Phys. Chem*. **98**, 12893-12898 (1994).

(57) M. Andrzejak, and H. Witek, *Theor. Chem. Acc*. **129**, 161-172 (2011).
(58) E. Stendardo, F. Avila Ferrer, F. Santoro, and R. Improta, *J. Chem. Theory Comput*. **8**, 4483-4493 (2012).
(59) H. Chosrovian, S. Rentsch, D. Grebner, D. U. Dahm, E. Birckner, and H. Naarmann, *Synth. Met*. **60**, 23-26 (1993).
(60) W. Paa, J.-P. Yang, M. Helbing, J. Hein, and S. Rentsch, *Chem. Phys. Lett*. **292**, 607-614 (1998).
(61) S. Rentsch, J. P. Yang, W. Paa, E. Birckner, J. Schiedt, and R. Weinkauf, *Phys. Chem. Chem. Phys*. **1**, 1707-1714 (1999).
(62) I. Zheldakov, J. M. Wasylenko, and C. G. Elles, *Phys. Chem. Chem. Phys*. **14**, 6211-6218 (2012).
(63) G. Zerbi, C. Castiglioni, and M. Del Zoppo *Electronic Materials: The Oligomer Approach* Wiley, 2008.

Chapter 5. Structural Heterogeneity in the Localized Excited States of Poly(3-hexylthiophene)

This chapter is based on work that was previously published[45] *in*
W. Yu, T. J. Magnanelli, J. Zhou, and A. E. Bragg. Structural Heterogeneity in the Localized Excited States of Poly(3-hexylthiophene). *J. Phys. Chem. B* **120**, 5093-5102 (2016)

5.1 Abstract

Transient hole-burning and resonantly enhanced Raman spectroscopies are used to probe heterogeneities amongst localized singlet excitons of poly(3-hexylthiophene) in solution. Transient hole-burning spectroscopy facilitated by population dumping through wavelength-selective stimulated emission exposes inhomogeneous broadening of the exciton absorption band in the near infrared, as reflected by correlations between stimulated emission and excited-state absorption transition energies. Dump-induced spectral diffusion of the exciton absorption band reflects structural fluctuations in locally excited polymer. This diffusion is observed to occur with rates slightly faster or slower than the non-equilibrium relaxation that follows direct excitation of the polymer (8-9 ps), with the timescale for diffusion varying with subpopulation: dumping across small vs. large band gaps results in diffusion over 5 vs. 35 ps, respectively. Furthermore, incomplete spectral relaxation of transient holes reflects that subsets of locally excited structural motifs prepared through photoexcitation cannot interchange through structural fluctuations that occur over the singlet-exciton lifetime. Raman spectra of the C=C/C-C stretching

region collected in resonance at energies across the exciton absorption band exhibit frequency and intensity trends (Raman “dispersion”) ascribed to variation in the local effective conjugation length. Together, results explicitly reveal heterogeneities amongst excitonic states associated with variations and fluctuations in local conformational order.

5.2 Introduction

The photophysical properties and dynamics of conjugated polymers (CPs) have received considerable attention in recent years that is fueled by interest in understanding the behaviors of organic electronic materials down to the molecular level.[1,2] CP photophysics present significant fundamental challenges regarding transport and charge separation of excitations within heterogeneous molecular and material environments.[3-6] Molecular-level understanding of these processes are complicated by the nature of CP electronic excitations (bound charge-pair excitons), which localize in various structural motifs along the backbone of a polymer and that exist due to its structural disorder.[7,8] A conceptual framework for CP photophysics should address which structural motifs trap and support excitons and how the nature of binding sites within a structurally disordered material impacts exciton properties and dynamics.[9,10] Understanding relationships between local structure and properties or behaviors of excitons will provide insights on how to manipulate their transport or charge separation in designer materials.

The canonical conjugated polymer poly(3-hexylthiophene) (P3HT) has received a large share of attention in efforts to characterize the trapping, relaxation, and properties of photogenerated excitons at a high level of photophysical detail. Fast spectral red-shifting and polarization anisotropy of transient absorption, stimulated emission, and time-resolved fluorescence have been ascribed to a combination of exciton localization (~100 fs)[6,11] and localized nuclear reorganization or excitonic energy transfer (~1-10s of

ps);[4,5,12-14] spectral dynamics on a timescale ~500ps is associated with singlet-exciton decay.[5,15] More recent exploration of polymer photophysics has utilized novel higher-order spectroscopies to gain deeper insights on relaxation of excitations,[6,11,16-18] as well as means for probing exciton binding strength and dissociation mechanisms.[19,20]

However, previous work has shed little light on the structural characteristics of localized excitations and correlations between local structure and photophysical properties, as the experimental methods applied generally have had limited ability to directly probe or differentiate amongst structural heterogeneities within an ensemble of photoexcited amorphous polymer, either in solution or films. This is noteworthy because polymer photophysics typically have been interpreted within a simplified conceptual framework that assumes that structural disorder along the polymer backbone fragments the extended pi network into a distribution of segments of variable length that are hosts for localized excitations;[10] thus the photoexcitation of polymer is expected to prepare an ensemble of excitons characterized by a distribution of conjugation lengths determined by variation in intrachain structure. The concept of an average, well-defined conjugated subunit is recognized to be an over-simplified paradigm for localized CP excitons,[9,21] yet, empirical data reporting characteristics of relevant structural motifs, their fluctuations, and how these impact exciton photophysical properties has remained limited. Experimental interrogation of structurally induced photophysical heterogeneities amongst CP excitons would provide further insights on mechanisms driving nonequilibrium

relaxation of photoexcited CPs and how the nature of the local structure impacts processes such as intramolecular charge-pair formation.

Here we present spectroscopic results that offer new perspective on structural heterogeneities amongst localized excitonic states of P3HT in solution. In our work we have interrogated the spectroscopy of singlet polymer excitons using a combination of pump-dump-probe transient hole burning (PDP THB) and resonant-enhanced excited-state Raman spectroscopies. Both techniques involve a wavelength-dependent perturbation of a photoprepared ensemble of excited polymer and thus enable preferential interrogation of photophysically distinct subpopulations of CP excitons and their correlations with local polymer structure.

THB spectroscopy is a common method used to interrogate spectral inhomogeneity – by definition, when variations in structure or physical and chemical environment are correlated with spectral variations amongst a set of related chromophores. In a THB experiment one prepares spectral "holes," typically through a photoinduced process, to expose the subpopulations that contribute to the equilibrated or quasi-equilibrated ensemble. When correlations between structure and spectroscopy exist THB can also reveal time-resolved physical or chemical exchange amongst subpopulations that occurs at or near equilibrium.[22,23] Through THB spectroscopy, fluctuations between specific excited-state subpopulations can be interrogated directly; in contrast fluctuations between subpopulations cannot be extracted directly from the non-equilibrium relaxation as

measured by TAS.

Here we have applied this technique to probe correlations between the electronic emission and absorption transitions of singlet excitons of P3HT; these correlations are attributed to structural heterogeneities within the ensemble of photoprepared excitons.[22,23] Transient hole-burning also allows us to explore dynamic exchange of exciton photophysical properties that is facilitated by structural fluctuations or energy transfer. We note that PDP THB spectroscopy is a unique complement to two other 3-pulse experiments that have been used previously to study non-equilibrium dynamics of ground-state[17] and doubly-excited[19] polymer.

Raman measurements of excited conjugated materials, on the other hand, provide a basis for directly probing nuclear structure and dynamics,[11,16,24-26] as well as correlating inhomogeneously broadened electronic absorption to variations in structural characteristics as probed with vibrational sensitivity. Here we utilize wavelength-dependent Raman excitation to photoselectively interrogate the vibrational spectroscopy of local structural features that underlie the inhomogeously broadened absorption of the CP exciton ensemble; this work complements our previous work on time-resolved Raman spectroscopy of excited polymers and oligomers.[11,16,24,26] We show that THB and Raman spectroscopies in combination illuminate photophysical heterogeneities that can be correlated with variations in structural order along the extended pi network of the polymer.

5.3. Experimental Methods

5.3.1 Sample Preparation and Characterization by Steady-State Spectroscopies

Regiorandom (RRa) poly-(3-hexylthiophene) (P3HT, Reike Metals, Mw=70-90K, used as-is) were dissolved in distilled THF to make 0.2 mg/mL solutions for transient absorption and pump-dump-probe transient hole-burning spectroscopies; 1 mg/mL solutions in deaerated chlorobenzene were prepared for excited-state Raman measurements. All measurements were conducted using sample solutions circulated with a peristaltic pump through a 0.5 mm UV-fused-silica flow cell (Spectrocell) at 15 mL/min.

Steady-state absorption and photoluminescence spectra of dilute P3HT solutions in quartz cuvettes were measured using a diode-array spectrophotometer (Stellarnet) and fluorescence spectrometer (Perkin-Elmer LS-B), respectively.

5.3.2 Pump-Dump-Probe Transient Hole-Burning Spectroscopy

5.3.2.1 Description of methodology

In this work we are interested in spectral correlations and diffusion associated with the electronic transitions of a photoprepared, quasi-equilibrated ensemble of polymer excitons. In our experiments an ensemble of excitons first was prepared through photoexcitation of P3HT dissolved in tetrahydrofuran (THF) solution with short "pump" pulses at 400 nm. Nascent excitons were allowed to relax for 100 picoseconds to enable redistribution and dissipation of excess internal energy. A spectral hole was then prepared through an interaction with a second "dump" pulse at 530, 560 or 600 nm, all of which are resonant with emission of excited polymer and can therefore deplete the ensemble population of quasi-equilibrated excitons.

A third broadband pulse was used to probe absorption of the remaining excitons in the NIR region (850 to 1130 nm) to interrogate the action of the dump pulse. Once a portion of the excited-state population has been dumped to the ground state, spectral diffusion associated with the remaining ensemble of excitons reflects structural fluctuations or energy transfer that drives evolution in photophysical properties. Notably, THB of an ensemble of excited states may reveal both dynamic and static heterogeneities. The latter results when structural fluctuations that occur over the course of the exciton lifetime are not sufficient to connect structural motifs with distinct photophysical properties and manifests as spectral diffusion that does not recover the

shape of the quasi-equilibrated excited-state spectrum prepared by the initial "pump" pulse. An illustrative cartoon and further description of THB spectroscopy is provided in the Supporting Information (Figure 5.1S).

5.3.2.2 Experimental Details

Laser pulses used for all experiments were derived from the output of an amplified Ti:Sapphire laser (Coherent Legend Elite, 4.5 mJ/pulse, 1 kHz rep. rate, 35-fs pulse duration). 400-nm pump pulses (4 μJ, 1 mm spot at sample) were generated by frequency doubling a portion of the fundamental. Dump pulses (2 μJ, 500 μm spot size at sample) were generated with an optical parametric amplifier (OPA; Coherent Opera Solo). The broadband white-light continuum probe (430-750 nm, for transient absorption, or 850-1100 nm, for TA and THB; 50 μm spot at sample) was prepared through white-light generation in sapphire. The effective time resolution of transient absorption and transient hole-burning experiments at the sample was determined to be 90 fs from coherent pulse interaction with the solvent.

Pump and dump pulses were aligned along two separate computer-controlled translation stages (Newport ESP301-2N) in order to control pulse arrival delays relative to the probe at the sample. The pump and dump beams were chopped separately at 500 Hz and 250 Hz to enable evaluation of each possible two- and three-pulse transient signal from a sequence of four successive laser shots; these include pump-probe transient

absorption (PP), dump-probe transient absorption (DP), and pump-dump-probe (PDP) signals. The crossing angles between probe pulse and pump or dump pulses were less than 5° through the sample. The polarization of pump and dump pulses was set to be parallel (vertical), while the probe pulse was set at the magic angle (54.7°) relative to vertical using a wire-grid polarizer immediately before the sample. Probe light was collected and dispersed with a 300-mm spectrograph (Acton-2360) onto a CCD camera (Pixis-100BR) that was configured to detect and read out the probe spectrum on each laser shot. Data acquisition, computation of spectra, and manipulation of translation stages were coordinated with a homebuilt LabView program.

The two- and three-pulse signals mentioned above must be used to isolate spectral correlations and diffusion associated with transient hole prepared by the dump pulse. These signals are calculated from the sequence of probe-continuum spectra measured in the pump-dump-probe experiment as follows:

$$PDP = -\log(I_{on\text{-}on}/I_{off\text{-}off}) \quad (5.1a)$$

$$DP = -\log(I_{off\text{-}on} / I_{off\text{-}off}) \quad (5.1b)$$

$$PP = -\log(I_{on\text{-}off} / I_{off\text{-}off}) \quad (5.1c)$$

I represents the intensity of the near-IR probe continuum and is a function of wavelength; here, for example, “on-off” refers to intensity of the probe with excitation by pump pulse,

but no interaction with dump pulse, etc. Pump-probe transient absorption spectra were collected for both near-IR and visible broadband probes by blocking the visible dump pulse. Transient absorption spectra in the visible and near-IR were averaged over 15000 chopping sequences to obtain spectra shown below; spectra associated with pump-dump-probe spectroscopy (Equations 6a-6c) were averaged over 7500 chopping sequences.

5.3.3 Excited-State Raman Spectroscopy by Femtosecond Stimulated Raman Spectroscopy (FSRS)

Excited-state Raman spectra were collected using FSRS[27,28] at fixed delays after 400-nm photoexcitation using various Raman-excitation wavelengths resonant with the excited-state absorption spectrum in the near-IR. Detailed description of our FSRS set-up can be found elsewhere.[11,16,24,26,29] Briefly, a second-harmonic bandwidth compressor (SHBC, Light conversion) was pumped with a portion of the fundamental output (800 nm, ~1 mJ/pulse) to generate narrowband pulses (~12 cm^{-1}) with 2-3 ps duration at 400 nm. The SHBC output was used to pump a white-light-seeded OPA (TOPAS-400, Light Conversion) in order to generate tunable narrowband Raman-excitation pulses (840, 880, 920 and 950 nm; 20 cm^{-1} bandwidth, 10-15 mJ/pulse, 500 mm diameter at sample). The time delay between Raman excitation and white-light probe pulses at the sample was adjusted with a translation stage (Newport) and optimized to give the best line-shapes for solvent Raman features.

Pump and Raman-excitation pulses were chopped at one-fourth and one-half of the laser repetition rate, respectively. As in our pump-dump-probe measurements described above, the spectrum of the probe continuum was collected in each of four chopping phases (excitation and Raman pump: on-on, on-off, off-on, off-off). Each set of four probe spectra were then used to calculate a transient absorption spectrum (TAS), a ground-state Raman spectrum (GSR) and a synchronously chopped spectral signature

(SC):

$$TAS = -\log(I_{on\text{-}off}/I_{off\text{-}off}) \quad (5.2a)$$

$$GSR = -\log(I_{off\text{-}on} / I_{off\text{-}off}) \quad (5.2b)$$

$$SC = -\log(I_{on\text{-}on} / I_{off\text{-}off}) \quad (5.2c)$$

Spectra obtained from equations 4-6 were obtained by averaging over 7500 collection cycles. Pure excited-state Raman (ESR) spectra were isolated as follows:[11]

$$ESR = SC - m*GSR - k*TA - Fit. \quad (5.3)$$

Here, *m* and *k* are scalar factors: *m* is optimized in order to remove contributions from solvent features, whereas *k* is optimized to remove baseline contributions due to the bleaching of excited-state absorption induced by the Raman-excitation pulse. "Fit" is a polynomial baseline fit that accounts for broadband discrepancies between the shape of the TAS and the broad baseline in the SC spectrum.

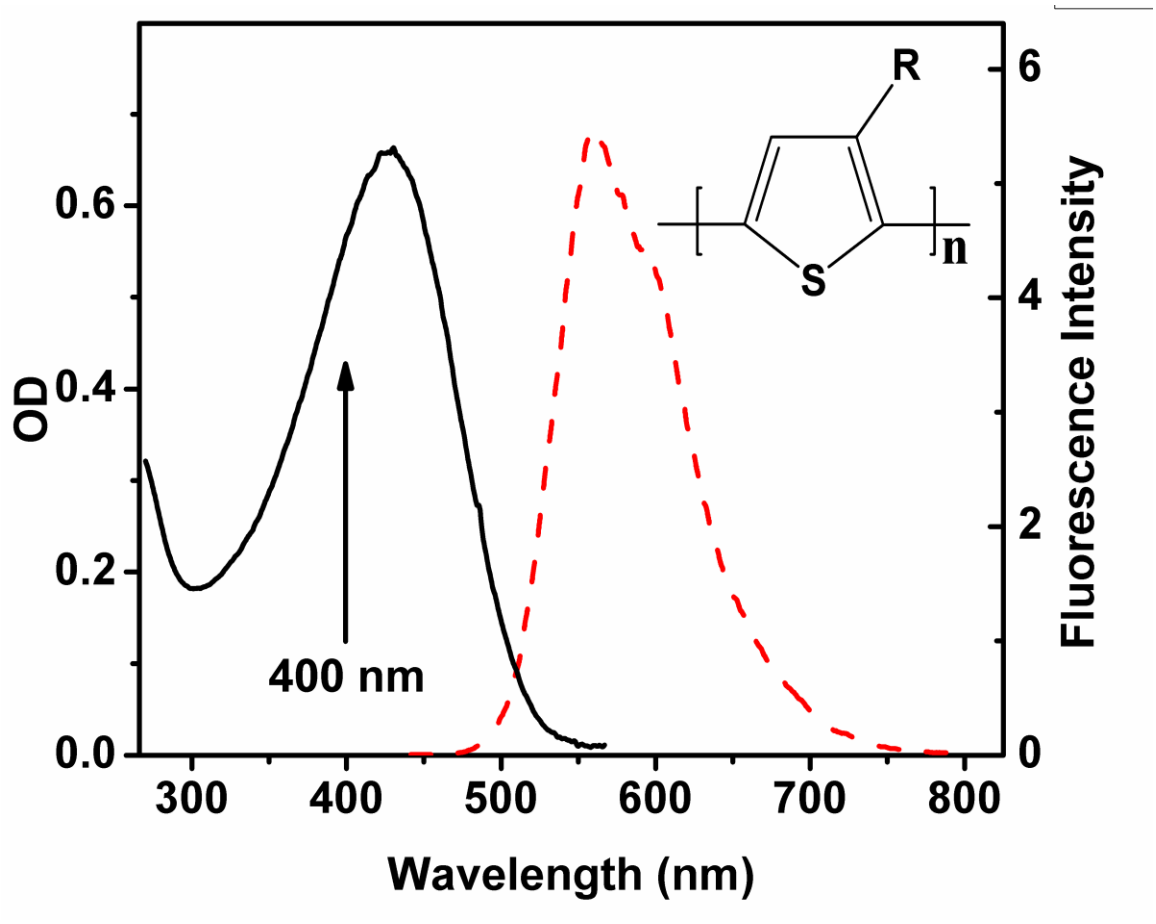

Figure 5.1: Steady-state absorption and dispersed fluorescence spectra of regiorandom poly(3-hexylthiophene) (RRa-P3HT) in THF solution (fluorescence excitation = 400 nm).

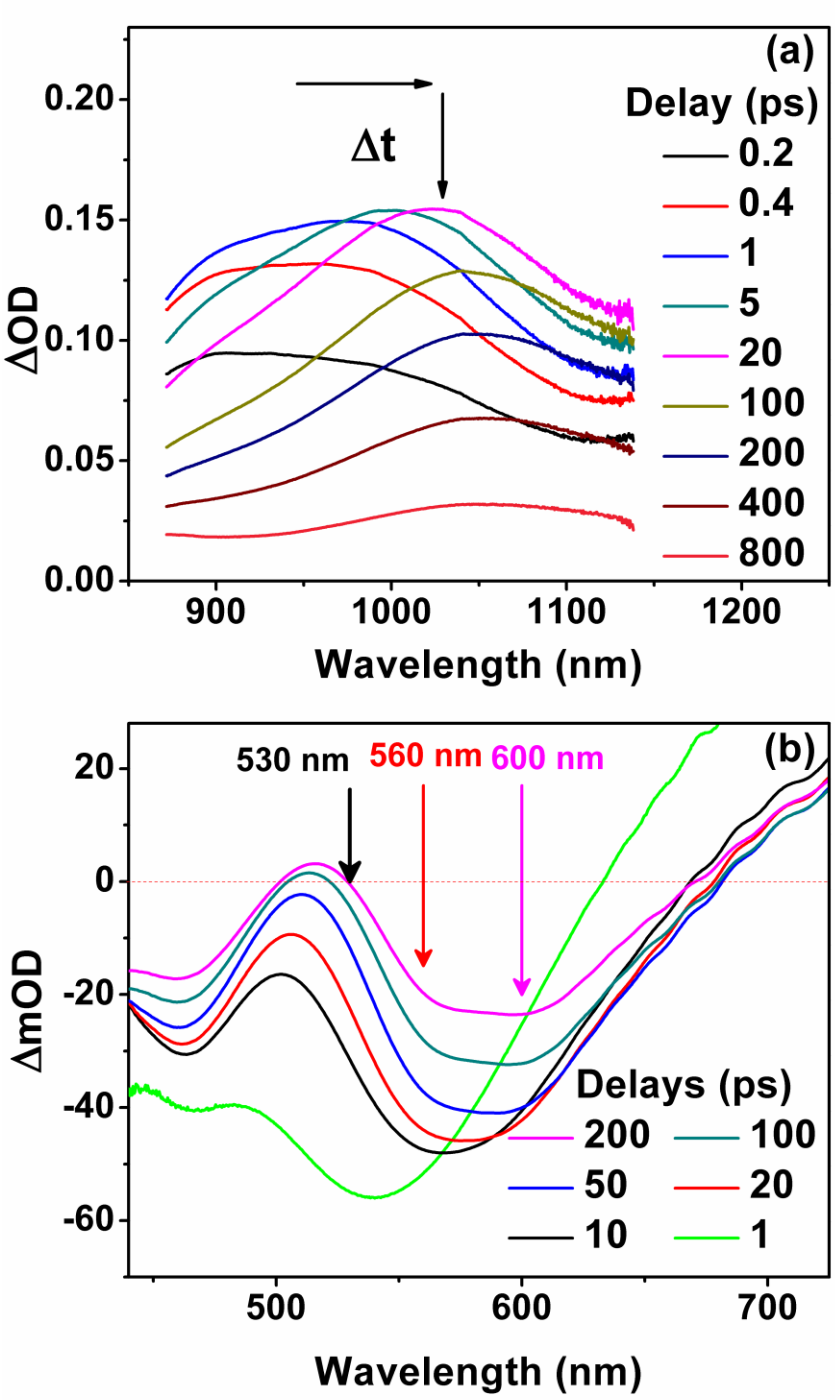

Figure 5.2: Pump-probe transient absorption spectroscopy of RRa-P3HT in THF solution following excitation at 400 nm: (a) Near-infrared transient spectra from photo-generated polymer excitons. (b) Transient spectroscopy of P3HT probed in the visible. In transient hole-burning experiments described here, dump pulses (530, 560 and 600 nm) selectively deplete excitons via stimulated emission.

5.4. Results and Discussion

5.4.1 Steady-State and Transient Absorption Spectroscopy of P3HT

The lowest-energy steady-state absorption feature for RRa-P3HT is a broad band peaked near 430 nm, as shown in Figure 5.1. We observe no signatures of stacked polymer strands in our steady-state spectroscopy (e.g. structured, red-shifted features associated with excitonic interactions); this is consistent with reports showing that RRa-P3HT takes on a highly amorphous (non-stacked) morphology even in films.[30,31]

In our experiments, polymer solutions were excited with 400-nm light pulses, as denoted with an arrow in Figure 5.1. Pump-probe transient absorption spectra collected after 400-nm photoexcitation of RRa-P3HT are presented in Figure 5.2(a) (near-IR absorption) and 2(b) (stimulated emission in the visible) at selected pump-probe delays. Spectral dynamics observed in these wavelength ranges are similar to what has been reported previously for both RRa and RR polymer:[5,15-17,32] Both exhibit signatures of non-equilibrium excited-state relaxation over 10's of picoseconds and exciton decay by a combination of fluorescence and intersystem crossing over hundreds of picoseconds. The sizable separation in these non-equilibrium singlet-exciton relaxation timescales is critical for our PDP THB spectroscopy, as vibrational relaxation to a quasi-equilibrated excited-state ensemble needs to be completed on a timescale that is short relative to the exciton lifetime itself.

5.4.2 Pump-Dump-Probe Transient Hole-Burning Spectroscopy

5.5.2.1 Selection of dump wavelengths

In our pump-dump-probe transient hole-burning experiments we have used three different dump wavelengths (530, 560, and 600 nm) ranging over the breadth of the polymer's weakly structured stimulated emission (Figure 5.2(b)) and fluorescence spectra (Figure 5.1) in order to induce selective population transfer of a subset of excitons back to the polymer ground state. The rationale for these dump wavelengths is as follows: 530 nm falls at the high-energy edge of the SE band and enables preferential dumping of excitons with large S_1-S_0 band gap that are anticipated to correspond predominantly with less ordered structural motifs (e.g. shorter conjugation length, conformationally or structurally disordered regions). In contrast, 600 nm corresponds with the low-energy edge of the SE band, and is expected to preferentially dump excitons with low band gap corresponding with predominantly more ordered structural motifs (e.g. longer conjugation length, more planar local conformations). Dumping through both high- and low-gap SE transitions enables exploration of correlations between TAS (Figure 5.2(a)) and SE (Figure 5.2(b)) transition energies for the ensemble of excited polymer.

Although it is desirable to tune the low-gap dump wavelength even further to the red, there is a significant overlap of the excited-state SE and TAS signals at wavelengths above 600 nm. The relative size of the absorption tail into the visible can be gauged from TAS (PP) data (Figure 5.2(b)): notably, a slightly positive absorption intensity

appears near 515 nm (between the SE and ground-state bleach bands) at time delays 100-200 ps after photoexcitation at 400 nm. Hence, we expect that pump-dump-probe signals will exhibit contributions associated with an alternative "pump-push" excitation pathway,[19,20] as demonstrate further below.

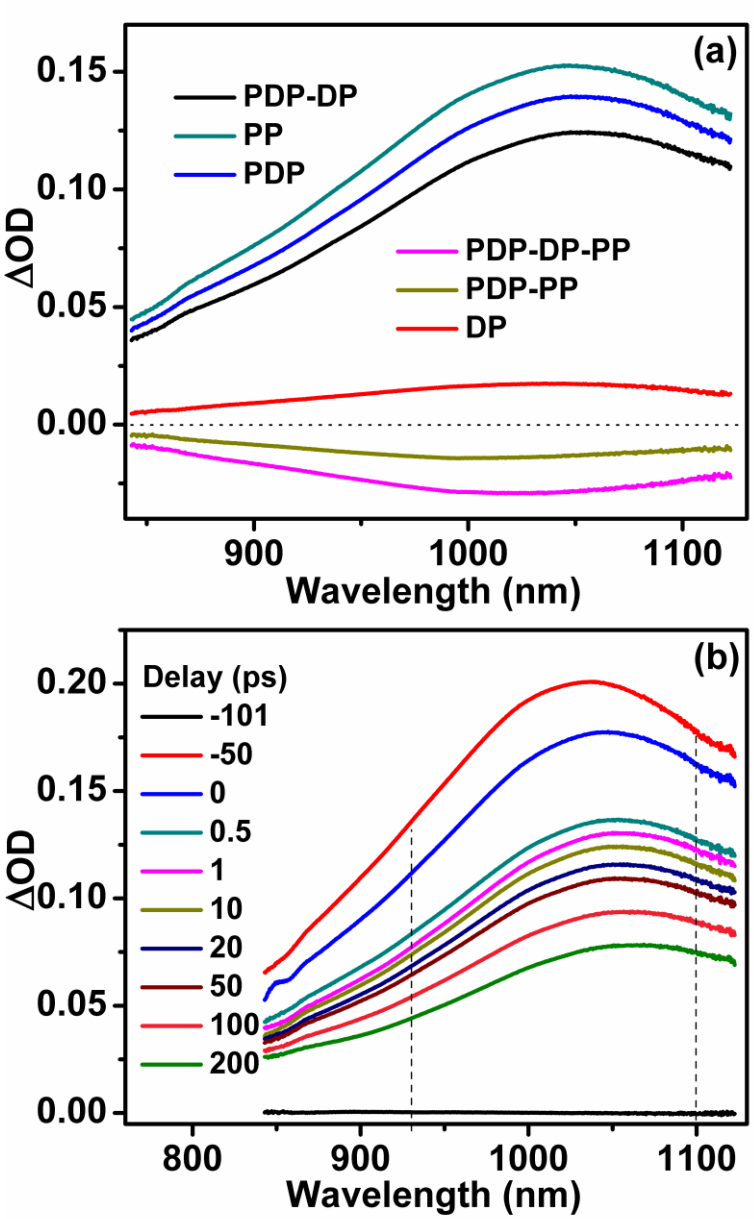

Figure 5.3: (a) Two- and three-pulse signal combinations obtained in the course of the pump-dump-probe (PDP) transient hole-burning (THB) experiments (pump = 400 nm, dump = 530 nm, pump-dump delay = 100 ps, dump-probe delay = 1 ps); PP = pump-probe, DP = dump-probe. (b) DP-corrected PDP spectra (PDP-0.89DP) of RRa-P3HT in THF solution at various dump-probe delays (pump = 400 nm, dump = 530 nm, pump dump delay = 100 ps); see text for details of correction for dump-probe contributions. Population dumping is apparent from the drop in near-IR absorption between -0.25 and 0 ps.

5.4.2.2 Correction for 2-pulse dump-probe signal contributions (530 nm).

Time-dependent pump-dump-probe signals contain the spectral diffusion associated with the non-equilibrated ensemble of CP excitons created through population dumping, but must be corrected for any 2-pulse "dump-probe" (DP) signal; this is essentially a pump-probe transient spectrum from direct S_0-S_1 excitation at the dump wavelength. No DP signal is observed with either 560 or 600 nm dump pulses, as both wavelengths are red of the polymer's ground-state absorption band, such that any spectral dynamics observed at these dump wavelengths is only due to the spectral diffusion of the transient spectral hole in the excited-state population. In contrast, 530 nm approaches the edge of ground-state absorption spectrum, such that this dump wavelength introduces a 2-pulse contribution to the total measured signal. Figure 5.3(a) plots examples of the 3-pulse PDP, as well as 2-pulse DP and PP signals obtained for a 100-ps pump-dump delay and a 1 ps dump-probe delay.

To accurately remove DP contributions to the PDP signal collected with 530 nm it is important to recognize that the former arises from the reduced ground-state population that remains after the initial 400-nm excitation of the sample; hence, the DP contribution to the three-pulse signal is smaller than the DP signal that would be collected when the 400-nm excitation beam is blocked. Based on the relative size of the steady-state absorption and the absorption bleach induced by the pump pulse, roughly 89% percent of the polymer is unaffected by the initial excitation at 400 nm. Hence, we scaled the pure DP signal by 0.89 for subtraction from the raw PDP signal in order to isolate spectral

changes induced by population transfer through stimulated emission at 530 nm. Specifically, the resulting corrected pump-dump-probe spectra (PDP-0.89DP) reflect the absorption of the remaining exciton population after the dump-pulse induced depletion. These are plotted in Figure 5.3(b); the abrupt drop in the signal near the dump-probe delay of 0 ps illustrates depopulation of the polymer excited state through action of the dump pulse.

5.4.2.3 Separation of 3-pulse signals: Pump-dump vs. pump-push pathways

Figure 5.4(a) plots the net time-dependent bleach in the near-IR exciton absorption (calculated as PDP-0.89DP-PP) for visualizing the action of 530-nm dump pulses. This plot illustrates that the dump pulse induces an instantaneous drop in the NIR excited-state absorption (also apparent in Figure 5.3(b)), which is a signature of laser-induced depopulation of the polymer excited state. The time-dependence of the peak bleach intensity at 1035 nm is plotted at all three dump wavelengths in Figure 5.4(b). Figures 5.4(a) and 5.4(b) illustrate that the dump-induced bleach evolves on two distinct timescales; the bleach decays with timescales of ~200 fs and ~300-400 ps when fitted with a bi-exponential functions (see Table 5.1). The longer of these two timescales represents the lifetime of the exciton population that remains after dump-induced depopulation, which is the same as the S_1 lifetime measured by pump-probe TAS. In contrast,[5,15-17,32] the former represents an ultrafast recovery of the hole that can only occur

if the dump pulse further excites, rather than deexcites, polymer excitons (i.e., a pump-push pathway).

Pump-push excitation of P3HT was recently investigated by Tapping and Kee.[19,20] These authors used a near-IR push pulse to further excite excitons prepared by the 400-nm excitation of ground-state polymer in solution to even higher-lying electronic excited states. Doubly-excited polymer was observed to have a lifetime of ~200 fs, as gauged by the recovery of near-IR exciton absorption after action of the push pulse. Most of these high-energy excitons were observed to relax back to the S_1 state within a picosecond, whereas a small fraction (~11%) of these dissociated as they were given sufficient energy to overcome the exciton binding energy and form separated charge carriers on a single polymer chain.[19]

Based on their findings, and given the overlap in exciton SE and TA spectra apparent in Figure 5.2(b), we ascribe the signal decay on a timescale of a few hundred fs observed in Figure 4 to a pump-push contribution. This is corroborated by the variation in the size of this component with dump wavelength: As the relative size of the stimulated emission compared to the exciton absorption decreases between 600 and 530 nm (Figure 5.2(b)), we expect that the relative contribution of the pump-push pathway to the total 3-pulse signal will increase as the dump pulse is tuned to the blue. The time-dependent bleach intensities obtained at the various dump wavelengths, as plotted in Figure 5.4(b), indeed show that the fraction of the ultrafast component increases from 13% to 23% to 36%

as the dump wavelength is tuned to the blue. The presence of this ultrafast component makes it difficult to isolate ultrafast spectral diffusion associated with dump-induced hole burning. However, and as we illustrate further below, the 3-pulse signal obtained in our experiment is dominated by the dump-induced emission pathway and the spectral dynamics of the PDP signal on timescales >2 ps can be ascribed to spectral diffusion of the transient spectral hole.

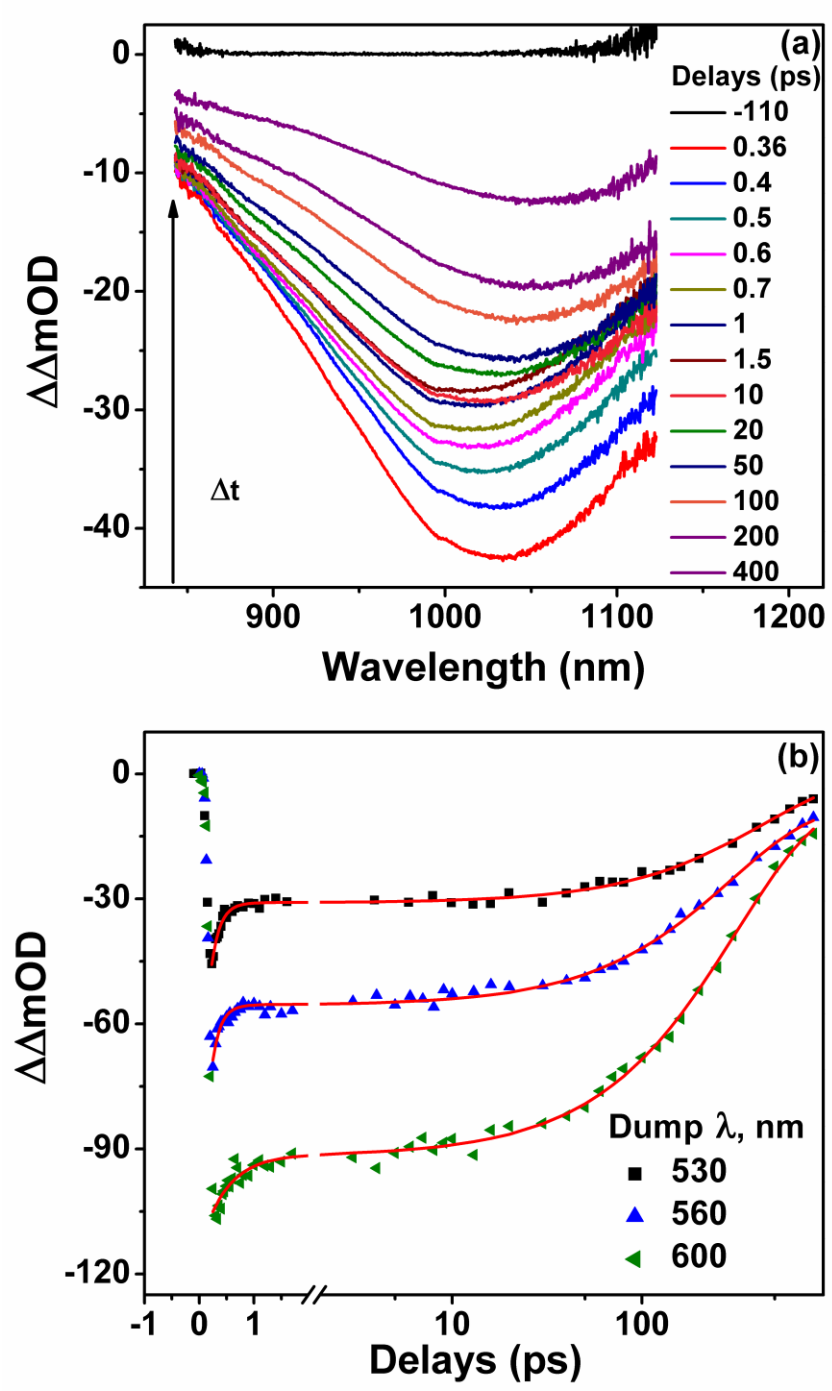

Figure 5.4: (a) Transient spectral hole (PDP-0.89DP-PP) in the excited-state absorption of RRa-P3HT as induced with a dump pulse at 530 nm. (b) Time-dependent intensity of bleach (PDP-DP-PP) induced by visible dump pulses. Timescales obtained by fitting bleach recovery to biexponential functions are given in Table 5.1.

Table 5.1: Timescales obtained by fitting excited-state bleach recovery (probed at 1035 nm, Figure 5.4(b)) at different dump pulse energies to a biexponential function. The pump pulse is 400 nm, pump-dump delay is 100 ps.

	530 nm	560 nm	600 nm
t_1/fs	150±20	150±20	320±50
t_2/ps	440±50	290±20	310±10

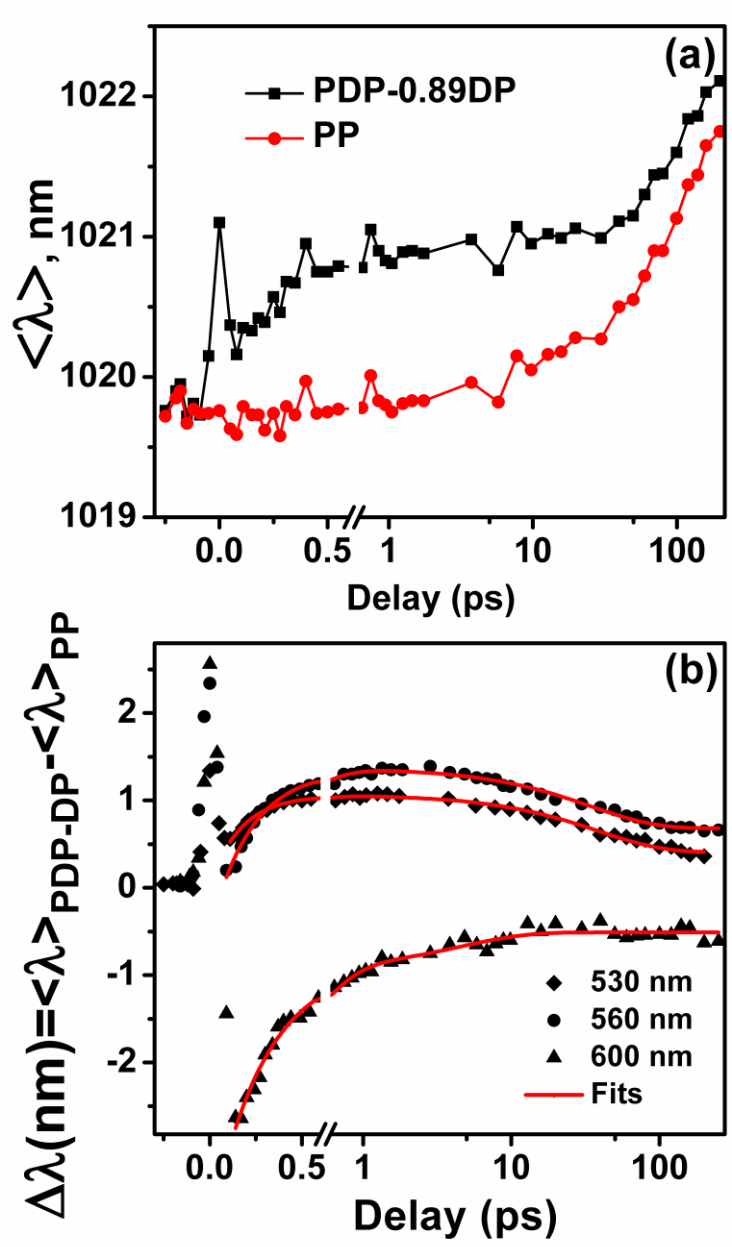

Figure 5.5: Spectral Correlations and Diffusion: (a) Comparison of the intensity-weighted average peak position of the pump-probe (PP) and corrected pump-dump-probe (PDP) spectra (930-1100 nm), illustrating response to dump-induced exciton depletion. (b) Dump-induced changes in spectra and spectral diffusion are illustrated with the difference in weighted spectral peak position of PDP and PP signals for all dump wavelengths. The pump pulse is 400 nm and the pump-dump delay is 100 ps. The sharp initial features around 0 ps arise from the dump-probe instrument temporal response. Spectral diffusion associated with excited-state hole burning is apparent on timescales > 2 ps. The fast red-shift appearing in the first 2 ps is due to bleach recovery from a pump-push excitation pathway explained in the text.

5.4.2.4 Characterization of dump-induced spectral diffusion

The dump-induced transient hole and its spectral diffusion can be visualized from the (DP-corrected) time-dependent bleach of the near-IR exciton absorption plotted in Figure 5.4(a): whereas the ultrafast decay of the spectral hole corresponds with bleach recovery via the pump-push pathway, a redshift observed at later times (>2 ps) corresponds with spectral diffusion of the hole created through the pump-dump pathway. The spectral diffusion of the transient hole vs. that of the remaining excited-state population occur in opposite directions, and hence it is most intuitive to characterize the spectral diffusion directly from the spectral evolution of DP-corrected PDP signal (e.g. Figure 5.3(b)).

We accomplish this here by comparing the intensity-weighted peak position of corrected PDP and PP signals with dump-probe delay; this is determined by an intensity-weighted averaging of the spectral shape over the range of 930 and 1100 nm, as illustrated in Figure 5.3(b)). Given that the inhomogeneous breadth of the excited-state absorption is most likely due to a large number of underlying conformational/structural motifs, characterization of the ensemble average seems to be the most conservative way to characterize spectral evolution/diffusion in this system. The integration range used here was chosen specifically to avoid overlap with spectral signature of the triplet (absorbing below 900 nm at long delays) and due to the limited reliability of the spectral response of the detector beyond 1100 nm; we also note that this range should not be chosen to be narrower, as it would not span the breadth of the near-IR absorption peak

and would therefore provide a poorer metric of the average peak position. We plot the intensity-weighted peak positions of PP and corrected-PDP signals in Figure 5.5(a) for a 530-nm dump applied 100 ps after initial excitation of the sample to illustrate the action of the dump pulse on the average wavelength of the near-IR exciton absorption.

The action of the dump pulse can be summarized by the difference in weighted band centers for the corrected PDP and PP signals, which we plot for all three dump wavelengths in Figure 5.5(b). Negative (positive) values of $\Delta\lambda$ correspond with a net blue-shift (red-shift) relative to the PP exciton absorption that is induced by the action of the dump pulse. A number of behaviors are apparent from this plot: (1) high-energy dumping (530 and 560 nm) results in a redshifted non-equilibrated exciton absorption spectrum, whereas low-energy dumping (600 nm) results in a net blueshift relative to the exciton absorption spectrum; (2) the spectral diffusion induced at all dump wavelengths reduces the magnitude of $\Delta\lambda$ over 10s of ps; (3) incomplete recovery ($|\Delta\lambda|>0$) is apparent at 300 ps; (4) dumping at all three wavelengths induces spectral redshifts on ultrafast timescales (100 fs to 1 ps) following an instrument-limited response at 0 fs.

The first three observations result from dump-induced formation of a spectral hole in the exciton population and the spectral diffusion that results from structural fluctuations of the remaining excitons. The dependence of the net shift of Dl on dump wavelength reflects a direct correlation between low (high) energy stimulated emission and low (high) energy exciton absorption; this correlation is a signature of inhomogenous broadening of

the exciton transitions attributed to grossly different exciton subpopulations.

Secondly, spectral diffusion observed on picosecond timescales for all dump wavelengths reflects that excitons remaining after the dump-induced population transfer experience structural fluctuations that fill in some of the spectral hole prepared by the dump pulse. We have applied exponential fits to the data in Figure 5.5(b) and find that the spectral recovery occurs predominantly on timescales of 4.6 ps at 600 nm, 34 ps at 560 nm and 39 ps at 530 nm, as reported in Table 5.2. These timescales are not far from the nonequilibrium exciton relaxation timescale obtained directly via pump-probe measurements (9 ps[16]). Similar magnitudes of these timescales should not be surprising, as the timescales of nonequilibrium dynamics and thermal fluctuations between quasi-equilibrated configurations are related through the fluctuation-dissipation theorem.[33] However, it is notable that spectral evolution associated with dumping via a low-gap transition (600 nm) is slightly faster than the non-equilibrium timescale, whereas spectral evolution initiated by high-gap transitions (560 and 530 nm) occurs more slowly. As spectral diffusion reflects some exchange amongst excited-state subpopulations, these differences in timescale indicate that the rate of exchange depends on starting and ending configuration.

Table 5.2: Timescales obtained by fitting $\Delta\lambda(t)$ acquired with different dump pulse energies to a biexponential function (as plotted in Figure 5.5(b)). The pump pulse is 400 nm, pump-dump delay is 100 ps.

	530 nm	560 nm	600 nm
t_1/fs	170 ± 10	220 ± 10	280 ± 20
t_2/ps	39 ± 3	34 ± 3	4.6 ± 1.4

Finally, incomplete spectral diffusion on a timescale of 100s of ps reflects that the subset of excitonic states depleted from the ensemble of excited polymer cannot be recovered completely by physical exchange driven by structural fluctuations of the remaining excitons. This indicates that static heterogeneities (static relative to the singlet exciton lifetime) exist within the initial quasi-equilibrated distribution of photoprepared excitons. In total, a key conclusion from this experiment is that electronic absorption of the excited polymer in the near-IR is inhomogeneously broadened, with limited conformational exchange between underlying subpopulations of excitons via thermal fluctuations.

Spectral dynamics on the fastest timescales probed (<2 ps), on the other hand, result from the alternate "pump-push" pathway described above.[19,20] Despite the presence of both pathways, dynamics of the spectral hole due to direct dumping of the S_1 population to the ground state appears to dominate the 3-pulse spectrum at time delays after this initial ultrafast bleach recovery for various reasons:

(1) "Pushed" excitons primarily recover to the singlet excited state regardless of push wavelength, with only a ~11% lost to photo-induced charge-pair formation.[19] Compounding this fraction with the relative contribution of pump-push vs. pump-dump signals in the total 3-pulse signal implies that the bleach remaining after the ultrafast recovery is dominated by the dump pathway by a factor of 20-100 (i.e., only ~1-5% of the transient bleach signal on longer timescales could be due to bleach obtained by

push-induced charge-separation).

(2) The spectral diffusion we observe on the ~10 ps timescale and greater is considerably slower than the push-recovery timescales noted previously (0.16 ps and 2.4 ps accounting for an 89% bleach recovery[19]), supporting its association with a separate photophysical pathway.

(3) Spectral relaxation of "hot" S_1 excitons populated from a short-lived S_N excited state would be expected to exhibit similar spectral dynamics regardless of the push energy in the visible. Rather, the dump-wavelength dependence to the relative spectral shifts (PDP-PP) shows opposite behavior for low- and high-energy dumping, and is consistent with expected behavior for THB.

Hence, we can conclude that our three-pulse PDP data on picosecond timescales reflect correlations between inhomogeneously broadened TAS and SE transitions, as well as spectral diffusion associated with fluctuations of the local polymer structure.

5.4.3 Structural Heterogeneities of Excitonic States Probed by FSRS

As P3HT is a homo-polymer, it is most conceivable that the heterogeneities that underlie the observed correlations in electronic spectroscopy and THB spectral diffusion are related to structural variations and fluctuations along polymer chains. Here we have examined correlations between excited-state electronic spectroscopy and local polymer structure using resonantly enhanced femtosecond stimulated Raman spectroscopy

(FSRS).[27,28] We have previously used this method to interrogate the relaxation of photoexcited polymers (P3HT and poly-(3-cyclohexyl,4-methyl)thiophene, or PCMT) and oligothiophenes according to time-dependent resonant enhancements and peak shifts of key Raman-active modes at selected Raman-excitation wavelengths.[11,16,26] In this work we have measured the stimulated Raman spectrum at various Raman-excitation wavelengths after photoexcitation of the polymer. The narrow-band (20 cm^{-1}) Raman-excitation pulse used in these measurements enables photoselective interrogation of local structures that underlie the inhomogeneous breadth of the exciton absorption band.

A comparison of Raman spectra of photoexcited RRa-P3HT collected in the carbon-carbon stretching region with various Raman-excitation wavelengths is presented in Figure 5.6(a). The most intense feature at 1470 cm^{-1} corresponds with the C=C symmetric stretch[11,16,24,26,34,35] and exhibits a sizable redshift in peak frequency as the Raman-excitation pulse is tuned to longer wavelength. Figure 5.6(b) illustrates that the wavelength-dependence of the peak position is essentially the same over a timescale of several picoseconds (similar behavior is also observed for RR-P3HT, Figure 5.4S). This is consistent with our previously reported time-resolved data (Raman excitation at 880 and 950 nm),[16] as well as recent findings with oligothiophenes demonstrating that the symmetric C=C stretching frequency (which dominates the Raman spectrum of the polymer) is very weakly sensitive at best to conformational relaxation.[26]

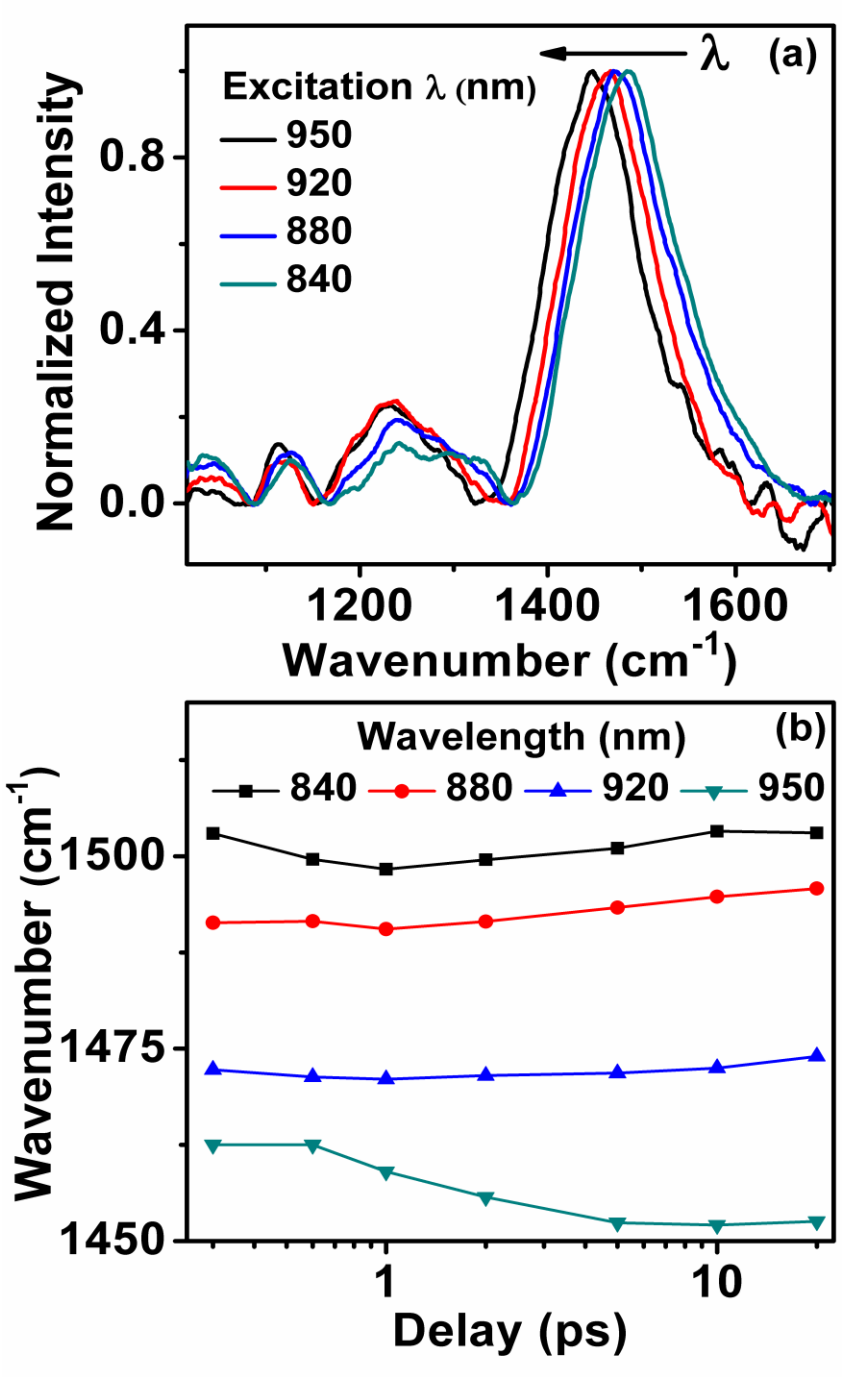

Figure 5.6: (a) Raman spectra of photoexcited RRa-P3HT collected at various Raman-excitation wavelengths spanning the near-IR exciton absorption band 1 ps after 400-nm excitation (c.f. Figure 5.2(a)). (b) Time-dependent weighted peak position of the C=C stretching feature obtained with RRa-P3HT at various Raman-excitation wavelengths.

The variation in C=C stretching frequency with excitation wavelength is reminiscent of the length-dependent frequency variation observed in the Raman spectra of conjugated oligomers with low monomer aromaticity.[36,37] For oligomers, this variation with length reflects increasing non-local electron exchange with greater conjugation that softens the C=C stretching potential.[36-38] For excited P3HT, which has greater delocalized character relative to its ground state and therefore effectively lower monomer aromaticity, the frequency shift apparent in Figure 5.6(a) can be interpreted as the variation in effective delocalization amongst exciton subpopulations that are interrogated at the selected Raman-excitation wavelengths; this variation in effective conjugation lengths is a consequence of variation in local structure of the polymer.

A useful comparison as regards the degree of frequency shift to expect in our wavelength-dependent measurements is to note that the ground-state C=C stretching frequency of oligofurans and oligoenes, which have low monomer aromaticities, exhibit comparable frequency shifts (20-40 cm^{-1}) for changes in oligomer length of only a few monomer units.[36-38] As electronic delocalization (and monomer aromaticity) in localized excited states of P3HT should be roughly comparable with what is observed for these ground-state oligomers, it is not surprising that such a variation in C=C stretching frequency would be observed even amongst a modest distribution of effective conjugation lengths within an ensemble of excited polymer.

Thus, the spectra in Figure 5.6(a) illustrate specifically that excitons probed via

lower Raman-excitation energies have greater effective conjugation than those probed at higher energies, which is consistent with the correlation between exciton absorption and emission gaps gleaned from THB data discussed above. Intensity variations observed in the C-C stretching region (1150-1350 cm^{-1}) are also correlated with Raman-excitation wavelength and further support that variations in structural order underlie the spectral inhomogeneity of the exciton absorption band.

We note that we have observed a similar correlation in C=C stretching frequency with Raman-excitation energy for photoexcited PCMT that likewise reflects a distribution of effective conjugation lengths in the ensemble of excited polymer.[11] For PCMT this variation in stretching frequency with Raman-excitation energy is corroborated by intersystem crossing dynamics (rather than correlations with electron spectroscopy via THB): ISC rates determined from FSRS measurements resonant with the red and blue edges of the PCMT S_1 transient absorption band reveal that faster ISC rates from the S_1 state are correlated with higher transitions energies in the S_1 absorption band. Faster ISC rates have been correlated with greater torsional disorder for small thiophene[39-41] and mixed phenyl-thiophene oligomers.[42] Thus we interpret the correlations in both C=C stretch frequency and ISC rates measured at different Raman-excitation wavelengths for S_1 PCMT to indicate wavelength-selective probing of structural heterogeneities that underlie the excited-state absorption band.

5.5 Conclusions

Results of THB and Raman measurements report on structural heterogeneities according to correlations in the spectroscopy of excitonic states prepared through the photoexcitation of P3HT. These photophysical variations can be understood in terms of the distribution of structural domains that are expected to be present in amorphous poly(3-alkylthiophenes): The persistence length of amorphous P3ATs has been estimated to be ~3 nm (~6-8 monomer units, much shorter than the ~500 unit length of a polymer strand studied here) from small-angle neutron diffraction scattering measurements[43] and is attributed to mixtures of anti and syn inter-ring conformations. Thus, variations in the spectroscopic and photophysical properties of excitons observed here likely arise from variations in the density of conformational defects along the polymer chain. For instance, an increased prevalence of conformational defects is expected to change the balance between the inter-ring mechanical and quantum-mechanical (i.e. delocalization) couplings that determine the frequencies of Raman-active modes and also introduce changes to the C-C stretching region.[36] Although linkage irregularity would also introduce structural distortions along the polymer backbone,[44] we note that we have observed similar wavelength-dependent Raman responses for both regioregular and regiorandom polymers (see Supporting Information). Thus, variations observed in photophysical and spectroscopic properties most likely originate from intrinsic conformational disorder in the polymer, rather than synthetic structural defects.

The observation of spectral diffusion in our THB measurements reflects that some

fluctuations between conformations affecting the effective delocalization length are possible and indicates that the ensemble of photoprepared excitons is characterized by a somewhat dynamic distribution of effective conjugation lengths. The similarity in timescales for nonequilibrium exciton relaxation and THB spectral diffusion highlight the important role of evolving conformational order in the relaxation of P3HT excitons. However, our results also reflect that the timescales for these fluctuations are sensitive to the nature of the starting and ending configurations: specifically fluctuations from disordered to ordered configurations occur considerably faster than fluctuations from ordered to disordered configurations, as illustrated from by differences in spectral diffusion observed for small and large band-gap dumping. These results are consistent with non-equlibrium relaxation favoring relaxation towards low-energy, conformationally ordered configurations. Furthermore, our THB measurements reveal signatures of incomplete spectral diffusion, indicating that the conformational fluctuations necessary to drive some structural exchange occur on timescales much longer than the exciton lifetime, consistent with the characterization of local structural motifs as exciton traps.

In conclusion, this work provides new perspective on the nature of excitonic states with respect to local structural order in amorphous CPs, with implications for nonequilibrium exciton relaxation and exciton photophysics. Specifically, our findings demonstrate explicitly that relaxation does not produce uniformly ordered localized excitations via a combination of structural reorganization and energy transfer along P3HT.

Rather a distribution of configurations that vary in terms of structural characteristics is prepared; some of these configurations fluctuate dynamically, but with significant contribution from effectively static motifs relative to the exciton lifetime (i.e. exciton traps). The combination of energy-selective electronic and Raman probes of exciton subpopulations enable a connection between the local electronic and structural properties of these disordered, heterogeneous multichromophoric materials.

5.6 Supplementary Information

5.6.1 Illustrative description of transient hole-burning (THB) spectroscopy

Figure 5.1S presents a descriptive illustration of the principles of transient hole-burning (THB) spectroscopy. THB begins with a (quasi)equilibrated ensemble of chromophores. The red, blue and green circles in Figure 5.1S(a) represent a chromophore present in a heterogeneous distribution of physical (or chemical) environments; correlations between physical environment and spectral position give rise to an inhomogeneously broadened spectrum (total spectral breadth represented with the dotted line). In a THB measurement, a portion of this distribution is selectively removed; in panel (b), we illustrate this by selectively removing a handful of red chromophores, producing a non-equilibrated distribution of chromophores with a corresponding spectral depletion at longer wavelengths relative to the original spectrum (the non-equilibrated spectrum, which includes a hole in the distribution of red circles, is plotted as a blue dashed line). As a result of this depletion the average wavelength exhibits a net dump-induced blue shift.

After depletion, the physical or/and chemical properties of the remaining chromophores may take on photophysical characteristics of depleted states via thermally-driven exchange (e.g. energy transfer or structural fluctuations) (panel (c)); the non-equilibrated spectrum (dashed blue) will consequently red shift and evolve towards the shape of the original equilibrated spectrum (red solid line). If some depleted motifs cannot be recovered by thermal fluctuations, as may be possible for an ensemble of

excited-state motifs, the spectral recovery will be incomplete (relaxing somewhere between the blue dashed and red solid lines). Incomplete relaxation is a reflection that an effectively static heterogeneity exists.

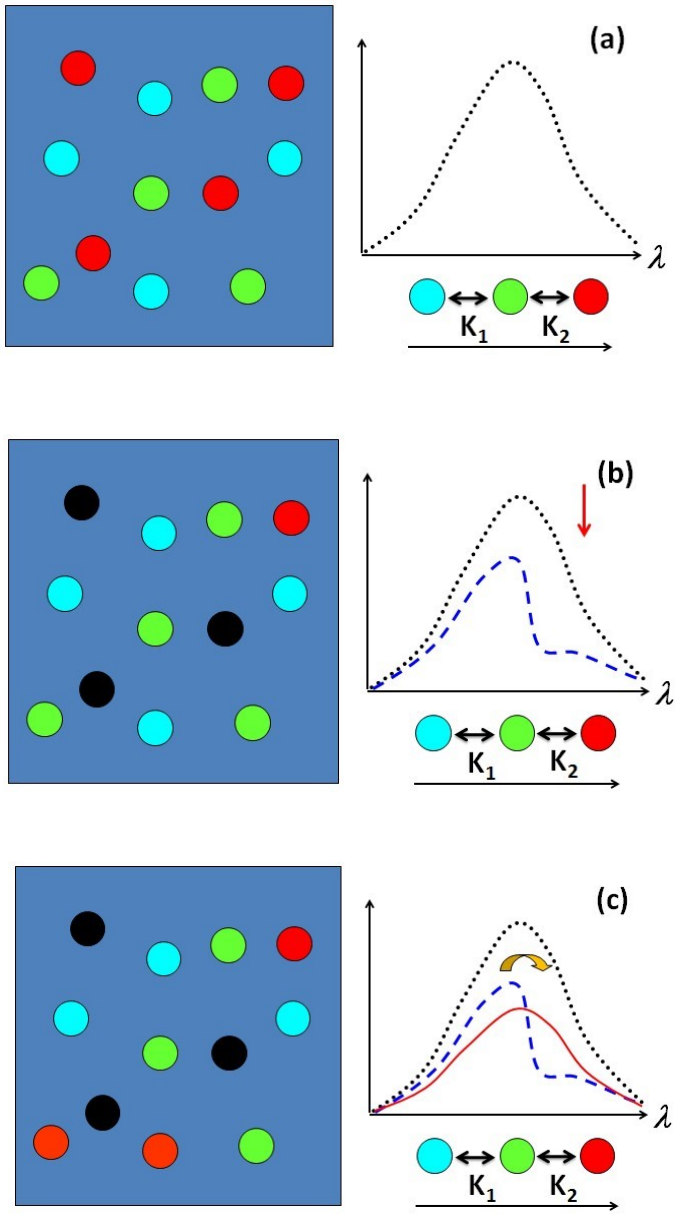

Figure 5.1S: A descriptive illustration of transient hole-burning (THB) spectroscopy
(a) Spectroscopy of a distribution of chromophores in different physical or chemical environments (represented with colored circles); (b) photoselective laser excitation removes ("burns") chromophores of a specific sub-ensemble (red), generating a *non-equilibrated* population and its corresponding absorption spectrum; (c) physical or chemical exchange, associated with microscopic fluctuations between different sub-ensembles, gives rise to spectral diffusion.

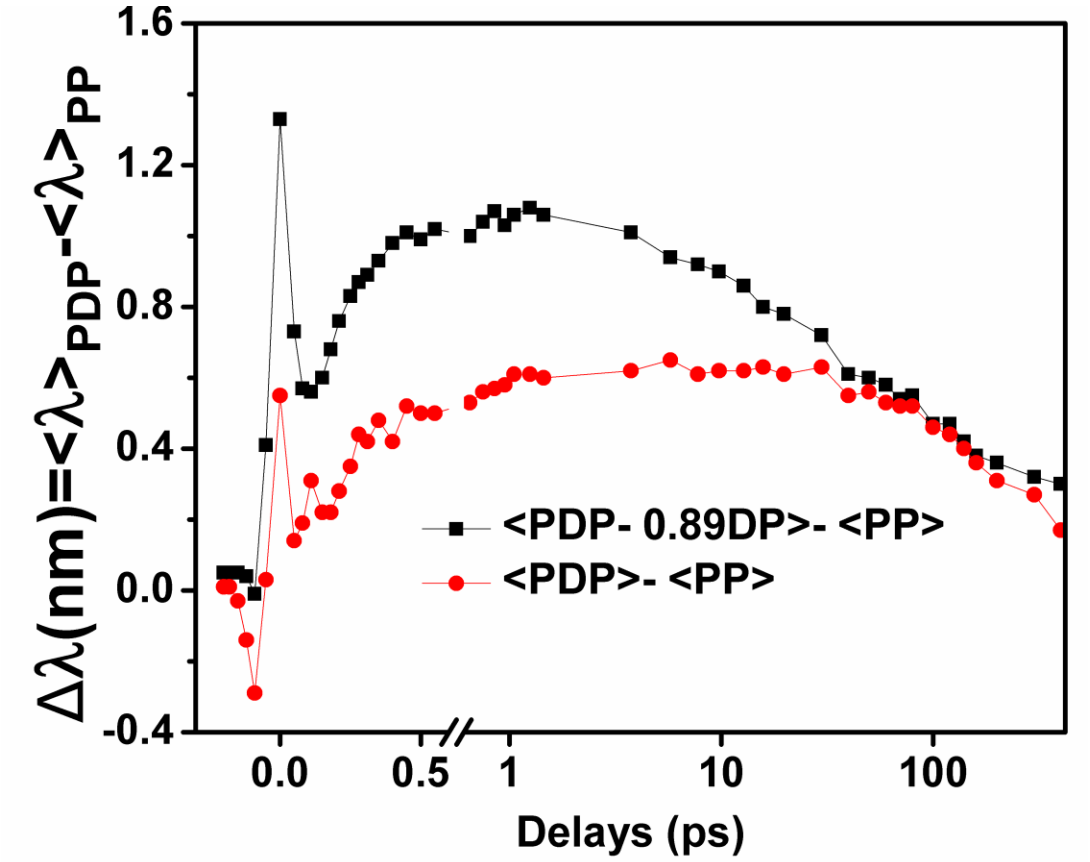

Figure 5.2S: Time-dependent weighted-average peak positions (relative PP TA) as obtained from THB measurements with a 530-nm dump pulse applied 100 ps after polymer excitation at 400 nm: corrected (PDP-0.89DP, black) vs. uncorrected (raw PDP, red) for two-pulse dump-probe-only (DP) contributions.

5.6.2. Effect of dump-probe (DP) correction on spectral evolution of 3-pulse pump-dump-probe (PDP) signals

The weighted-average peak position (relative to the pump-probe TA) for corrected (PDP-0.89DP) and uncorrected/raw PDP results are compared in Figure 5.2S. The DP signal contribution at 530 nm can be seen to have a substantial impact on the time-dependent spectral dynamics of the uncorrected PDP signal. This is because the direct excitation of polymer with the "dump" pulse contributes a transient signal with a spectral redshift (e.g. Figure 5.2(a)) associated with non-equilibrium exciton relaxation. This non-equilibrium spectral redshift counteracts the blue-shifting spectral diffusion of the PDP signal (the manifestation of transient hole burning), as illustrated by comparing the corrected and uncorrected PDP signals in Figure 5.2S. At 530 nm the DP only signal is roughly half the magnitude of the spectral hole (but opposite in sign; Figure 5.3S(a)). Nonetheless, similar THB spectral diffusion is observed when the raw PDP signal is corrected for DP contributions using a realistic range of scaling factors based on the size of the pump-induced bleach and steady-state absorption spectra (0.89 ± 0.1).

5.6.3. Effect of pump-dump delay on spectral evolution of 3-pulse pump-dump-probe (PDP) signals

In our experiments we have specifically chosen a pump-dump delay of 100 ps to ensure preparation of a quasi-equilibrated ensemble of excitons for transient hole burning. In order to demonstrate that the PDP THB dynamics are not affected by the chosen pump-dump delay, experiments were conducted with variable pump-dump delays ranging between 10 and 200 ps. Results (i.e. weighted-average peak wavelengths of DP-corrected pump-dump-probe signals) are plotted in Figure 5.3S for data collected with a 530-nm dump. Spectral diffusion is qualitatively consistent across all pump-dump delays, exhibiting an overall red-shift in weighted peak position upon dumping followed by a dynamic blue-shift as a function of dump-probe time delay. For each specific pump-dump delay, a tri-exponential fit recovers three distinguishable time scales; fitting results are summarized in Table 5.1S. The ultrafast timescales are all around 200 fs, which corresponds with the ultrafast bleach recovery from the "push" pathway induced by the visible dump pulse (described in more detail in the text). Measurements described in the main text used a 100-ps pump-dump delay, as this delay ensures an adequate time for exciton equilibration and is well before the appearance of the triplet excitons via intersystem crossing.

Table 5.1S: Timescales obtained by fitting $\Delta\lambda(t)$ acquired at different pump-dump delays to a tri-exponential function. The pump and dump pulses are 400 nm and 530 nm, respectively.

Pump-dump delay	10 ps	30 ps	50 ps	100 ps	200 ps
τ_1/fs	85	178	199	220	222
τ_2/ps	7.5	10.4	9.1	13.3	11.2
τ_3/ps	71	121	97.6	107	123

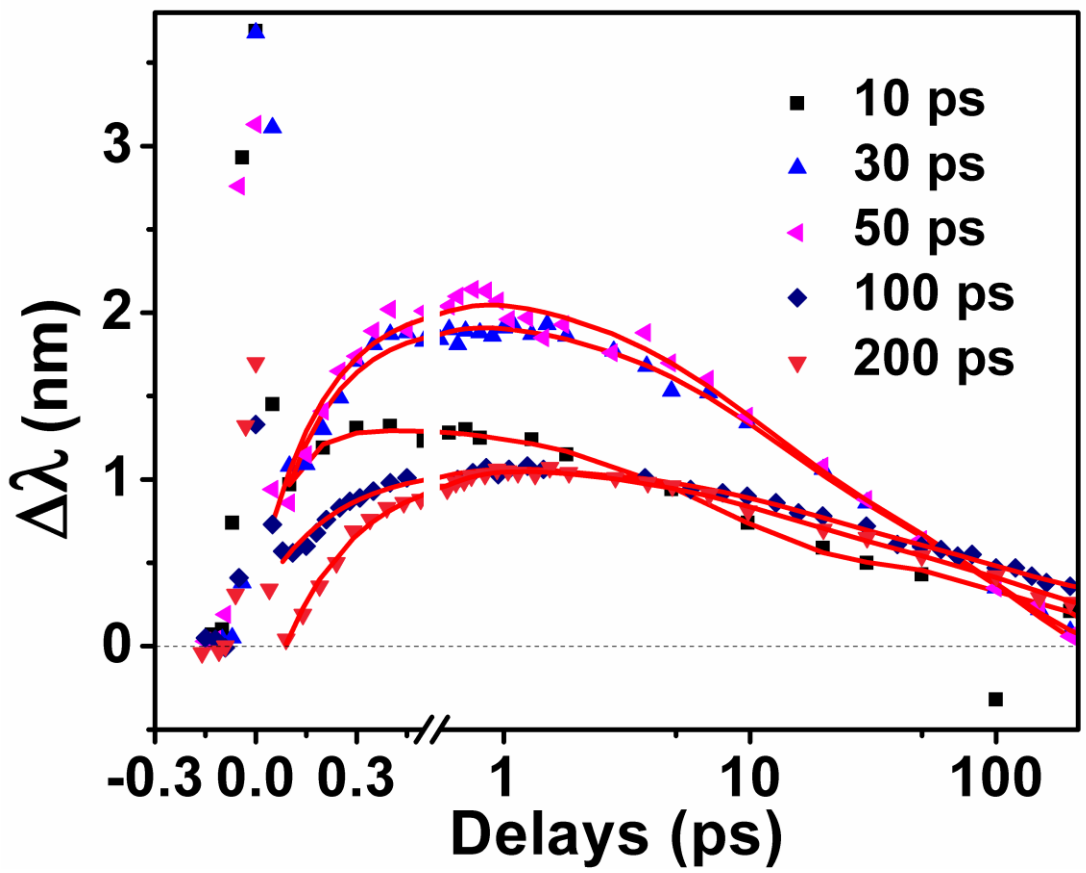

Figure 5.3S: Time-dependent weighted peak positions of PDP-DP spectra (relative to PP spectra, $\Delta\lambda$) at various pump-dump delays given in the legend. Pump and dump pulses are 400 and 530 nm, respectively.

5.6.4. Excited-state Raman spectroscopy of excitons in regioregular P3HT.

In order to demonstrate that exciton heterogeneities arise from intrinsic structural variations and not as a consequence of synthetic defects along the RRa polymer, we also investigated the wavelength-dependent Raman spectra of excitons on regioregular (RR) P3HT. Figure 5.4S shows that RR-P3HT also has wavelength-dependent Raman dispersion of the C=C stretch, as well as similar variations in the intensity distribution within the C=C/C-C stretching region as we observed with RRa-P3HT (notably the disappearance of intensity near 1300 cm^{-1}) at longer Raman-excitation wavelengths.

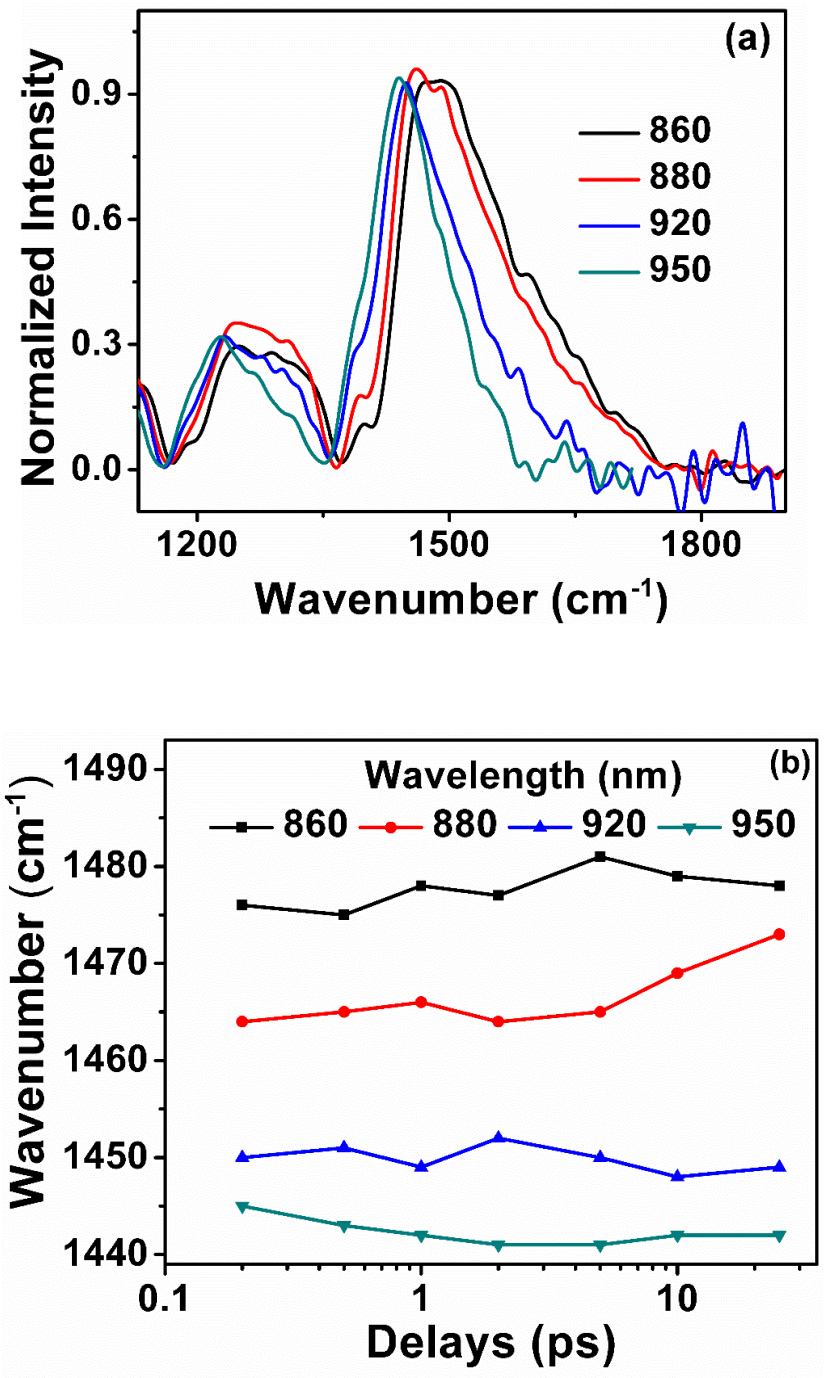

Figure 5.4S: FSRS Raman dispersion for RR-P3HT.(a) Raman spectra collected with different Raman-excitation energies at 1 ps after 510-nm photoexcitation. The main feature near 1500 cm^{-1} corresponds with the C=C symmetric stretch, which red shifts as Raman-excitation energy decreases. (b) Time-dependent weighted peak position of the C=C stretching feature obtained with RR-P3HT at various Raman-excitation wavelengths.

5.7 References

(1) Paquin, F.; Yamagata, H.; Hestland, N. J.; Sakowicz, M.; Bérubé, N.; Côté, M.; Reynolds, L. X.; Haque, S. A.; Stingelin, N.; Spano, F. C. *et al.* Two-Dimensional Spatial Coherence of Excitons in Semicrystalline Polymeric Semiconductors: Effect of Molecular Weight. *Phys. Rev. B* **2013**, *88*, 155202.

(2) Falke, S. M.; Rozzi, C. A.; Brida, D.; Maiuri, M.; Amato, M.; Sommer, E.; De Sio, A.; Cerullo, G.; Molinari, E.; Lienau, C. Coherent Ultrafast Charge Transfer in an Organic Photovoltaic Blend. *Science* **2014**, *344*, 1001-1005.

(3) Dykstra, T.; Kovalevskij, V.; Yang, X.; Scholes, G. D. Excited State Dynamics of a Conformationally Disordered Conjugated Polymer: A Comparison of Solutions and Films. *Chem. Phys.* **2005**, *318*, 21-32.

(4) Westenhoff, S.; Beenken, W. J. D.; Friend, R., H.; Greenham, N. C.; Yartsev, A.; Sundström, V. Anomalous Energy Transfer Dyanmics Due to Torsional Relaxation in a Conjugated Polymer. *Phys. Rev. Lett.* **2006**, *97*, 166804.

(5) Wells, N. P.; Boudouris, B. W.; Hillmyer, M. A.; Blank, D. A. Intramolecular Exciton Relaxation and Migration Dynamics in Poly(3-Hexylthiophene). *J. Phys. Chem. C* **2007**, *111*, 15404-15414.

(6) Wells, N. P.; Blank, D. A. Correlated Exciton Relaxation in Poly(3-Hexylthiophene). *Phys. Rev. Lett.* **2008**, *100*, 086403.

(7) Barford, W.; Lidzey, D. G.; Makhov, D.; Meijer, J. H. Exciton Localization in Disordered Poly(3-Hexylthiophene). *J. Chem. Phys.* **2010**, *133*, 044504.

(8) Westenhoff, S.; Beenken, W. J. D.; Yartsev, A.; Greenham, N. C. Conformational Disorder of Conjugated Polymers. *J. Chem. Phys.* **2006**, *125*, 154903.

(9) Beenken, W. J.; Pullerits, T. Spectroscopic Units in Conjugated Polymers: A Quantum Chemically Founded Concept? *J. Phys. Chem. B* **2004**, *108*, 6164-6169.

(10) Yaliraki, S. N.; Silbey, R. J. Conformational Disorder of Conjugated Polymers: Implications for Optical Properties. *J. Chem. Phys.* **1996**, *104*, 1245-1253.

(11) Yu, W.; Donohoo-Vallett, P. J.; Zhou, J.; Bragg, A. E. Ultrafast Photo-Induced Nuclear Relaxation of a Conformationally Disordered Conjugated Polymer Probed with Transient Absorption and Femtosecond Stimulated Raman Spectroscopies. *J. Chem. Phys.* **2014**, *141*, 044

(12) Parkinson, P.; Müller, C.; Stingelin, N.; Johnston, M. B.; Herz, L. M. Role of Ultrafast Torional Relaxation in the Emission from Polythiophene Aggregates. *J. Phys. Chem. Lett.* **2010**, *1*, 2788-2792.

(13) Tretiak, S.; Saxena, A.; Martin, R. L.; Bishop, A. R. Conformational Dynamics of Photoexcited Conjugated Materials. *Phys. Rev. Lett.* **2002**, *89*, 097402.

(14) Grage, M. M.-L.; Pullerits, T.; Ruseckas, A.; Theander, M.; Inganäs, O.; Sundström, V. Conformational Disorder of a Substituted Polythiophene in Solution Revealed by Excitation Transfer. *Chem. Phys. Lett.* **2001**, *339*, 96-102.

(15) Banerji, N.; Cowan, S.; Vauthey, E.; Heeger, A. J. Ultrafast Relaxation of the Poly(3-Hexylthiphene) Emission Spectrum. *J. Phys. Chem. C* **2011**, *115*, 9726-9739.

(16) Yu, W.; Zhou, J.; Bragg, A. E. Exciton Conformational Dynamics of Poly(3-hexylthiophene) (P3HT) in Solution with Time-Resolved Resonant Raman Spectroscopy. *J. Phys. Chem. Lett.* **2012**, *3*, 1321-1328.
(17) Busby, E.; Carroll, E. C.; Chinn, E. M.; Chang, L.; Moulé, A. J.; Larsen, D. S. Excited-State Self-Trapping and Ground-State Relaxation Dynamics in Poly(3-hexylthiophene) Resolved with Broadband Pump-Dump-Probe Spectroscopy. *J. Phys. Chem. Lett.* **2011**, *2*, 2764-2769.
(18) Clark, J.; Nelson, T.; Tretiak, S.; Cirmi, G.; Lanzani, G. Femtosecond Torsional Relaxation. *Nat. Phys.* **2012**, *8*, 225-231.
(19) Tapping, P. C.; Kee, T. W. Optical Pumping of Poly(3-hexylthiophene) Singlet Excitons Induces Charge Carrier Generation. *J. Phys. Chem. Lett.* **2014**, *5*, 1040-1047.
(20) Kee, T. W. Femtosecond Pump-Push-Probe and Pump-Dump-Probe Spectroscopy of Conjugated Polymers: New Insight and Opportunities. *J. Phys. Chem. Lett.* **2014**, *5*, 3231-3240.
(21) Schwartz, B. J. What Makes a Chromophore? *Nat. Phys.* **2008**, *7*, 427-428.
(22) Bragg, A. E.; Glover, W. J.; Schwartz, B. J. Watching the Solvation of Atoms in Liquids One Solvent Molecule at a Time. *Phys. Rev. Lett.* **2010**, *104*, 233005.
(23) Fleming, G. R. *Chemical Applications of Ultrafast Spectroscopy*; Oxford University Press: New York, 1986.
(24) Magnanelli, T. J.; Bragg, A. E. Time-Resolved Raman Spectroscopy of Polaron Pair Formation in Poly(3-hexylthiophene) Aggregates. *J. Phys. Chem. Lett.* **2015**, *2015*, 438-445.
(25) Wang, C.; Angelella, M.; Doyle, S. J.; Lytwak, L. A.; Rossky, P. J.; Holliday, B. J.; Tauber, M. J. Resonance Raman Spectroscopy of the T_1 Triplet Excited State of Oligothiophenes. *J. Phys. Chem. Lett.* **2015**, *6*, 3521-3527.
(26) Zhou, J.; Yu, W.; Bragg, A. E. Structural Relaxation of Photoexcited Quarterthiophenes Probed with Vibrational Specificity. *J. Phys. Chem. Lett.* **2015**, *6*, 3496-3502.
(27) Dietze, D. R.; Mathies, R. A. Femtosecond Stimulated Raman Spectroscopy. *Chem. Phys. Chem.* **2016**, DOI: 10.1002/cphc.201600104.
(28) Kukura, P.; McCamant, D. W.; Mathies, R. A. Femtosecond Stimulated Raman Spectroscopy. *Annu. Rev. Phys. Chem.* **2007**, *58*, 461-488.
(29) Zhou, J.; Surampudi, S.; Bragg, A.; Klausen, R. Photoinduced Charge Separation in Molecular Silicon. *Chem. Eur. J.* **2016**, *22*, 6204-6207.
(30) Gao, Y. Q.; Grey, J. K. Resonance Chemical Imaging of Polythiophene/Fullerene Photovoltaic Thin Films: Mapping Morphology-Dependent Aggregated and Unaggregated C=C Species. *J. Am. Chem. Soc.* **2009**, *131*, 9654-9662.
(31) Tsoi, W. C.; James, D. T.; Kim, J. S.; Nicholson, P. G.; Murphy, C. E.; Bradley, D. D. C.; Nelson, J. The Nature of In-Plane Skeleton Raman Modes of P3HT and Their Correlation to the Degree of Molecular Order in P3HT:PCBM Blend Thin Films. *J. Am. Chem. Soc.* **2011**, *133*, 9834-9843.
(32) Guo, J.; Ohkita, H.; Benten, H.; Ito, S. Near-IR Femtosecond Transient Absorption Spectroscopy of Ultrafast Polaron and Triplet Exciton Formation in Polythiophene Films with Different Regioregularities. *J. Am. Chem. Soc.* **2009**, *131*, 16869-16880.

(33) Callen, H. B.; Welton, T. A. Irreversibility and Generalized Noise. *Phys. Rev.* **1951**, *83*, 34-40.

(34) Louarn, G.; Trznadel, M.; Buisson, J. P.; Laska, J.; Pron, A.; Lapkowski, M.; Lefrant, S. Raman Spectroscopic Studies of Regioregular Poly(3-alkylthiophenes). *J. Phys. Chem.* **1996**, *100*, 12532-12539.

(35) Yin, J.; Wang, Z.; Fazzi, D.; Shen, Z.; Soci, C. First-Principles Study of the Nuclear Dynamics of Doped Conjugated Polymers. *J. Phys. Chem. C* **2016**, *120*, 1994-2001.

(36) Donohoo-Vallett, P. J.; Bragg, A. E. p-Delocalization and the Vibrational Spectroscopy of Conjugated Materials: Computational Insights on Raman Frequency Dispersion in Thiophene, Furan, and Pyrrole Oligomers. *J. Phys. Chem. B* **2015**, *119*, 3583-3594.

(37) Hernandez, V.; Castiglioni, C.; Del Zoppo, M.; Zerbi, G. Confinement Potential and p-Electron Delocalization in Polyconjugated Organic Materials. *Phys. Rev. B* **1994**, *50*, 9815-9823.

(38 Zerbi, G.; Castiglioni, C.; Del Zoppo, M. *Electronic Materials: The Oligomer Approach* Wiley, 2008.

(39) Beljonne, D.; Shuai, Z.; Pourtois, G.; Bredas, J. L. Spin-Orbit Coupling and Intersystem Crossing in Conjugated Polymers: A Configuration Interaction Description. *J. Phys. Chem. A* **2001**, *105*, 3899-3907.

(40) Yang, J.-P.; Paa, W.; Rentsch, S. Femtosecond Investigations of Photophysics of Ultrafast Intersystem Crossing in Terthiophene by Wavelength Dependent Excitation. *Chem. Phys. Lett.* **2000**, *320*, 665-672.

(41) Grebner, D.; Helbing, M.; Rentsch, S. Size-Dependent Properties of Oligothiophenes by Picosecond Time-Resolved Spectroscpoy. *J. Phys. Chem.* **1995**, *99*, 16991-16998.

(42) Zheldakov, I.; Wasylenko, J. M.; Elles, C. G. Excited-State Dynamics and Efficient Triplet Formation in Phenylthiophene Compounds. *Phys. Chem. Chem. Phys.* **2012**, *14*, 6211-6218.

(43) McCulloch, B.; Ho, V.; Hoarfrost, M.; Stanley, C.; Do, C.; Heller, W. T.; Segalman, R. A. Polymer Chain Shape of Poly(3-alkylthiophenes) in Solution Using Small-Angle Neutron Scattering. *Macromolecules* **2013**, *46*, 1899-1907.

(44) Chen, T. A.; Rieke, R. D. The First Regioregular Head-to-Tail Poly(3-hexylthiophene-2,5,-diyl) and a Regiorandom Isopolymer: Nickel Versus Palladium Catalysis of 2(5)-Bromo-5(2)-(Bromozincio)-3-Hexylthiophene Polymerization. *J. Am. Chem. Soc.* **1992**, *114*, 10087-10088.

(45) Yu, W., Magnanelli, T., Zhou, J., Bragg, A. E. Structural Heterogeneity in the Localized Excited States of Poly(3-hexylthiophene) J. Phys. Chem. B, **2016**, 120(22), 5093-5102

Curriculum Vitae

Wenjian Yu

Department of Chemistry
Johns Hopkins University
3400 North Charles Street, Baltimore, MD 21218 USA

Personal Information

Name: Wenjian Yu
Born Feb 16, 1987 in Shandong, China
Email: wenjianyu.chem@gmail.com
Address: 4008 Linkwood Rd, Apt C, Baltimore, MD, 21210 USA

Education

Johns Hopkins University, Baltimore, Maryland, USA *9/2010-09/2016 (expected)*
PhD of Physical Chemistry in Dr. Art Bragg Lab

Fudan University, Shanghai, China *09/2006-07/2010*
B. Sc. Degree in Applied Chemistry

Awards and Honors

Mary Lydston Kilpatrick Fellowship	06/2013
Excellent student of Fudan University	11/2007
Dow Scholarship	11/2007

Publications

- Art Bragg, **Wenjian Yu**, Jiawang Zhou, and Timothy Magnanelli. Ultrafast Raman Spectroscopy as a Probe of Local Structure and Dynamics in Photoexcited Conjugated Materials. *J.Phys.Chem.Lett. (Perspective), 2016 (accepted)*
- **Wenjian Yu**, Timothy J. Magnanelli, Jiawang Zhou and Art Bragg, "Structural and photophysical heterogeneities of localized excited states of the conjugated polymer poly(3-hexylthiophene) (P3HT)", *J. Phys. Chem. B, 2016, 120(22), 5093-5102*
- Jiawang Zhou, **Wenjian Yu** and Art Bragg, "Structural Relaxation of Photoexcited Quaterthiophenes Probed with Vibrational Specificity", *J. Phys. Chem. Lett. 2015, 6, 3496-3502*
- **Wenjian Yu,** Paul J. Donohoo-vallett, Jiawang Zhou and Art Bragg, **"**Ultrafast photo-induced nuclear relaxation of a conformationally disordered conjugated polymer probed with transient absorption and femtosecond stimulated Raman spectroscopies", *J. Chem. Phys, 2014, 141, 044201*

- **Wenjian Yu**, Jiawang Zhou and Art Bragg, “Exciton conformational dynamics of poly(3-hexylthiophene) (P3HT) in solution from time-resolved resonant-Raman spectroscopy”, *J. Phys. Chem. Lett.*, *2012, 3, 1321-1328*
- Ji Ni, **Wen-Jian Yu**, Lin He, Hao Sun, Yong Cao, He-Yong He and Kang-Nian Fan,"A green and efficient oxidation of alcohols by supported gold catalysts using aqueous H_2O_2 under organic solvent-free conditions", *Green Chem., 2009, 11, 756–759*

Skills

- Experienced in ultrafast laser operation, includes tuning oscillator, choosing suitable optics, signal detection and related experiment set-up.
- Experienced in time-resolved Transient Absorption (TA)， Femtosecond stimulated Raman spectroscopy (FSRS) and three-pulses pump-dump-probe (PDP), pump-push-probe (PPP) spectroscopy
- Experienced in Labview, Origin and MatLab
- Experienced in making and characterizing supported gold and iridium nanoparticles

Teaching Experience

Teaching Assistant in General Chemistry	09/2010-06/2011
Teaching Assistant in Physical Chemistry Lab	09/2011-06/2012
Teaching Assistant in Physical Chemistry Lab	09/2014-12/2015

Research

Undergraduate research

During my undergraduate study, I joined the Lab of Surface Chemistry. Under the instruction of Prof. Yong Cao, I studied the supported gold and iridium nanoparticles using ZnO and TiO_2 as carriers and their application as catalysts in the oxidation of alcohols and the reduction of nitro-benzene.

PHD Research

My PHD research focuses on the relaxation dynamics of excited conjugated polymers, like poly-(3-hexyl-thiophene) (P3HT), poly-(3-cyclohexyl-4-methylthiophene) (PCMT) and poly-(thiophene-methano annulene-thiophene) (PTMT). Various ultrafast spectroscopies methods have been used to investigate these systems, include transient absorption (TA), Femtosecond stimulated Raman spectroscopy (FSRS), pump-dump-probe etc. We focus primarily on the conformational relaxation process after benzoidal ground state structures in the polymer have been excited to form quinoidal structures. The time-dependent

Raman spectroscopy is a very helpful method when exploring the relaxation process because it can show the dynamics of specific nuclear motions. Because Raman frequencies and exciton energy are sensitive to exciton length, we also focus on the exciton size change after photoexcitation. Pump-dump-probe technique can perform transient hole-burning measurement for excitons, which can explore the exciton inhomogeneity. The goal of my research is to get the full picture of exciton relaxation dynamics using ultrafast spectroscopic methods.